University of Reno, Nevada

Synthesis, Fabrication and Functionalization

of

Two-Dimensional Polymers

A dissertation submitted in partial fulfillment of the requirements for

the degree of Doctor of Philosophy in Chemistry

by

Zachary R. Kehoe

Dr. Benjamin T. King/Dissertation Advisor

December, 2023

THE GRADUTE SCHOOL

We recommend that the dissertation
Prepared under our supervision by

Zachary Ryan Kehoe

Entitled

Synthesis, Fabrication and Functionalization of
Two-Dimensional Polymers

Be accepted in partial fulfilment of the
Requirements for the degree of

DOCTOR OF PHILOSOPHY

Benjamin King, Ph D., Advisor

Wesley Chalifoux, Ph. D., Committee Member

Lawrence Scott, Ph. D., Committee Member

Dylan Kosma, Ph. D., Committee Member

Joonhee Lee, Ph. D., Graduate School Representative

Markus Kemmelmeier, Ph. D., Dean of Graduate School

December, 2023

Abstract

The synthesis of two-dimensional polymers (2DPs) is an emerging field with expected applications in nano-electronics, separation membranes, and memory storage devices. Unlike linear or branched polymers, 2DPs are defined as topologically planar sheets having a thickness consistent to their monomer species. This dissertation revolves around the synthesis, fabrication, and surface functionalization of a 2DP coined poly(carboxy fantrip).

Chapter one focuses on the definition, synthetic approaches, and applications of 2DPs. Both natural and synthetic two dimensional (2D) materials are reviewed, including different polymerization approaches, transfer processes and, surface modifications.

Chapter two reports the optimization of a 2D monomer, carboxy fantrip, and derivatized versions on a preparative scale. This chapter addresses inconsistencies from previous procedures increasing monomer yields from a few milligrams to hundreds. Synthetic strategies, both working and unsuccessful are reported, including experimental protocol and characterization of intermediates.

Chapter three discusses new photo-polymerization strategies at the air/water interface, polymer deposition onto solid substrates, and covalent surface modifications of the resulting film. The results of these experiments are monitored and analyzed by Brewster angle microscopy (BAM), differential interference contrast (DIC) microscopy, high speed videography, and contact angle measurements.

Dedication

To my family and friends for all their love and support.

Acknowledgements

I would like to thank my **Parents**, for their support throughout my life. They have given me so much over the years and I hope to give one day that back.

I would like to thank my fiancé **Alexandra English** for her constant love, support, and understanding both intellectually and emotionally. Every day is brighter with you in the world.

I would like to thank **William Thompson**, for his guidance and friendship during my time pursuing the synthesis of Fantrip. His willingness to help troubleshoot issues, and time spent reviewing this dissertation is greatly appreciated.

I would like to thank **Benjamin King** for taking the time to share his chemical knowledge with me while advising my PhD journey.

I would like to thank **Jerry Kier** for his help refining my writing and helping me wind down from all the stress.

UNR **chemistry department**, both faculty and students for the knowledge and friendships I have gained.

Contents

List of Figures

Chapter 1

Chapter 2

Chapter 3

List of Abbreviations

1D	One Dimensional
2D	Two Dimensional
3D	Three Dimensional
2DP	Two Dimensional Polymer
AFM	Atomic Force Microscopy
BAM	Brewster Angle Microscopy
COF	Covalent Organic Framework
CVD	Chemical Vapor Deposition
DIC	Differential Interference Contrast
GC-MS	Gas Chromatography Mass Spectrometry
GI-XRD	Grazing Incidence X-Ray Diffraction
HOPG	Highly Ordered Pyrolytic Graphite
HRMS	High Resolution Mass Spectrometry
MMA	Mean Molecular Area
NMR	Nuclear Magnetic Resonance
PDC	Pyridinium Dichromate
SEM	Scanning Electron Microscopy
SP	Surface Pressure
STM	Scanning Tunneling Microscopy
TFA	Trichloroacetic acid
TOF	Time of Flight

UV	Ultraviolet
UV/Vis	Ultraviolet/Visible
XRD	X-Ray Diffraction

Chapter 1: Introduction

Scientific confinement in two dimensions (2D) and freestanding 2D macromolecules are a scientific field much unexplored. Notable and ubiquitous applications of 2DPs is a preeminent field of inquiry. Monomer design and polymerization techniques lead to vast arrays of 2D structures tailored to the application at hand.

1.1 Introduction of 1D Macromolecules

The extraction and utilization of naturally occurring polymers has been conducted since 1600 BC, long before the scientific method. Natural rubber derived from latex, secreted from the *Hevea Brasiliensis* tree in South America was exploited by Mayas and Aztecs in daily life and religious ceremonies.[1] Natural latex tapped from this same tree now constitutes over 30% of the world's rubber hydrocarbon consumption.[2] Although Mayan culture provided the first documented utilization of rubber, the quotidian use of plastics did not occur until the Second World War, where natural latex was vulcanized and used in military tire production.[3] Today, unimaginable production (380 metric tons in 2015) of plastics are produced and sold in the global market.[4]

Over the last century, polymer chemists have gained a refined understanding over synthetic control. When synthesizing 1D polymers, a categorization of the physical properties by structural aspects of these macromolecules is now commonly known. Indeed, synthetic polymers represent a critically important class of materials.[5,6] Today, polymer applications range from coatings, adhesives, fibers, building materials, and many more.[7–9]

Recent advancements in the polymer field are functional materials, now commonly used in electronic devices, batteries, and solar cells.[10–12]

The first 100 years of synthetic polymerization have seen two dominant structural paradigms: 1) topologically linear chains and amorphous, cross-linked networks, (Figure 1.1 and 1.2) macromolecular dimensionality. Each of these structural paradigms can be best understood by monomer composition. One-dimensional polymers are comprised of monomers as the smallest repeat unit. These small organic molecules with sizes no greater than a few nanometers can be considered as having no dimensions. As these monomers covalently bond forming a linear chain, they are viewed as one dimension (1D), in the same way a string is one-dimensional. Chain interactions occur via intramolecular forces including van der Waals, and hydrogen bond interactions acting on multiple linear and/or branched chains to create the solid plastics widely used today. Another interaction is crosslinking neighboring chains through covalent intramolecular bonds to form an amorphous three dimensional, (3D) networks.

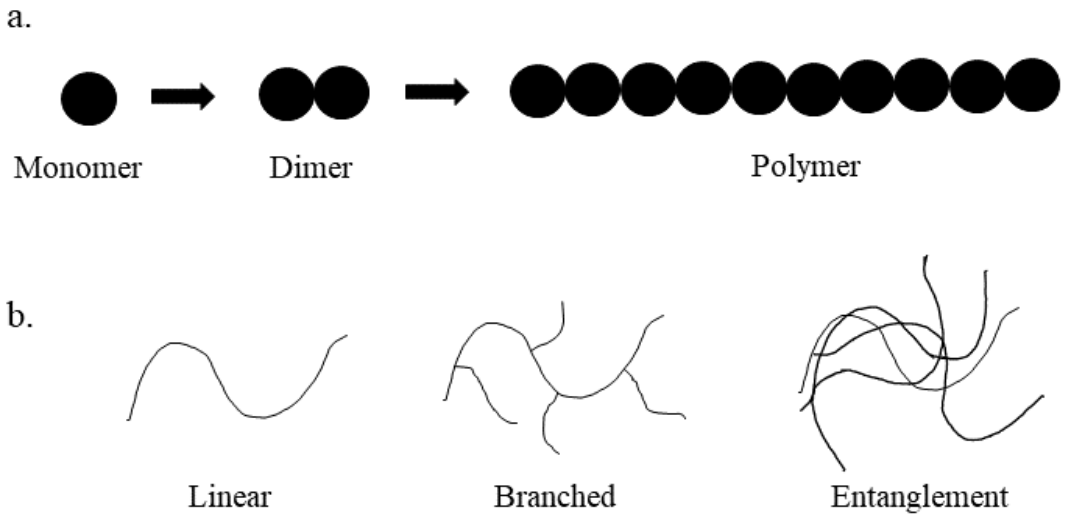

Figure 1.1 Chain growth polymerization: (a.) Linear growth polymerization in one dimension (1DP). (b.) Different growths of chain polymerizations and entanglement of chains.

Prolonged research has sought to provide answers to grow polymers of higher dimensions for the better part of a century. Nature has provided the canonical example of a 2D polymer, graphene, a single atomically thick layer of the commonly found material, graphite. Isolation of single layers from its crystal-like parent, graphite, can be done by rubbing onto a solid surface. Then a perfectly cleaved single layer is tediously searched for within the bulk fragments of tens of hundreds of layers.[13] This mechanical rubbing, similar to "drawing on a chalkboard" has been used to also isolate free standing 2D crystals from a large variety of strongly layered 3D crystals including, boron nitride, dichalcogenides, and complex oxides.[14]

This "needle in a haystack" approach was the first successful isolation of atomically thin films and led to the discovery of useful properties compared to their bulk counterparts.

Although the isolation was a success, sheets are only the size of a few nanometers. Another particularly daunting issue is the thermodynamically stability of these free-standing films below a certain thickness. Many 2D crystals decompose or segregate typically below a few dozen layers.

Different methods have been explored in order to synthesize graphene and other two-dimensional materials, such as using chemical vapor deposition (CVD) process on copper foils at high temperatures (1000^{o}C) to grow graphene onto copper foil.[15] CVD growth is an energy taxing process and results in defect free sheet sizes of only a few nanometers, rendering large scale manufacturing non-viable. For 2D materials to become used in industrial applications, it is necessary to produce economically viable, thermodynamically stable, large area free standing sheets.

Despite these established methods, there are still many possibilities unexplored, and more research is needed to understand the potential applications of these materials. A synthetic covalent 2D grid approach, while drastically different than the methods previously discussed, supports a more rational approach to create large area molecularly thin films through a bottom-up modular approach. The next sections will provide the necessary information to elucidate this question and is the aim of my dissertation.

1.2 Introduction of 2D Macromolecules

Roald Hoffmann provided insight into a chemist paradigm between relying on nature for the discovery of new materials verses relying on the limited human perspective to identify ideal mathematical forms for inspiration. He writes,

> *"Organic chemists are masterful at exercising control in zero dimensions... One subculture of organic chemists has learned to exercise control in one dimension. These are polymer chemists, the chain builders…*
>
> *But in two or three dimensions, it's a synthetic wasteland. The methodology for exercising control so that one can make unstable but persistent extended structures on demand is nearly absent. Or to put it in a positive way—this is a certain growth point of the chemistry of the future."*[16]

This passage is particularly relevant today given the status of the field of 2D polymers. Despite the tremendous potential synthetic 2D polymers have to advance various applications to scientific and engineering fields, surprisingly little research has been done in this area. Despite numerous approaches attempted over the years, few have resulted in the successful creation of a single, molecularly thick, covalently bonded sheet with an organized internal structure.[17] While the concept of covalent macromolecules is not new, dating as early as 1935, chemists suggested the same techniques to form linear strands and interlinked networks may be applied to establish macromolecular sheets. Examples of such early contributions to this area of inquiry include functionalized β-eleostearic acids, most notably by Talmud coining the term 2D polymerizations to describe cross-linking of stearic aldehydes and polyfunctional amines.[18,19] While these early attempts were novel given the time period, these preliminary outcomes most undoubtedly resulted in linear chains irregularly cross-linked, rendering them non-crystalline and not molecularly thin.

The lack in indistinctness between 2D or not 2D remains a complex task that continues without substantive resolution. While no current definition is accepted across the field of chemists, there are 5 fundamental criteria that 2D films must identify given by Dieter Schlüter.[20]

1. Planarity: Two-dimensional polymers are topologically planar sheets.
2. Repeat units: Two-dimensional polymers have repeat units rendering them crystalline in at least one conformation.
3. Covalent bonds: The repeat units of two-dimensional polymers are connected by covalent bonds.
4. Thickness: Two-dimensional polymer molecules have the thickness of the constituent repeat unit (monolayers).
5. Separability: Two-dimensional polymers are strong enough to be manipulable as individual entities.

Two-dimensional polymers differ from chain polymers in a manner that monomer repeat units must contain at least three reactive sites which lie in a topological plane, rather than one or two reactive sites which react linearly. This creates a repeating pattern that is similar to a fisherman's net (Figure 1.2).

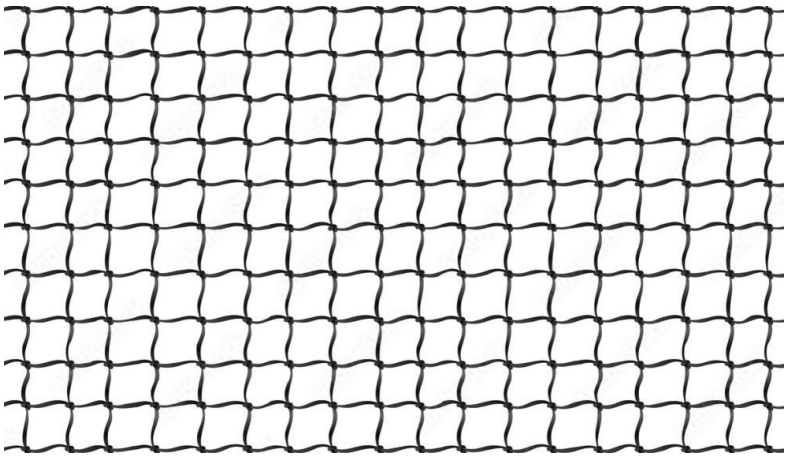

Figure 1.2 Illustration of a fisherman's net: A 2D network of repeating knots tied with rope.

A 2D polymer must be planar, one unit thick and contain a periodic internal structure installing long-range order.[17] This topology can be viewed by the field of tessellations; in other words, an arrangement of shapes closely fitting together in a repeated pattern without gaps or overlaps. Tiles are a closed polygon created by a set of edges and vertices, if they can be arranged with no gaps or overlap, then they are considered a tiling.

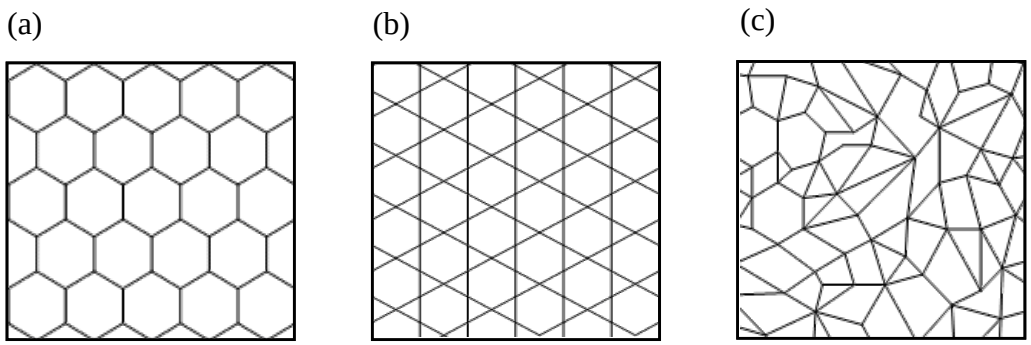

Figure 1.3 Types of tiling: (a) regular tiling, (b) semi-regular or alternating, (c) non-periodic.

Tilings may be periodic or non-periodic, therefore one or many polygons may be used if there are no overlapping points or gaps. Periodic tiling have multiple sub categories, including the most common, regular or semi-regular tiling. As these patterns are made by connecting one or more polygons together periodically forming a repeating pattern. Non-periodic, or random tiling uses any arrangement of polygons to form a pattern having no periodic order (Figure 1.3).

Tessellation theory is a tool that can lay the structural groundwork for a bottom-up 2DP synthesis by providing a template for monomer characteristics. Structural design of monomers are illustrated by two different examples (Figure 1.4). In both, the red dots are reactive atoms, or vertices and the black lines are covalent bonds, edges. In example (a), graphene may be broken down to a trigonal star made of 2 sp^2 hybridized carbon atoms. Three monomers, when covalently bonded together, form a hexagonal lattice. Example (b) would be the simplest tiling having a vertex configuration of 4.4.4.4 or 44 which creates a square lattice. As a result, monomers designed using tessellation theory will result in a periodic polymer with no gaps or overlaps within a single topological plane.

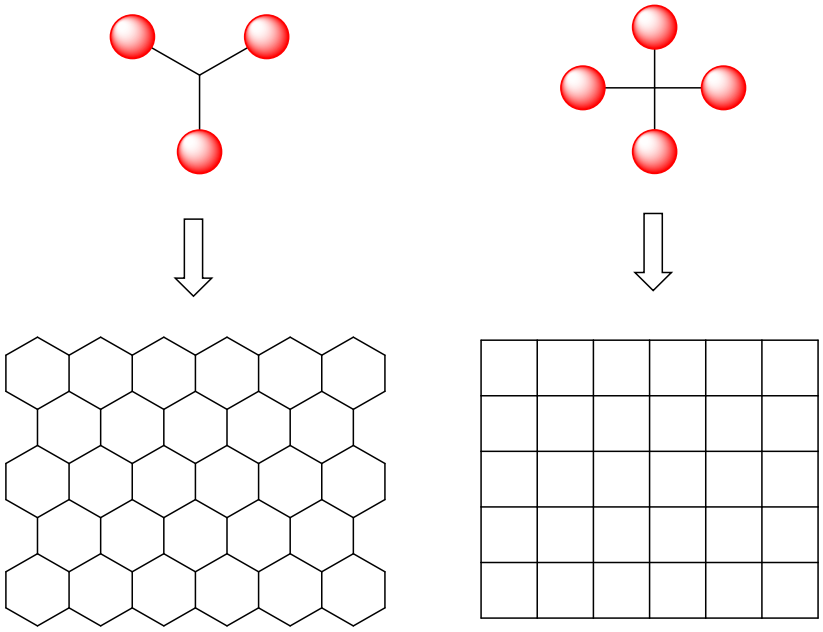

Figure 1.4 Two different reactive monomers: Triangular shaped monomers create a honeycomb lattice (a). A cross shaped monomer forms a square lattice (b).

1.3 Potential Applications of 2D Polymers

Two-dimensional polymers (2DPs) demonstrate unique characteristics not obtainable in other macromolecules systems. The mix of properties identified in 2DPs are mainly due to their ordered, flat, and anisotropic nature, which results in clearly defined shapes.[19] Due to these qualities, 2DPs have been studied to explore varied possibilities in industrial applications, including molecular separations, organic electronics, and sensors for electronics or biological fields.

1.3.1 Separation membranes

2DP films could offer a reasonable solution to the global challenges surrounding water scarcity. Population growth and global warming are accelerating the need to access fresh water. One-in-four people do not have access to safe drinking water.[21] A bottom-up approach to synthesize 2DPs offers sheets with tunable pore size that could facilitate selective, ultrafast separation of targeted molecules via pore size exclusion. Membrane flux is inversely proportional to thickness, and 2DPs inherent nanometer molecular thinness allow for incomparable efficient water flux when compared to current state of-the-art 200 nm-thick poly(amide) membranes (Figure 1.5).[22] Computational studies support flux enhancement of molecularly thin films by studying nonporous graphene.[23–25]

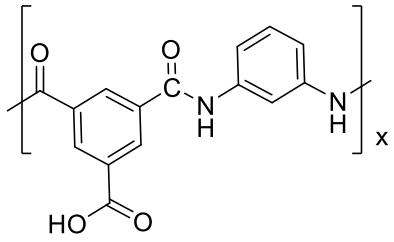

Figure 1.5 Polyamide structure: Current backbone for many RO filters.

A bottom-up approach results in pore uniformity which more efficiently separates molecules when compared to current RO membranes typically made of poly(amides) or cellulose acetate both of which do not have molecular thinness or uniform pores. Figure 1.6 illustrates the difference in thickness and pore uniformity in both polymer membranes and a 2DPs (Figure 1.6).

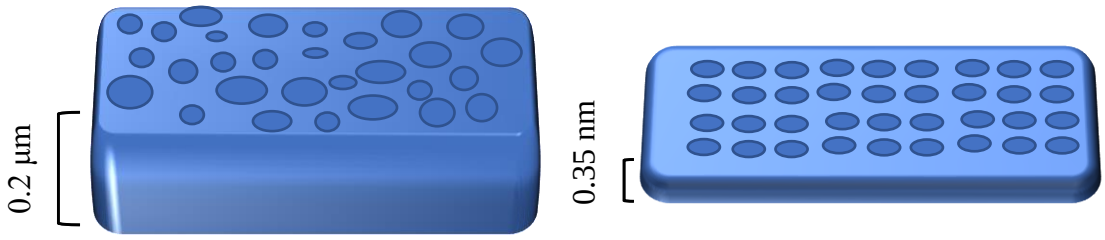

Figure 1.6 Different types of separation membranes: Polyamide membrane consisting of many layers and uneven pores (left). Single layer graphene membrane with uniform porosity (right).

1.3.2 Electronic Properties

K. S. Novoselov first reported useful electronic properties of few-layer graphene (FLG) in 2004.[13] Two-dimensional (2D) materials generated much attention including nano- and atomic electronic device manufacturing and prospective use in battery separation membranes given the unique charge carrier mobility of FLG.[26] Atomically thin graphene support higher mobilities for charge carriers and have a greater susceptibility to electric fields allowing the most efficient materials to date for transistor applications.[13] These electronic properties can be attributed to graphene's fully conjugated hexagonal structure.[27] Another example of 2D conjugated covalent organic frameworks (COF) is a triazine bridged by sp^2 carbon linkers,[28] but other examples are lacking and remain a current synthetic challenge investigated through polycondensation reactions of porphyrin-containing monolayers.[29]

1.3.3 Functional Surfaces

2DPs are particularly appealing for use in functionalized surfaces. The highly ordered repeat units (RU) offer a regular, periodic platform with ordered repeating functionality.

Incorporating a reactive tether onto one or both sides of the monomer introduces opportunity for post functionalization of the 2DP surface. Density of functionalization could be calculated from the number of active sites per monomer and area of RU post polymerization. This result could serve applications involving catalysis, sensors, and quantum memory storage. Designing a monomer with post-functional capabilities require multiple conditions when transferred to a solid support to ensure the reactive tether is facing in the right direction.

Post-polymerization modification of the surface requires accessible reactive sites. Film deposition onto solid supports requires specific reactive tether orientation in which the sites face away from the support; this can be imagined as an egg prepared “sunny-side-up” where the yolk of the egg is the functional tether. If the yolk is facing down or “onto the pan”, modification of the functional tether is hindered. Monomer orientation on the air/water interface is influenced through polar reactive tethers that are attracted to water, subsequently aligning the rest of the monomer up, much like the keel of a boat (Figure 1.7). Tether reactivity is also important, it cannot react during the polymerization and must have proper reactivity to facilitate surface modifications after the polymer is transferred to a substrate.

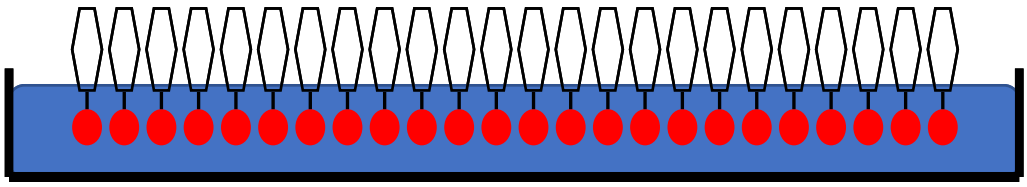

Figure 1.7 Monomers floating on the air/water surface: Monomer orientation is influenced by reactive polar tethers, represented as red ovals anchored in water.

1.4 Synthetic Approaches to 2D Polymers

This section discusses past and current synthetic strategies employed to create and characterize 2DPs. Herein, solid support, single crystal, and air/water interface approaches are discussed as these are pertinent and successful approaches cited in the research literature. Within this section, the air/water approach provide a brief literature overview of advancements in the field and will be discussed in greater detail as it pertains to the work completed in this dissertation in Chapter 3.

1.4.1 Solid Support

Substrates have been used to facilitate the growth of supramolecular systems including self-assembled monolayers (SAM) and covalent 2D systems. Exploiting principles from nature, H-bonding has been used to synthesize many self-assembled polymers. One of the earliest examples of extended 2D molecular networks reported by *Grissel et al.*[30] who utilized 1,3,5-benzenetricarboxillic acid (TMA) monomer, previously known to form six-molecule polymorphs through intermolecular hydrogen-bonding between carboxylic acid groups (Figure 1.8).[31] Solid support was used to overcome the energetically unstable close packing of a single molecule. TMA was evaporated under ultrahigh vacuum (UHV) onto highly ordered pyrolytic graphite (HOPG) substrate and imaged with scanning tunneling microscopy (STM). Two geometries were observed in ambient conditions, coined “chicken wire or honeycomb” and “flower,” both consisting of six-fold rings held together by intermolecular hydrogen bonds. The existence of the 2DP in ambient conditions validated the thermodynamic stability of close packing monolayers sublimed to solid support.

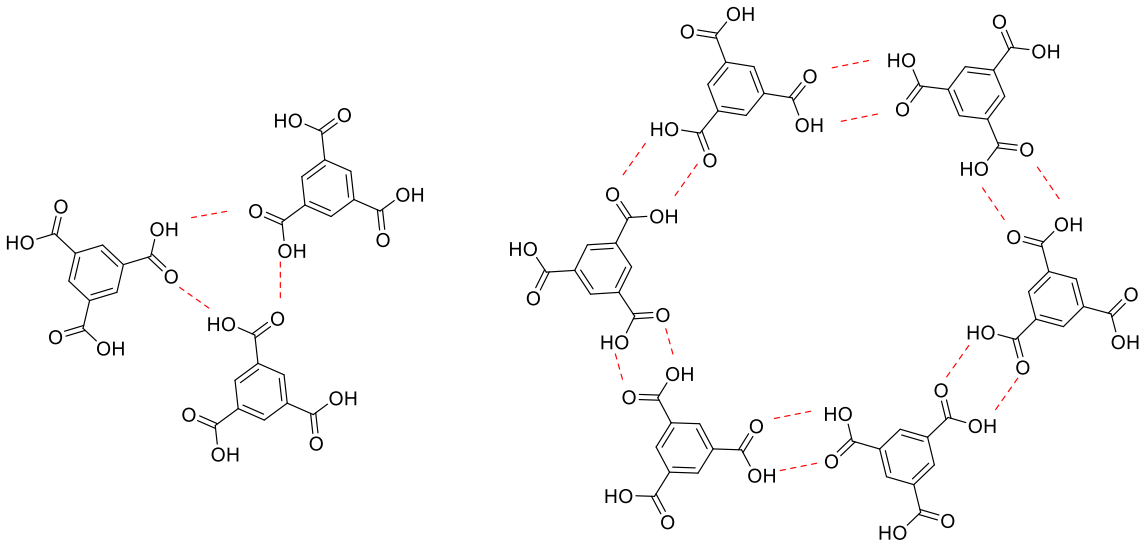

Figure 1.8 Trimesic Acid (TMA) Monomer: Two different hydrogen bonding 2D lattices are formed, flower (right) and chicken wire (left).

Other non-covalent 2D lattices have been prepared on substrates. Examples of these aggregating monomers include dialkylbenzenes through Van der waal forces,[32] cyanophenyl substituents through dipole-dipole interactions,[33] and metal containing coordination compounds.[34] Thermal stability is considerably weak in non-covalent 2D SAMs, and few have been reported as free-standing films at room temperature. Molecular thin-films connected through covalent bonds offer the greatest thermal stability and are more appealing for consumer applications.[35,36]

An example of a covalent, surface supported 2DP was reported by *Bieri et al.* which utilized a Ullman reaction at elevated temperatures (525K) to couple hexaiodo-substituted cyclohexa-*m*-phenylene monomers as they were UHV deposited onto Cu (II) surfaces (Figure 1.9).[36] STM imaging provided conclusive evidence of the ordered 2DP. Covalently bonded 2D surfaces synthesized via UHV offer increased thermal stability but suffer from

network defects in large (> 10 nm) domains. One explanation why this issue persists is the irreversibility of covalent bonds. Once the monomer is deposited on the surface and reacted, it is anchored to the surface permanently. Any hope of a post correction to the network has vanished.[36] This process also eliminates any applications which need the polymer to be transferred onto another surface. These shortcomings are still unresolved.

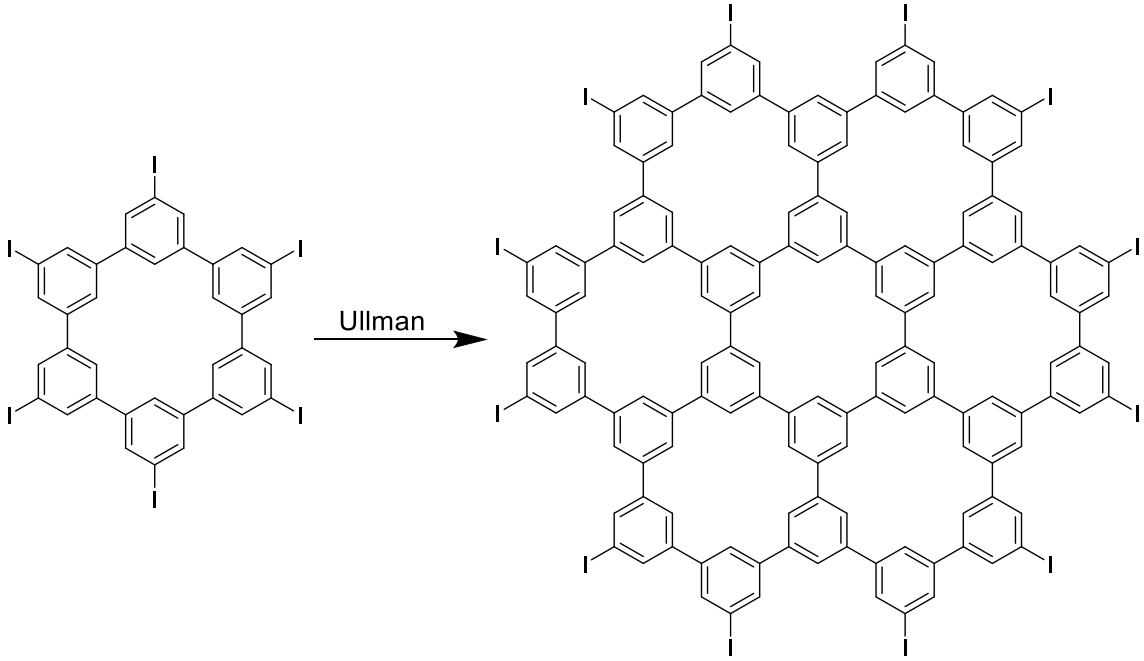

Figure 1.9 Ullman coupling of 2DP on solid support: Chemical structure of hexaiodo-substituted CHP (left). A fraction of the 2DP chemical structure (right).

1.4.2 Single Crystal Approach

Single crystal approach is a highly effective synthetic approach towards 2DPs. Efficiency of this method results from monomer preorganization and the availability to obtain structural data on both the monomer and polymer by use of X-ray diffraction (XRD). The single crystal approach allows monomers to crystallize into a lamellar lattice, which

aligns the monomers reactive units parallel to each other. The resulting crystal is polymerized, forming a polymer lamellar crystal. Molecularly thin 2DPs are exfoliated from the parent crystal by dispersing it in a solvent for many days (Figure 1.10). Solvent-suspended, single sheets can be transferred onto substrates and imaged by AFM or STM.

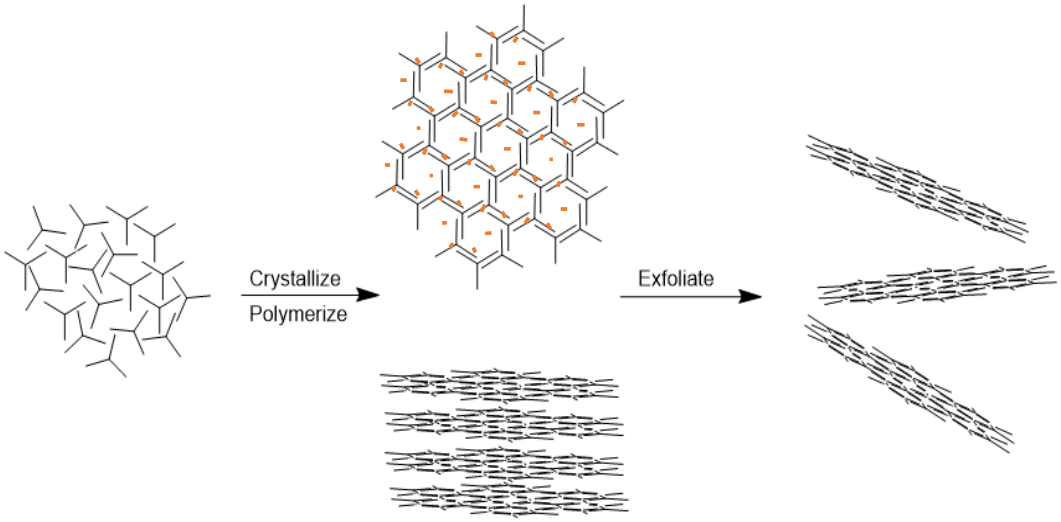

Figure 1.10 Single crystal approach: Liquid state of monomers dissolved in solutions (left). Crystallization and polymerization of aligned monomers (middle). Exfoliation of lamellar polymer crystal exposing molecularly thin sheets (right).

Kissel et al. reported the first organic 2DP by using the single crystal approach in 2012. An anthracene-based ridged macrocycle was made in a 25 step synthesis to yield a monomer containing photoreactive 1,8-diethynylanthrylene units (DEAs) and three terphenylene bridges (TPBs) units.[37] Successful monomer crystallization was attained from various solvent mixtures of 1,1,2,2-tetrachloroethane (TCE)/tetrahydrofuran (THF). The crystals were confirmed by XRD and showed birefringence under polarized light. Upon

irradiation (λ = 470 nm, 300 mW) neighboring monomers reacted in a [4+2] cycloaddition between the alkyne and 9,10-anthracene positions (Figure 1.11). Fluorescence, birefringence, and solubility of the irradiated product dropped significantly indicating the presence of the desired polymer. Structural rearrangements during the photo-polymerization resulted in a loss in crystallinity and inhibited structural elucidation by XRD. Unwrapping the crystal to a molecularly thin sheet provides evidence the film's weight can support the 2D network. Exfoliation in 1-methyl-2-pyrrolidone (NMP) at 150 ^{o}C for 2 days resulted in round sheets having lateral dimensions of 1–2 μm observed by AFM on mica.

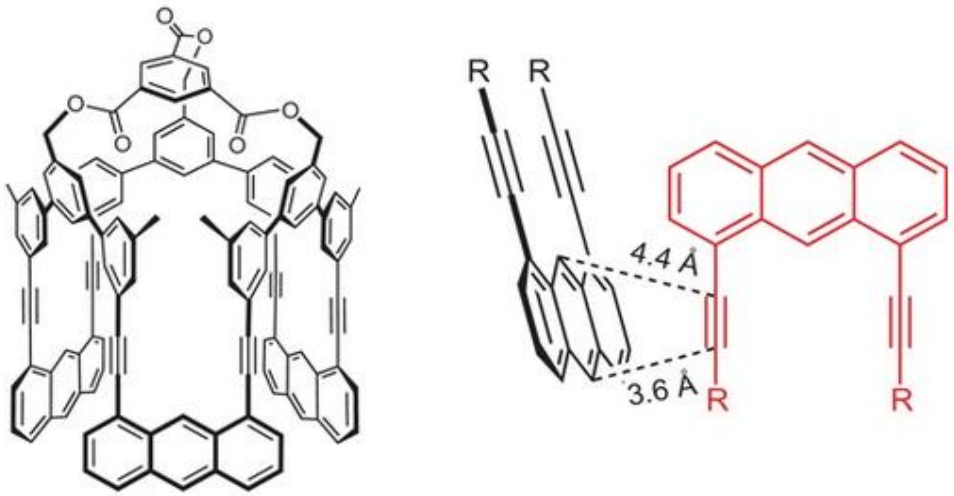

Figure 1.11 Single crystal 2DP: Monomer of a photoreactive crystal (left), and the alignment of two adjacent monomers (right).

Shortly after, *Bhola et al.* reported a second example of an organic 2DP.[38] A triptycene monomer with anthracene extended blades coined "antrip", was reported to crystallize in a pseudolamellar structure. Polymerization through a photoinduced [4+4]

cycloaddition dimerized neighboring anthracene blades. Solid-state NMR, IR and exfoliation of the molecular sheets analyzed by AFM confirmed bond formation. Similar to *Kissel et al*., rearrangement of the pseudolamellar monomer crystal during polymerization resulted in a loss of crystallinity, thus inhibiting structural elucidation by SC-XRD (Figure 1.12).

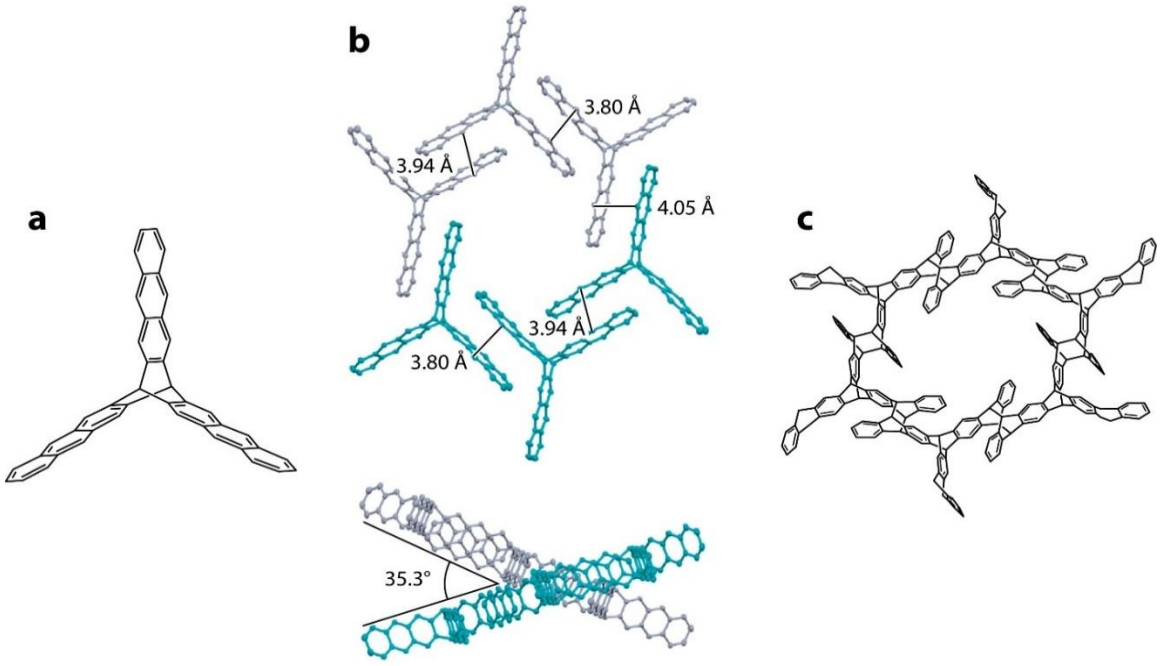

Figure 1.12 Photo-Polymerization of Antrip: Antrip monomer (a), pseudolamellar monomer crystal (b), and dimerization adduct of monomer creating a honeycomb 2D lattice (c).

While these first two monomers undoubtably resulted in 2DPs, a loss in crystallinity after polymerization limited the use of SC-XRD to elucidate the structures. A true single-crystal-to-single-crystal (SCSC) approach should proceed topochemically maintaining a lamellar crystal upon polymerization, allowing for structural elucidation by SC-XRD. In

2014, King and Schlueter independently reported 2DPs from the SCSC approach. Both methods utilized a photoinduced [4+4] cycloaddition that resulted in a 2DP without loss of crystallinity.[39–41]

A beneficial outcome that makes the crystal approach effective is the ease of structural analysis obtained via XRD of both monomer and polymer crystal which is otherwise not possible with solid support methods, where STM or AFM are needed. Another benefit of this method is lamellar crystal packing. Monomer confinement within the crystal lattice ensures a pre-organized, highly ordered domain is installed before polymerization, resulting in near defect free 2DP sheets. The single crystal approach also uses mild reaction conditions compared to UHV and intensely elevated temperatures needed for a solid support method. This approach also provides free standing sheets allowing for transfer onto surfaces.

Inherent shortcomings to the single crystal method includes size limitation and crystallization time. Exfoliated sheets are limited to the size of the crystal, and in practice are much smaller due to shear forces acting upon the unraveling crystal. Crystal size greatly depends on solvent choice and concentration which takes time to optimize. In a manufacturing setting, solvent optimization, slow crystal growth, and limited sheet size ultimately renders this method untenable for industrial applications.

1.4.3 History of the Air/Liquid Interface

Langmuir methods are not new – they were developed by Agnes Pockels, Irving Langmuir, and Katherine Blodgett 100 years ago. The dawn of the technique, while rudimentary, has been dated as early as the 18th century BC. The first accounts are from

Babylonia times, when oil was dropped onto water invoking patterns used to guide divination rituals.[42] Centuries later, Benjamin Franklin reported calming water effects when he poured a teaspoon of oil onto the surface of a pond in 1773.[43] Interestingly enough, he was told by a ship captain that he too noticed the effects of a calmer sea when the wasted fish oil from meals were poured overboard. It was not until 100 years later that Lord Rayleigh was able to repeat Franklin's oil experiment and further contribute to the field by calculating the oils monolayer thickness by measuring the volume of oil used and the area it spread.[44] Monomer thinness was calculated by converting the volume of oil used to the number of molecules using Avogadro's number, then dividing by the area the oil covered, this set the stage for further scientific experiments.

Since these rudimentary, but essential experiments, Pockels, Langmuir, and Blodgett have developed a scientific foundation to study monomers at the air/liquid interface. This was accomplished by engineering troughs with movable barriers, sensitive surface-pressure detectors, and elaborate dippers to control and transfer monolayers within a laboratory environment. Technological advancements have since allowed for some needed control in the laboratory, but the homogenous transfer of monolayers onto solid surfaces remains an often confounding experimental problem to this day.

The confinement of molecules on a liquid surface is a promising method for large area production of 2DPs. The first laboratory trough was made in 1890 by Agnes Pockels and since, many amphiphiles have been observed to pre-organize on a 2-dimensional liquid surface. As early as 1935, scientists explored the idea of interlocking linear fatty acids at the liquids surface to create 2D films. This work established the nascent understanding of

molecularly thin 2D films. Subsequent cross-linking of fatty acids undoubtedly resulted in unordered random Diels-Alder cycloaddition adducts between maleic anhydride and β-eleostearic acid producing an amorphous structure offing no long range order.[45]

Cross-linked UV-initiated polymerizations of long saturated chains containing acrylate polar heads at the air/water interface have been reported to form two-dimensional networks. Pioneering these light induced polymerization was Dubault, who used a mercury lamp to crosslink 1-n-octadecyloxy-2-3-diacryloloxy propane (Figure 1.13) on the surface of water.[46] After drying, a white deposit remained and was insoluble in solvents, suggesting a polymer product.

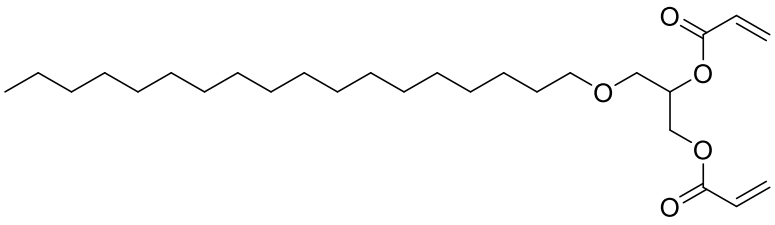

1-n-octadecyloxy-2-3-diacryloloxy propane

Figure 1.13 UV-initiated 2DP: Diacrylate polar head floats in water and cross links with neighboring monomers

Other 2D dipolar long-chain polymerizations at the air/liquid interface include 2-pentadecylaniline (PDA) and 1,2,2-bis(2-aminophenyl)docosane (BAD) (Figure 1.14). These crosslink reactions are carried out in an acidic liquid subphase containing sulfuric acid and ammonium peroxydisulfate as an oxidizing agent.[47–49]

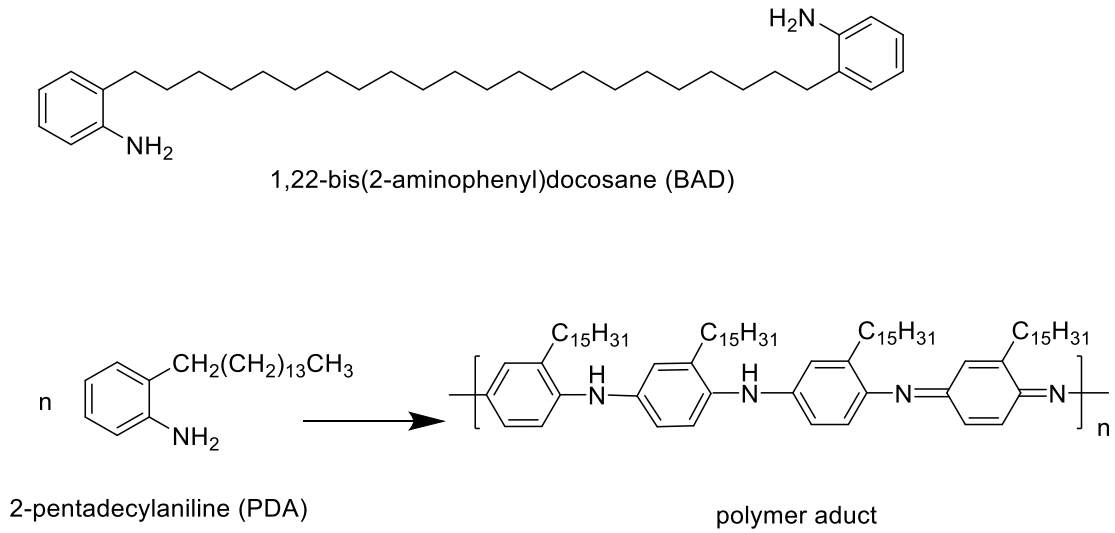

Figure 1.14 Polyalkylaniline 2D crosslinking: Dipolar monomer (BAD) (top), manopolar analine monomer (PAD) (bottom left) and its polymer aduct (bottom right).

Metal complexes have since been used to "sandwich" organic monomers using connecters to form a covalent 2DP. Michl made advancements in this field using lanthanum-tetrapyridylporphyrin complexes floating on a mercury subphase.[50] Para-xylene dibromide was subsequently used as a linear coupling agent (Figure 1.14). Michl was able to transfer the 2DP onto HOPG by first laying a thin blanket of polystyrene over the films surface to aid in extraction from an air/mercury interface, then was transferred onto HOPG. To image the 2DP by AFM, the polystyrene transfer agent had to be dissolved from the surface. Mercury oxide impurities were removed by boiling the deposited film in hydrochloric acid. AFM imaging revealed that transferring the film with a polystyrene support onto HOPG followed by the demanding purification caused mechanical folding and a rough surface. Regardless, Michl was able to image small flakes with dimeters of

100-150 nm having a thickness of 0.7 nm. The imaged chips showed local ordered (< 20 nm) but large domain order (> 100 nm) was poor, suggesting many defects (Figure 1.15).

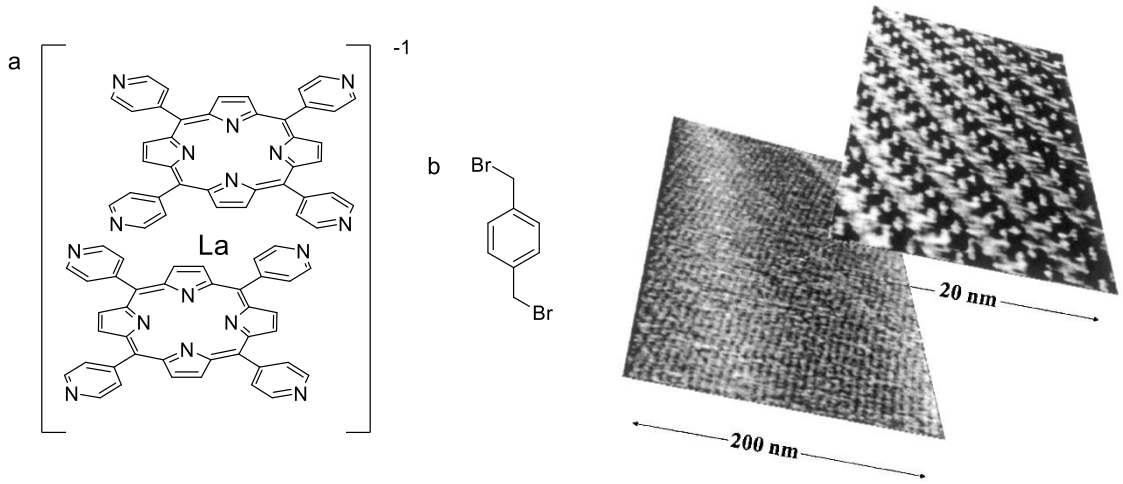

Figure 1.15 Lanthanum sandwich 2DP: Lanthanum-tetrapyridylporphyrin complexes (a). Para-xylene dibromide linear linker (b). Michl's AFM image of resulting 2DP transferred onto HOPG (c).

Another synthesis of a 2DP at the air/liquid interface is poly(antrip-DEG) reported by King group.[51] The King group utilized a light initiated (365 nm) [4+4] photopolymerization on the air/water interface of antrip-DEG monomer. Antrip-DEG monomer is rigid, amphiphilic and consists of three anthraceno blades organized on a central triptycene core with a polar diethylene glycol tail at one bridgehead acting as an anchor when deposited on the air/water interface. The resulting 2DP was successfully transferred onto SiO_2 and HOPG for structural elucidation, confirming hexagonal packing observed by XRD in the crystal packing.

Preparing 2DPs at the air/water interface offers benefits that each previously discussed techniques lack. These benefits include mild reaction conditions, large area films (as large as the trough) and there is no need for exfoliations and fishing out monolayers from a solution of different layered films. Compression of monomers at the water interface forces intermolecular alignment, pre-organizing the monomers into a periodic domain which spans the surface between the barriers. After polymerization occurs, this newly formed 2DP can be effectively transferred off the air/water interface for desired applications.

1.4.4 General Trough Operations

A monolayer is deposited at the air-water interface, usually by dropping a solution target molecule in the center of the trough between two barriers and allowing the solvent to evaporate. Distinct phase changes of the monomer on the waters interface occur upon barrier compression which is compared to a 2D P-V diagram for solid/liquid/gas phase changes. When surface tension is equal to zero, the molecules do not interact with one another and remain in the gaseous state (G). Upon compression, molecules come into contact and share weak intramolecular interactions, at which point they considered to be in an amorphous liquid state (L). At higher surface pressures, the monomers transition into a solid state (S) where the molecules orient in a tightly packed crystal lattice on the surface of the liquid. Phase changes are detected by plotting the area between the barriers vs surface pressure of the liquid upon barrier compression. Extrapolating the slope of the solid phase to a surface pressure of 0 provides the molecules mean molecular area (MMA) for a given solid packing (Figure 1.16).

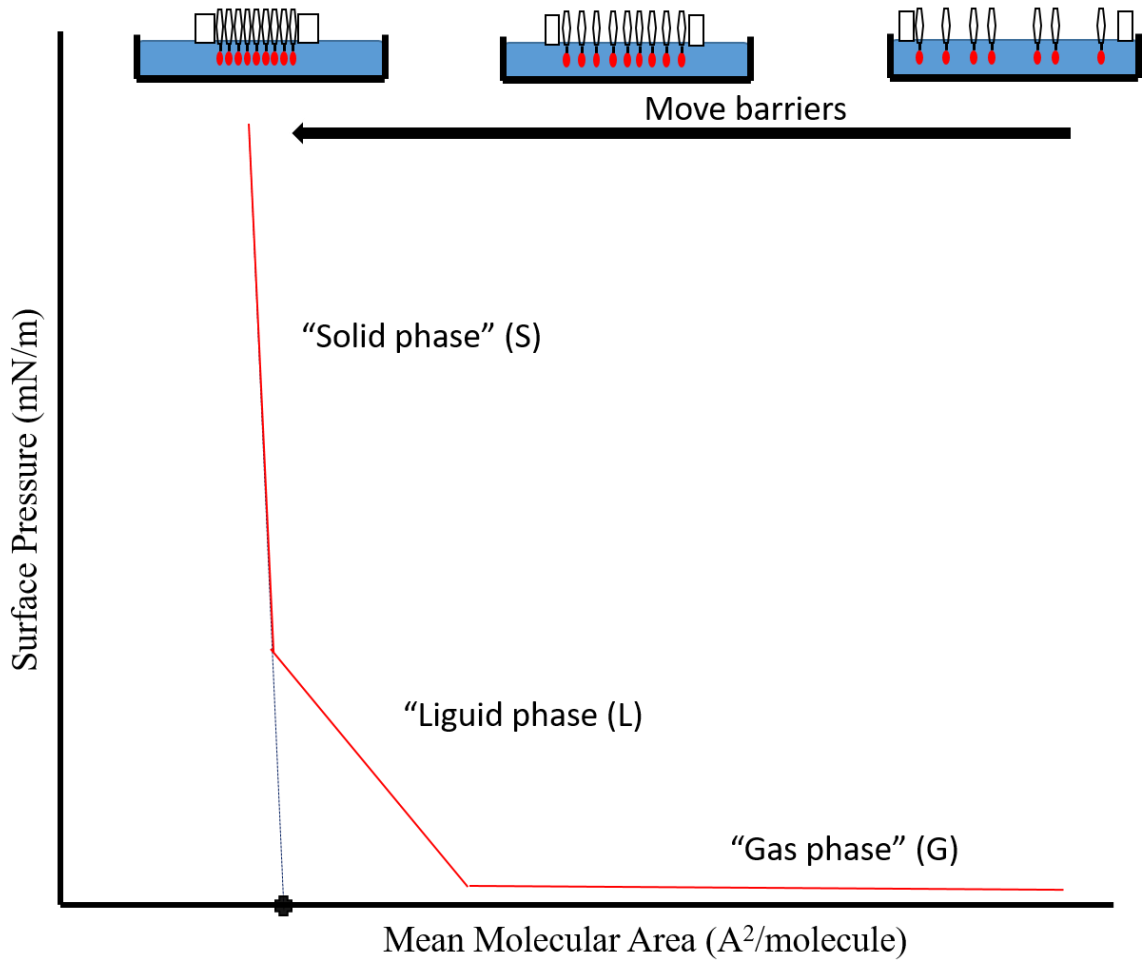

Figure 1.16 Surface pressure diagram: Red line represents surface pressure changing with reduction of area. As trough barriers close, surface pressure raises from gas phase (G), to a liquid phase (L), followed by a solid phase (S). Extrapolating solid phase slope to y= 0 represents the mean molecular area (MMA) of the monomer.

Multiple dipping techniques have been developed to transfer films to solid substrates from the air-water interface, including Langmuir-Blodgett (vertical), and Langmuir-Schaefer (horizontal). Each of these methods can be done either by emersion

(retraction or upstroke) or immersion (dipping or downstroke) (Figure 1.17). Dipping techniques determine the films orientation when transferred onto the substrate and can be chosen per application.

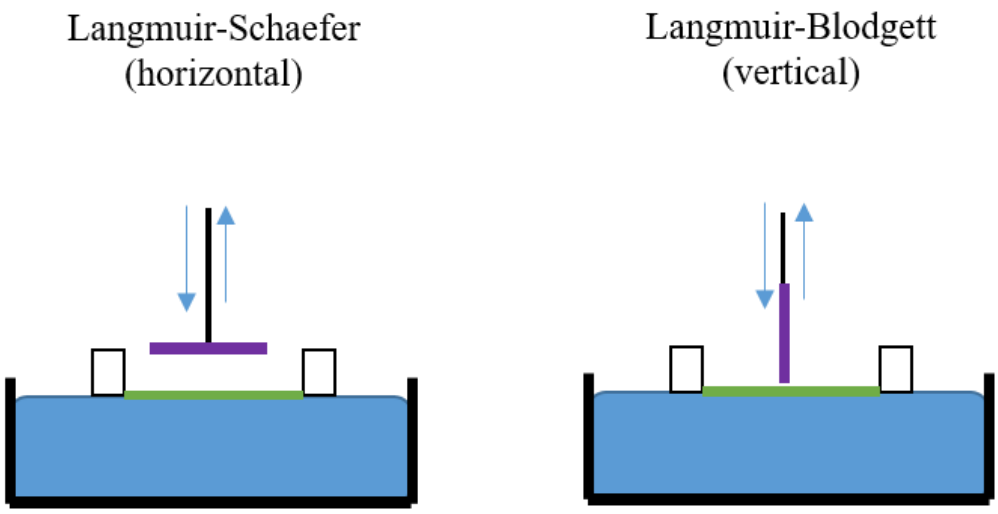

Figure 1.17 Langmuir deposition techniques: Left represents emersion or immersion of a horizontal substrate and right represents emersion or immersion of a vertical substrate.

1.5 Functionalized Surfaces

2DPs are composed of periodic repeat units that offer control over size and shape of the 2DP, piquing interest for use as a scaffold for predictable surface modifications. If a functional group is installed on the repeat unit, the resulting 2DP will contain a highly ordered surface containing a reactive tether on each monomer. Modification of the functional group can be performed post polymerization on the surface of a transferred film. This reactive tune-ability is intriguing in specific areas including molecular bio sensors, spin coupled electronics, and tailoring poor size for exclusion membranes. Chapter 3 of

this dissertation will focus on post modification of my target polymer poly(carboxy fantrip).

1.6 Anthracene and its Dimer

Anthracene is a molecule consisting of three linearly fused benzene rings discovered by French chemists, Dumas and Laurent while distilling coal tar in 1832.[52] Anthracene is cheap and abundant, proving a desirable starting material for organic synthesis and polymer crosslinking. Anthracene is uniquely suited for cross-linking, as the reaction is easily triggered by photoirradiation, stereospecific, clean, and does not form byproducts.

The earliest recorded photodimerization was of anthracene, discovered by the precipitation of the dimer adduct in solution in 1867 by Fritzsche.[53] This discovery occurred when Fritsch left a solution of anthracene in benzene in contact with sunlight and small, insoluble crystals formed on the glass container. He also observed that heating the crystal past its melting point regenerated the soluble starting material.

Anthracene is an economic starting material for synthesizing higher ordered acenes and their dimers, as its reactivity lends itself to symmetrical dimerization explained through Clar aromatic sextets.[52,54–56] Clar's rule states that the greatest local aromaticity will lie in the resonance structure with the highest number of disjointed aromatic π-sextets. For example, phenanthrene and anthracene both possess 14-π electrons but their local resonance is held in different areas of the molecule. Phenanthrene's greatest Clar sextet resides in resonance structure in the bottom left of figure 1.18. In contrast, anthracene displays a delocalization of one disjointed aromatic π-sextet throughout the system.

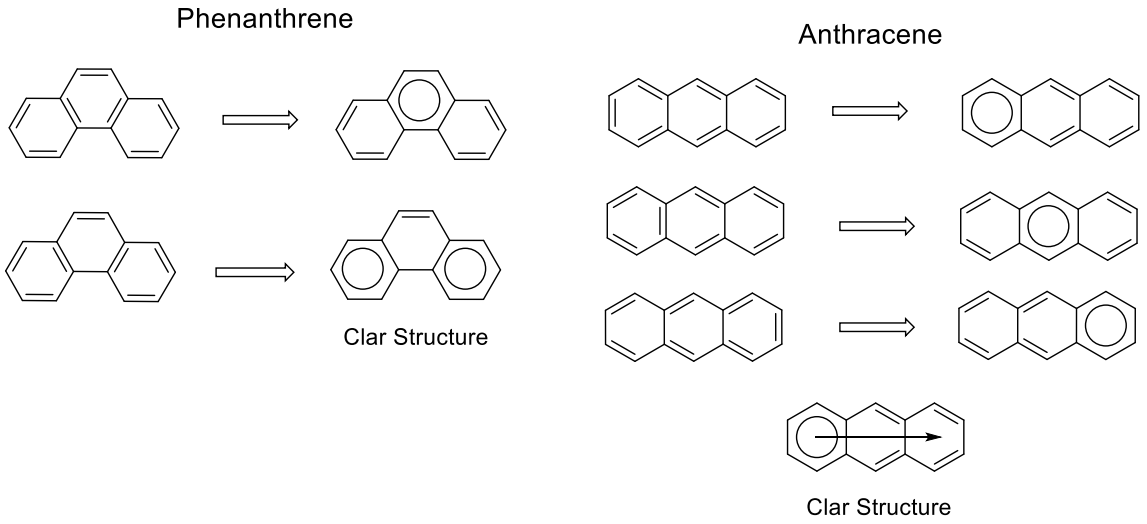

Figure 1.18 Migrating Clar sextets: Resonance structures of phenanthrene (left) and anthracene (right).

Despite anthracene exhibiting a migrating Clar sextet, its photoreactive sites are explicit to the 9,10-position. This is a result of maximizing Clar sextets within the resulting dimer, thus having the greatest aromatic delocalization as shown in figure 1.18. The dimer is a photoadduct of two anthracene monomers reacting through a [4+4] cycloaddition with 365 nm light. The dimerization is thermally reversible and photochemically reversible with high energy light (> 270 nm), reverting the dimer to its respective anthracene monomers (Figure 1.19).

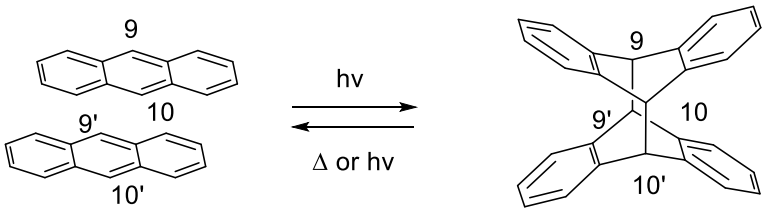

Figure 1.19 Dimerization of anthracene: Light induced [4+4] photopolymerization of anthracene (left), dimer unit exclusively at the 9,10 position (right).

The dimerization of anthracene for use as a cross-linker in the assembly of 2DPs is attractive for a few reasons. The excited state of the anthracene monomer does not undergo conformational change, allowing for pre-organized networks of anthracene monomers to retain shape during polymerization.[57,58] Another compelling characteristic is anthracenes reactivity being limited to only the medial 9,10 position, thereby installing a high degree of order in the polymerized product. Lastly, the void space of two monomers is close to the dimer adduct, as result, a pre-organized 2D network of anthracene monomers have a similar mean molecular area to the dimer adduct, allowing for minimal contraction which reduces network disruption during the polymerization process. Perhaps the most enticing characteristic is that the photodimerization is quantitative, offering no side products and needs no catalysts or reagents. These characteristics lead to highly ordered large domains of molecular thin sheets with minimal defects.

1.7 Antrip and Fantrip Monomer

Swager and Long first reported a triptycene based molecule containing three-fold anthracene blades (Figure 1.20)[59] for use as a molecular anchor in conventional polymers.

Their design was guided by the need to maximizing internal free volume, that is, the void volume around the molecule.

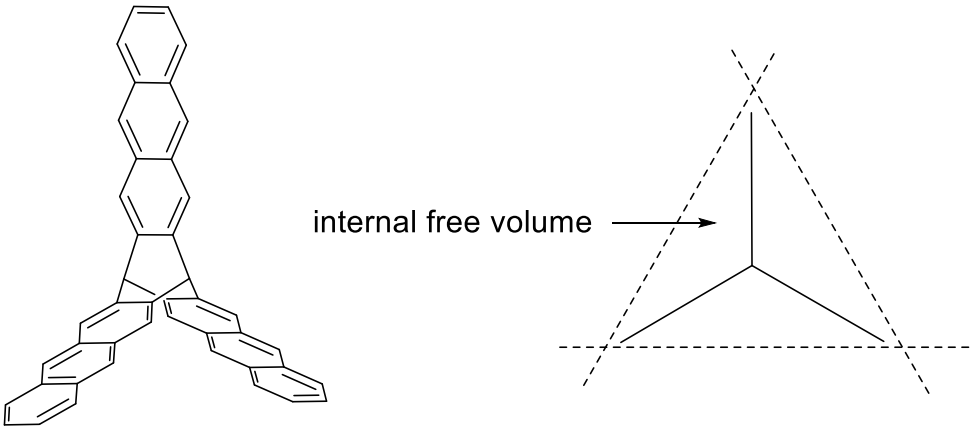

Figure 1.20 Structure of Antrip: A triptycene core with three anthracene extended blades (left). Illustration of internal free volume created by triptycene ridged core (right).

Swager successfully synthesized this molecule, through Friedel-Crafts alkylation of triptycene with phthalic anhydride to give the corresponding tris-ketoacid.[59] The acid adduct was cyclized with sulfuric acid and the anthraquinone adduct with reduced using aluminum amalgam (Al-$HgCl_2$). After silica chromatography and recrystallization, they reported antrip product in very low yields (2.3 %).

The King group utilized this strategy to synthesize antrip in an attempt to create a 2DP through a single-crystal approach, but was found to be unsuccessful in reproducing Swager's synthesis. Dr. Bhola and Dr. Patterson employed modifications to Swager's harsh synthesis and obtained antrip product in similar yields.[38] During Friedel-Crafts cyclization, non-linear regioisomers are formed by free rotation of the tris-ketoacid starting material. This established the main cause of the poor yields (Figure 1.21). In order to increase the

efficiency of this synthesis, the King group took a different synthetic approach to eliminate the unwanted regioisomers.

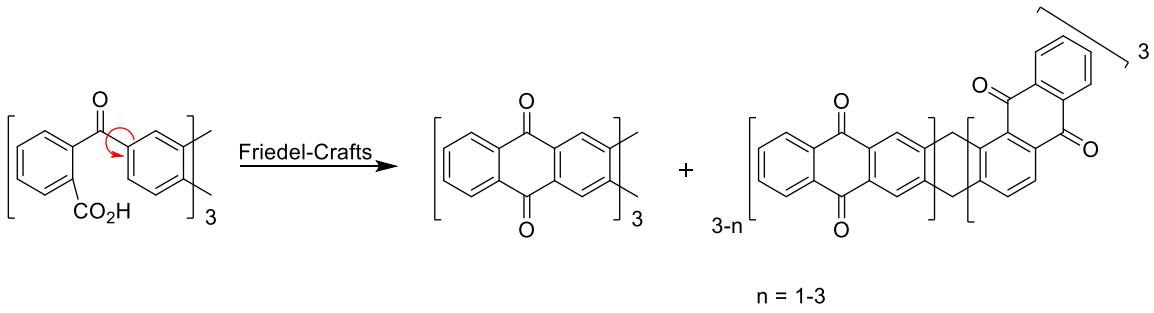

Figure 1.21 Friedel-Crafts antrip route: Tris-ketoacid with red arrow depicting free rotation around acyl bond (left). Two possible regioisomers formed in the cyclization, antrip precursor (middle) and non-linear side product (left).

Dr. King and coworkers developed a Diels-Alder cycloaddition route using a hexabrominated triptycene dienophile precursor trapped with N-methyl-isoindole (Figure 1.22), a strategy pioneered by Gribble.[37,60] The benzyne intermediate generated by lithium-halogen exchange and subsequent LiBr elimination does not have the possibility of non-linear acene products. This synthetic strategy eliminated the possibility of non-linear acene homologation which plagued the Friedel-Crafts reaction.

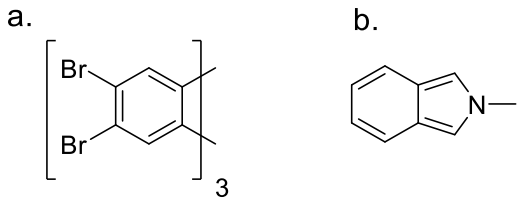

Figure 1.22 Diels-Alder cycloaddition starting materials: Hexabrominated triptycene (a), isoindole (b)

Dr. King's benzyne synthetic route took inspiration from Gribble's (1985) when ortho-dihalogenated benzene was submitted to alkyl halide conditions which underwent lithium-halogen exchange and elimination, forming the benzyne in situ and was trapped by isoindole forming an amine-bridged acene intermediate which was cheletropically eliminated using meta-chloroperoxybenzoic acid (mCPBA) to establish the anthracene motif.[60]

Chapter 2: Synthesis of Carboxy Fantrip

2.1 Previous Synthetic Routes to Antrip Fantrip

The first synthetic route to antrip and fantrip monomers lacked scalability, rendering milligrams of final product. While this route was low yielding, sufficient quantities were isolated to demonstrate that stable macromolecular 2DP sheets are in fact possible with this three-fold scaffold using a crystal approach. The first successful synthesis was of antrip, an un-functionalized triptycene core containing three anthracene extended blades (Figure 2.1).[38,59] These low yielding reactions were satisfactory to demonstrate the viability of the single-crystal approach to 2DPs, but sheet size was limited to the size of the crystal grown. This size constraint shifted the synthetic focus to a monomer that could be polymerized by pre-organizing a monolayer of monomers at the air/water interface. The lateral dimensions of 2D polymers using the air/water interface approach is limited only by the size of the interface. It is noteworty that much less monomer is needed when polymerized on the air/water interface compared to a crystal approach. For example, one hundred milligrams of fantrip monomer, when polymerized as a single monolayer on the air/water interface, would cover 114 m^2. The same amount of monomer used in the crystal approach would only yield sheet sizes as large as a crystal grown in solution, dramatically reducing easy access to large sheets.

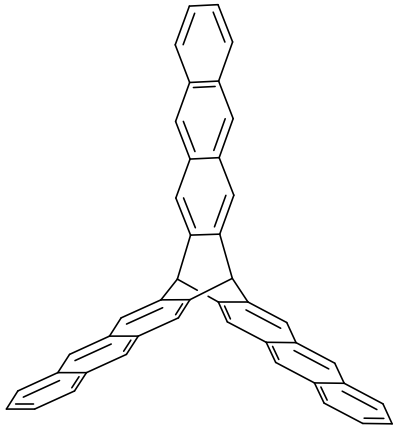

Figure 2.1 Illustration of antrip: A Y shaped two dimensional monomer.

The new target molecule required redesign to float on the air/water interface to allow for intramolecular blade alignment to facilitate photo-polymerization. The first 2DP scaffold introduced on the air/water interface was antrip-DEG, synthesized by former King group members, R. Bhola and D. Patterson. As before, the the rigid three-fold bicyclic anthracene core provides the same three-fold symmetry of fantrip, but the polar DEG group allows the monomer to correctly float on the air/water interface, to facilitate 2D crystal packing. A diethylene glycol tail on one bridgehead offers a polar anchor that enables the monomer to pre-organize and ultimately polymerize on the air/water interface. Once photo-polymerized, the resulting 2DP is periodic and has a high pore density, thereby confirming a three-fold motif is possible when polymerizing on the water's surface.

The group was led away from antrip-deg due a challenging synthesis of the DEG functionalization due to the hindered 9-OH on the antrip core. Additionally, antrip was found to pack poorly on the air/water interface, leading to challenging transfers onto multiple substrates including TEM grids and SiO_2 wafers. Pristine transferred film was no

larger than 1mm^2. Lack of large-scale transfers, in combination with very poor monomer yields, led the group to find an antrip analog to alleviate these issues.

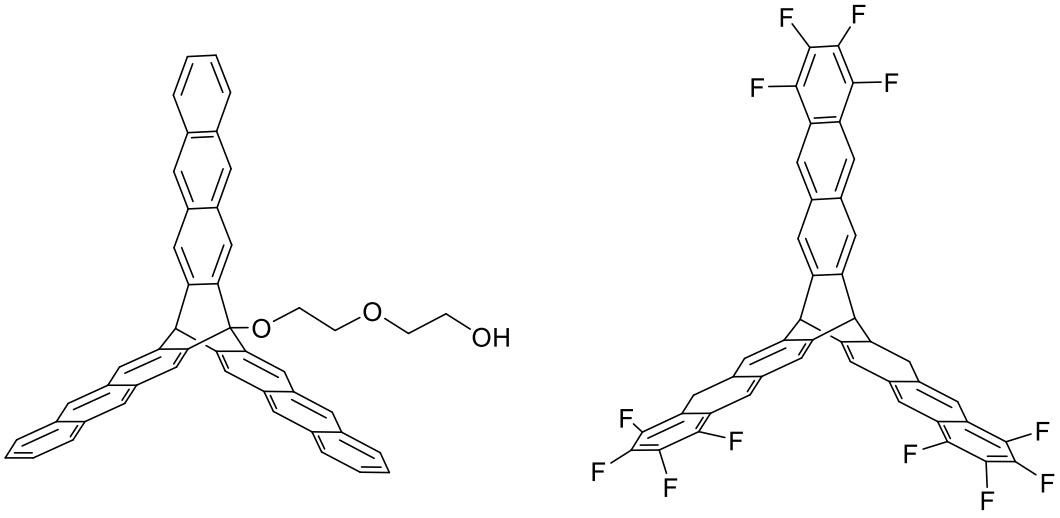

Figure 2.2 Antrip-deg (left), fantrip (right)

A fluorinated analog of antrip, fantrip, was targeted for two main reasons. Firstly, fantrip avoided an unstable intermediate in antrip synthesis, N-methylisoindole, which degrades within hours. This instability greatly limits the amount of product to be made at one time. Tetrafluoroisoindole, however, is much more stable than its nonfluorinated analog (Figure 2.3).

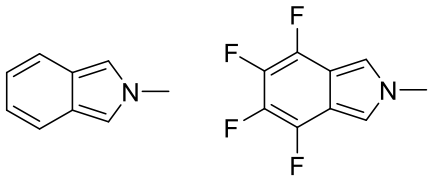

Figure 2.3 N-methylisoindole (left), and tetrafluoro-isoindol (right)

The use of tetrafluoro-N-methylisoindole has two added benefits for the fabrication of this trifold 2DP. The fluorinated isoindole was more robust and could be sublimed and then stored for long periods (years) under ambient conditions, enabling reactions in larger scales. Secondly, the resulting fluorinated anthracene is known to promote the essential cofacial, antiparallel arrangement that facilitates lateral polymerization through intermolecular photocyloadditions (Figure 2.4).

The packing arrangements of benzene and small acenes tend to align parallel-displaced, or edge-to-face when forming a crystal lattice.[61] This arrangement is not useful for photo-polymerization of anthracene due to the distant proximity of neighboring 9,10-positions (medial) which participate in the [4+4] Diels-Alder cycloaddition. Promoting cofacial pi-pi stacking is important to align the medial positions of intramolecular anthracene blades to promote the Diels-Alder reaction. The induced dipole moment on end-fluorinated acenes are observed to pack co-facial and antiparallel.[24,62] Fantrip utilizes fluorine substituents on the outer rims of its three anthraceno blades that induce antiparallel packing of neighboring anthaceno arms facilitating [4+4] cycloaddition (Figure 2.4).

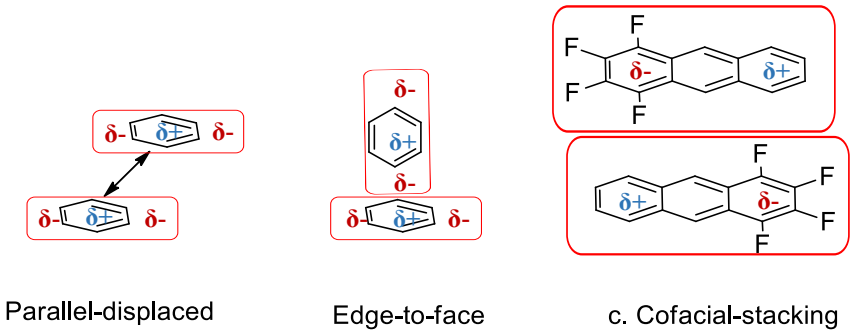

Figure 2.4 Intramolecular stacking: Different arrangements governed by dipole moments.

Dr. Kissel's single crystal polymerization to 2DPs approach laid the synthetic groundwork to the fantrip monomer.[39] His three-step synthetic route resulted in an overall yield of 0.9% for a total of 11 mg. These results were improved by Dr. Thompson who rendered yields of 16% overall with 1.13 g of fantrip monomer. A triple benzyne between hexabromo triptycene and isoindole resulted in the three anthracene blades creating the Y shape monomer (Figure 2.5).

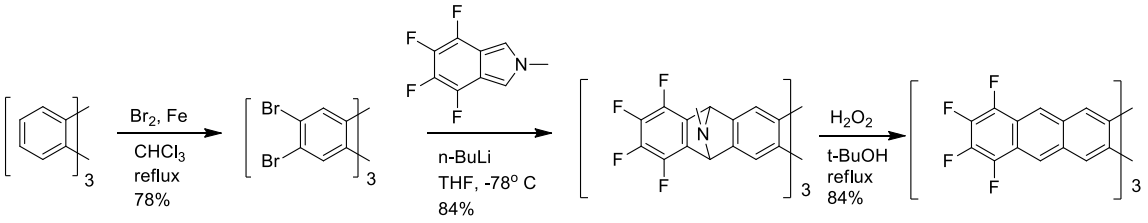

Figure 2.5 Fantrip Synthesis: Optimized three step synthetic route achieved by Dr. Thompson.

Proper monomer alignment on the air/water interface is critical for photopolymerization. A polar anchor must be fitted on the fantrip monomer to facilitate this alignment. Installation of a DEG bridgehead could suffice but lacks reactivity to post-functionalize the resulting polymer once transferred on a surface. Carboxy fantrip was the functional group chosen to serve as both an anchor on the air/water interface and as a reactive end for post functionalization work. The analogous triptycene bearing a bridgehead COOH group (and without the extended anthracene blades) has been reported to form Langmuir-Blodgett films at the air-water interface.[63] Self assembled monolayers containing terminal carboxylic acid functionality are also reported in the literature for reactivity towards nucleophiles forming esters and amides in high yields.[64]

The synthetic groundwork of carboxy fantrip was further advanced by King Group member, Dr. Thompson. While this original work was a successful route to carboxy fantrip, monomer yields were in the tens of milligrams and required to intensive chromatography work and preparative high-performance liquid chromatography (HPLC). My contribution to the synthetic route notably increased yields from milligrams to hundreds of milligrams. This was accomplished by two different methods. Optimizing the synthetic route greatly improved yields and avoided all time consuming preparative HPLC work. And by innovating a new synthetic route which utilized a lower bridgehead oxidation state, isolating carboxy fantrip in better yields and offering additional bridgehead functionality. The lower oxidation state was hypothesized to avoid a ring opening rearrangement of the triptycene core speculated to be the cause of the low yields. This method was developed as a secondary route to carboxy fantrip. Additionally, fantrip carbinol offers new functionality previously unexplored.

2.2 Optimization to the Synthesis of Carboxy Fantrip

The optimization of carboxy fantrip from former yields of a few milligrams to hundreds of milligrams is paramount for use in applications. Prior to my optimizations, our group was left with no backstock monomer, creating a bottleneck in polymerizations and transfers. It also eliminated the chance of shipping material to collaborators on a consistent basis to broaden the scope of possible applications. This section addresses key issues and resolutions to greatly improve the yields of carboxy fantrip.

The triptycene blades were homologated to the tetrafluoroanthraceno blades via the Diels-Alder cycloaddition reaction of an aryne with tetrafluoroisoindole. The arynes,

which reacted as they were formed, were obtained by the lithium-halogen exchange and subsequent elimination of LiBr. Oxidation of the resulting tertiary amines induced chelotropic elimination of ONMe and concomitant aromization (Figure 2.6).

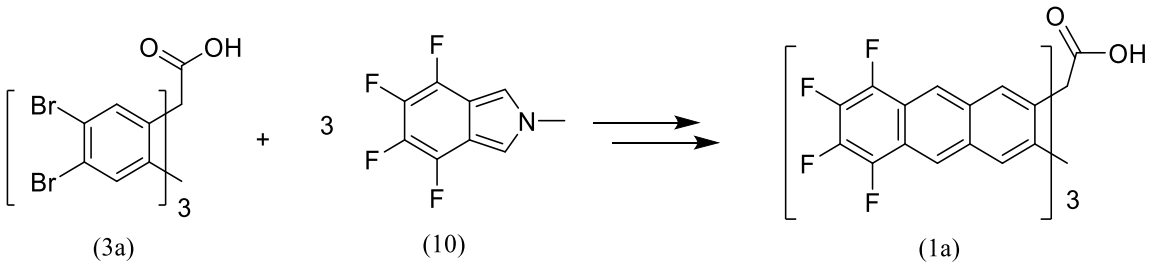

(3a) (10) (1a)

Figure 2.6 Triple Diels-Alder cycloaddition: Acene homologation step forming the carboxy fantrip core using carboxy hexabromotriptycene and fluorinated isoindole.

Carboxy substituted hexabromotriptycene (**3a**) and tetrafluoro-isoindole (**10**) were synthesized through previously developed methodology, but these preparation required optimization to provide safer conditions and increase yields as explained in Section 2.5.

2.2.1 Synthesis of Carboxy Hexabromo Triptycene

Bridgehead functionalization was introduced early in the synthesis by using 9-substituted anthracene as a starting material. A multitude of 9-substituted triptycene motifs have been reported in the literature, thus offering different bridgehead functionality depending on specific applications.[65,66]

The synthetic route towards carboxy fantrip begins with economic, readily available acetal-protected 9-anthraldehyde (**8**) and undergoes a [2+4] Diels-Alder cycloaddition with benzyne, generated in situ from the diazotization of anthranilic acid (**9**) (Figure 2.7).

It is worthy to note that, during this reaction, two moles of gas are released for every one mole of anthranilic acid. A diazotization—decarboxylation takes place when the amine of anthranilic acid reacts with a nitrosonium ion of isoamyl nitrite to form a diazonium salt. Elimination of both N_2 (g) and CO_2 (g) produce benzyne *in situ* which is quickly trapped by anthracene forming the triptycene core. Careful consideration of reaction size, temperature, and addition of anthranilic acid must be in place to avoid unmanageable pressure release. An optimized procedure is reported in the experimental section of this chapter.[67]

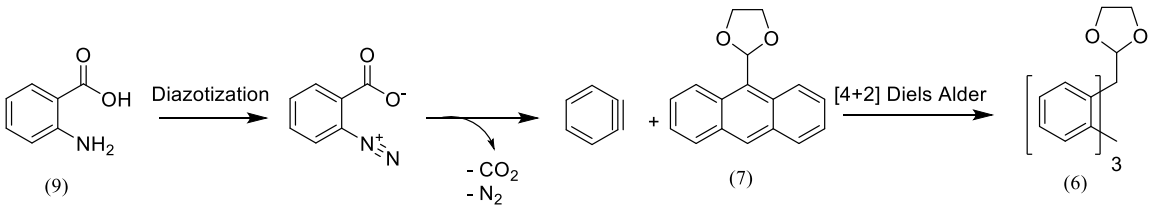

Figure 2.7 Synthesis of 9-substituted triptycene: Diazotization-decarboxylation of anthranilic acid forming reactive intermediate benzyne trapped with 9-acetal protected anthracene.

The Diels-Alder cycloaddition reactivity of anthracenes is sensitive to the functionality, especially at the 9 and 10 positions.[68] Additional considerations regarding this Diels-Alder cycloaddition sequence is the lack in reactivity of specific substituted anthracenes. Unprotected 9-anthraldehyde and the analogous carbinol are not reactive in the [2+4] Diels-Alder cycloaddition reaction. Acetal protection is necessary for the Diels-Alder cycloaddition reaction to proceed affording a triptycene core (Figure 2.8).

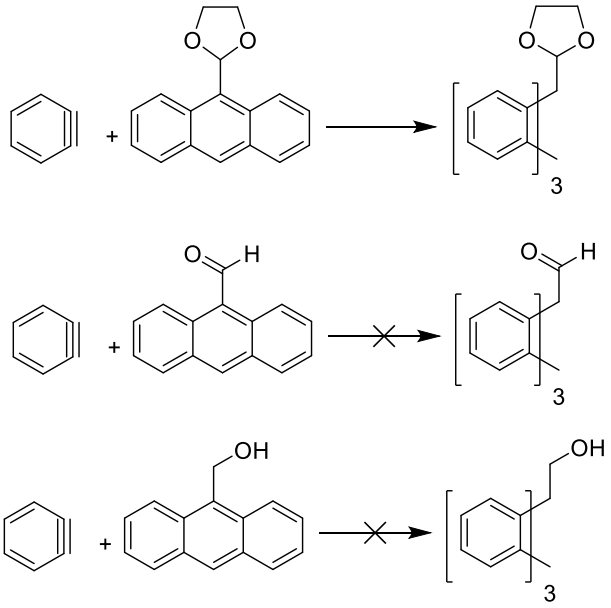

Figure 2.8 Reactivity of triptycene: 9-acetal protected anthracene (top), 9-Anthraldehyde (middle), and 9-anthracene carbinol (bottom).

The product from the Diels-Alder cycloaddition reaction, the acetal-protected triptycene-9-carbaldehyde (**6**), was easily deprotected with HCl in glacial acetic acid to afford 9-triptycene carbaldehyde. A simple water wash gave pure product. The aldehyde oxidized under Jones conditions resulting in the corresponding carboxylic acid.[69]

A recurring theme in these optimization reactions was the propensity of the triptycenes to occlude solvent of crystallization, and those occluded solvents interfered with subsequent reactions. Vacuum drying at elevated temperature (100 °C) was necessary to remove these occluded solvents, as other methods including concentrating under reduced pressure and high vacuum at room temperature did not suffice.

Bromination of carboxy triptycene proved challenging following previously reported experimental methods having inconsistent yields (10-65%). The progress of the reaction was monitored by ^{1}H NMR, and this enabled the reproducible preparation of hexabromocarboxytriptycene in acceptable yield. In particular, avoiding over-bromination is essential, as the over-brominated products are difficult to separate. Bromination of the distal carbons on the carboxy triptycene is done by reacting Br_2 and elemental iron in an electrophilic aromatic substitution type reaction. During bromination, reaction progression was monitored closely by ^{1}H NMR to avoid an inseparable over-brominated product. By monitoring the disappearance of many under brominated bridgeheads (5.43-5.19 ppm) and aromatic (7.00-8.20 ppm) signals between the 1-8th aliquots of the ^{1}H NMR allowed the reaction to halt before over bromination occurs (Figure 2.9). Key indications of a completed reaction is indicative of the elimination of multiple bridgeheads in the reaction mixture. Aliquot eight is reminiscent of the reaction entering completion with no observed over-brominated material present. The single bridgehead at 5.19 ppm and two aromatic signals at 7.64 and 8.06 ppm account for all protons, signaling for the reaction to be halted (Figure 2.9).

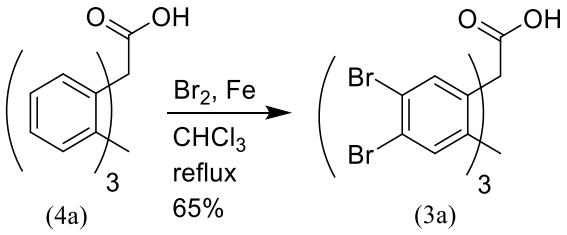

Figure 2.9 Bromination of carboxy triptycene.

Purification of this adduct can be simplified from previously reported methods by concentrating the reaction mixture under reduced pressure, then by running the resulting brown oil through a silica plug with THF. The concentrated material is a brown/tan powder which can easily be triturated with acetone multiple times until a white powder remains. The solubility of the product is poor in $CHCl_3$ but very good in DMSO and ethyl acetate. NMR analysis reported in experimental is done in d_3-CDCl3.

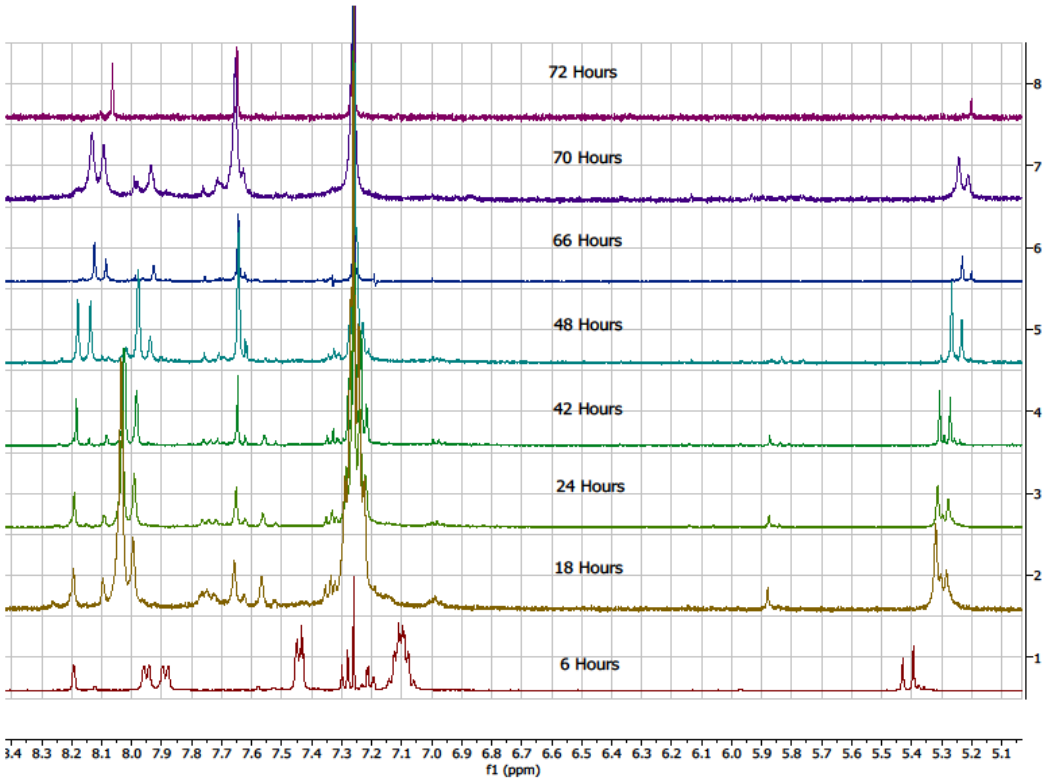

Figure 2.10 Stacked ^{1}H NMR of the progression of bromination in the preparation of carboxy hexabromotriptycene: Bromination of distal aromatic protons monitored as reaction moved forward.

Multiple additions of both Br_2 and elemental iron were required to bring the bromination to completion. Six equivalents of Br_2 are theoretically required for complete bromination, but in practice 11 equivalents were needed. It is still not fully understood why five additional equivalents of bromine is required. Some loss of bromine can possibly be attributed to the bromination of $CHCl_3$, which is used as the solvent. Some other possible reasons is the evaporation of Br_2 from the reaction flask or bromine reacting with amylene (used as a stabilizer in the chloroform). Although these processes account for why the reaction stalls, it does not, however account for the excess of bromine needed to complete the reaction.

2.2.2 Optimization of Triple Diels-Alder Cycloaddition Reaction

After brominating carboxy triptycene, a triple benzyne is generated by using excess tetrafluoroisoindole (**10**) as a diene. This process forms the three anthraceno blades of the monomer precursor (**2a**). The benzyne is produced in situ through lithium-halogen exchange of ortho-dibromides on the distal position of the triptycene dienophile when treated with n-BuLi at -78 °C. The elimination of lithium and bromine results in an aryne intermediate, which is then trapped by tetrafluoroisoindole in a [4+2] regiospecific Diels-Alder cycloaddition reaction. This leads to the formation of the carboxy fantrip precursor (**2a**) (refer to Figure 1.11).

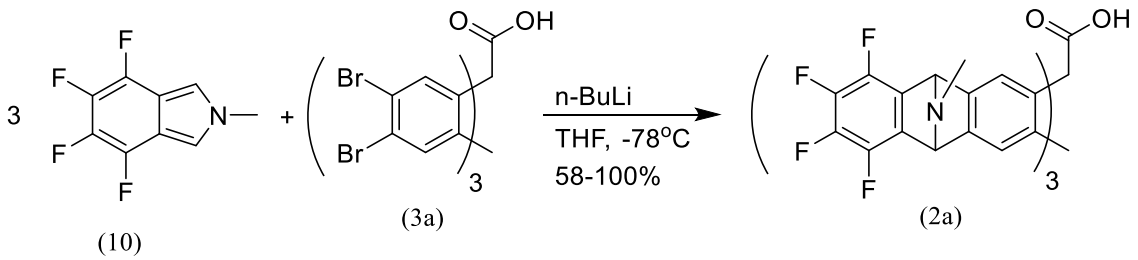

Figure 2.11 Carboxy fantrip precursor synthesis: Triple benzyne between tetrafluoroisoindol and carboxy hexabromotriptycene to generate carboxy fantrip precursor.

The purification of the trifold adduct through chromatography posed significant challenges due to the presence of anti and syn-isomeric conformations and the spontaneous elimination of the N-methyl bridges on the trifold adduct, resulting in poor yields of 25%. To address the broad differences in R_f and prevent material loss, a silica plug was selected to separate excess isoindole, which ran with the solvent front from the reaction mixture (mobile phase dichloromethane). The solvent polarity was increased (mobile phase 90:10 dichloromethane:MeOH) to intentionally extract the baseline off the silica, containing the product.

Acid-base extraction was explored to avoid chromatography. While this method supported the fantrip carbinol procedure, as explained in Section 2.3.2, it proved unsuccessful for the carboxy precursor. Poor recovery was attributed to the carboxylic acid being protonated and deprotonated at opposite times as the tertiary amines.

Considering other factors affecting yields is the dryness and purity of starting materials are crucial. The synthesis of N-methyl tetrafluoroisoindole (**10**) has been reported previously and was synthesized using a modified literature procedure.[70] To prevent

decomposition of the fluorinated isoindole, sublimation becomes necessary. Once sublimed, the compound remains shelf-stable under ambient conditions for years.

Carboxy hexabromotriptycene exhibits a high affinity to trap solvents within the free volume of the molecule. Water, acetic acid, and acetone cannot be removed from the molecule under high vacuum at ambient temperature. Hence, it is necessary to heat the material to 120 °C under vacuum overnight. Any intercalated solvents other than THF will negatively compete with the generated aryne. Solvent exchange is crucial as a final step to ensure any intercalated solvents from previous steps have been removed from the reaction mixture. This is achieved by dissolving the reaction mixture in freshly distilled THF and concentrating it under reduced pressure a minimum of three times before initiating the reaction.

2.2.3 Optimization of Cheletropic Elimination

The establishment of the anthracene blades is achieved through cheletropic elimination of the N-methyl bridges on the trifold adduct. Several oxidants were tested to induce elimination, including benzyltriethylammonium chloride and a sodium hydroxide solution, both of which resulted in trifold in poor yields. Alternative attempts using meta-chloroperoxybenzoic acid (mCPBA), as originally reported by Gribble (1985), showed effective elimination, but the method led to a cumbersome separation of the monomer and mCPBA or its reduced byproduct.[60]

Another approach involved the use of dimethyldioxirane (DMDO), which was prepared by treating acetone with potassium peroxymonosulfate ($KHSO_5$) in the form of Oxone. While this method provided fair yields, the preparation of DMDO was deemed

impractical, and the inherent instability of DMDO required fresh preparation for each reaction.

Hydrogen peroxide (H_2O_2) proved to be the most effective choice, offering the best results in terms of ease of use and overall yields. The N-methyl elimination of (**2a**) proceeded smoothly, eliminating the need for demanding purification of carboxy fantrip. This optimization significantly increased the yield from the initial 1-2% to an improved 23% (refer to Figure 2.12). Hydrogen peroxide generates the N-oxide, which then eliminates nitrosomethane (H3CNO), an octet satisfied species that leaves the reaction as a gas.

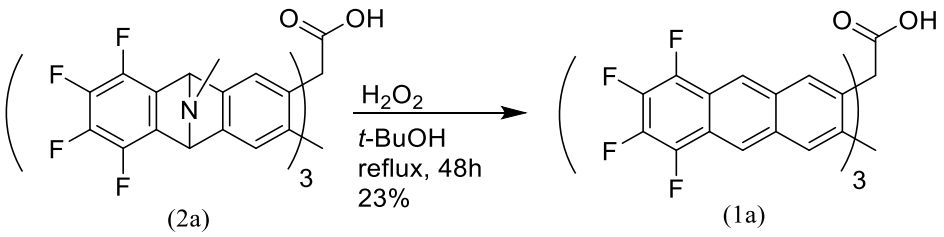

Figure 2.12 Cheletropic elimination: Synthesis of carboxy fantrip from precursor. Bicyclic nitrogen bridgeheads eliminate to establish anthracene aromaticity.

The isomeric mixture obtained from the triple aryne/Diels-Alder cycloaddition reaction is extracted from the silica plug baseline. The resulting oil is dissolved in tert-butyl alcohol (*t*-BuOH), to which hydrogen peroxide is added at reflux to cleave the N-methyl bridgeheads on (**2a**), establishing aromaticity. However, the reaction progression tends to slow over the course of five hours, and additional H_2O_2 is required to bring the reaction to completion. Monitoring the reaction progress is easily achieved through TLC, but it is crucial to consider that all *t*-BuOH must be evaporated before running the TLC plate. This

step is essential to prevent the reaction mixture from moving with the solvent front during TLC analysis (mobile phase: 7:3 EtOAc:Hex with 0.1% AcOH).

The workup of carboxy fantrip becomes challenging at this step due to its limited solubility in many organic solvents and its propensity to remain dissolved in water. Ethyl acetate has proven to be the most effective solvent for extraction. To prevent emulsion during aqueous extraction, it is advisable to remove *t*-BuOH by vacuum evaporation before proceeding with the workup. After the removal of *t*-BuOH from the reaction mixture, water is added, followed by extraction with ethyl acetate three times or until the extracted organic phase shows no presence of the product as indicated by TLC.

Efforts were undertaken to minimize the use of silica in order to enhance yields. However, the extracted powder exhibited a dark brown color upon recrystallization in various solvents, including $CHCl_3$, CH_2Cl_2, acetone, THF, and numerous solvent mixtures. Recrystallization of the crude product proved challenging, necessitating an alternative approach. The crude product must be run through a silica column covered in foil, conducted in the absence of light to prevent dimerization. TLC conditions (mobile phase: 7:3 EtOAc:Hex with 0.1% AcOH) are employed to monitor the separation process.

After the top three bands elute and are combined, the resulting mixture is concentrated under reduced pressure and high vacuum. The resulting solid is subjected to recrystallization from chloroform (10 mL) at –18 °C, followed by trituration in chloroform multiple times. This process yields carboxy fantrip monomer as a pale yellow/white solid. It is recommended to store the solid away from light at –20 °C.

Despite obtaining a relatively pure fantrip monomer through these steps, the Langmuir-Blodgett work requires further purification to remove trace impurities and any residual grease that interfere with the formation of monolayers. This purification can be accomplished by transferring 10 mg of the monomer into an NMR tube and performing further trituration with chloroform followed by trituration with HPLC grade pentane.

2.3 Synthesis of Fantrip Carbinol

After encountering low yields in the original synthesis of carboxy fantrip over several years, a new approach was pursued, involving the utilization of fantrip carbinol as a precursor to the target carboxy molecule. The primary goal was to initiate the triple benzyne with a substituted bridgehead featuring a lower oxidation state. This strategic choice aimed to circumvent a hypothesized rearrangement of the triptycene core. Previous literature, particularly from Penelle et al. and Minoura et al., suggested that some triptycene rings can undergo expansion via an anionic ring opening, particularly when the bridgehead is attached to a partial positive carbon.[71,72] This rearrangement phenomenon, while not conclusively characterized with carboxy fantrip, may have been the of lower intermediate yields compared to unfunctionalized and other antrip and fantrip derivatives.

Fantrip carbinol not only provides a pathway to carboxy fantrip but can also be functionalized to yield other derivatives at lower oxidation states, notably via reductive amination via the carbaldehyde. Serving as an alternative route to carboxy fantrip, fantrip carbinol offers the opportunity for additional tether functionality at the monomer level, thereby expanding possibilities for surface modification (refer to Figure 2.13). The

synthetic steps and purification of fantrip carbinol, as well as the preparation of amine tethers, are further discussed in this section.

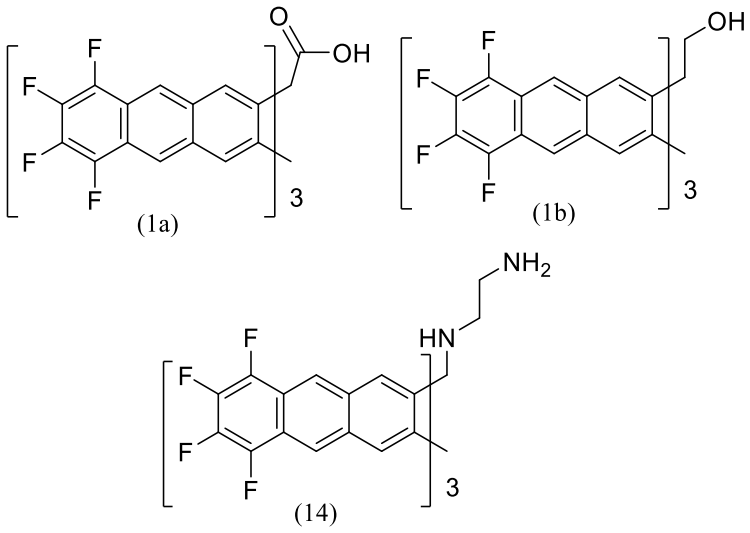

Figure 2.13 Functionalized Fantrip: Carboxy fantrip (left), fantrip carbinol (right) and ethylene diamine fantrip (bottom).

The synthesis of fantrip carbinol and its derivatives follows a parallel pathway to the synthesis of carboxy fantrip monomer. Similar to the process for carboxy fantrip, an benzyne is formed using anthranilic acid, which subsequently reacts with acetal-protected anthracene through a [4+2] Diels-Alder cycloaddition reaction, forming the triptycene core. The acetal triptycene is then deprotected using glacial acetic acid and HCl, resulting in triptycene aldehyde. Subsequently, the aldehyde is reduced using sodium borohydride, converting the aldehyde to a primary methyl alcohol or carbinol (refer to Figure 2.14).

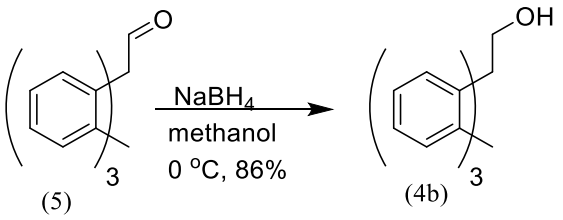

Figure 2.14 Reduction of triptycene aldehyde to triptycene carbinol.

2.3.1 Synthesis of Carboxy Hexabromo Triptycene Carbinol

As outlined in section 2.2.1, the bromination of triptoic acid was found to be more challenging than previously reported. Unfortunately, the bromination of triptycene carbinol presented a similar challenge. Careful monitoring of the reaction progress through ^{1}H NMR allowed for the addition of excess bromine and iron without causing overbromination (refer to Figure 2.15).

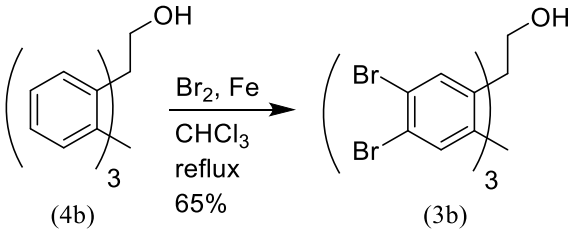

Figure 2.15 Reaction scheme of the bromination of triptycene carbinol: Reaction monitored by ^{1}H NMR to govern equivalents of bromine needed.

Below is a stacked ^{1}H NMR spectra of five aliquots taken during the progress of the reaction (Figure 2.16). The disappearance of signals associated with under-brominated bridgeheads (around 5.2-5.3 ppm) and aromatic signals (7.15-7.26 ppm) between the 1st and 4th aliquots indicates the successful progression of the reaction without over-bromination.

The observation of over-bromination, as indicated by the emergence of a new bridgehead signal at 5.31 ppm in the 5th aliquot, provides a clear indication of the reaction reaching a state of excess bromination. This careful monitoring strategy allows for precise control over the reaction, preventing undesired side products and ensuring the desired level of bromination is achieved.

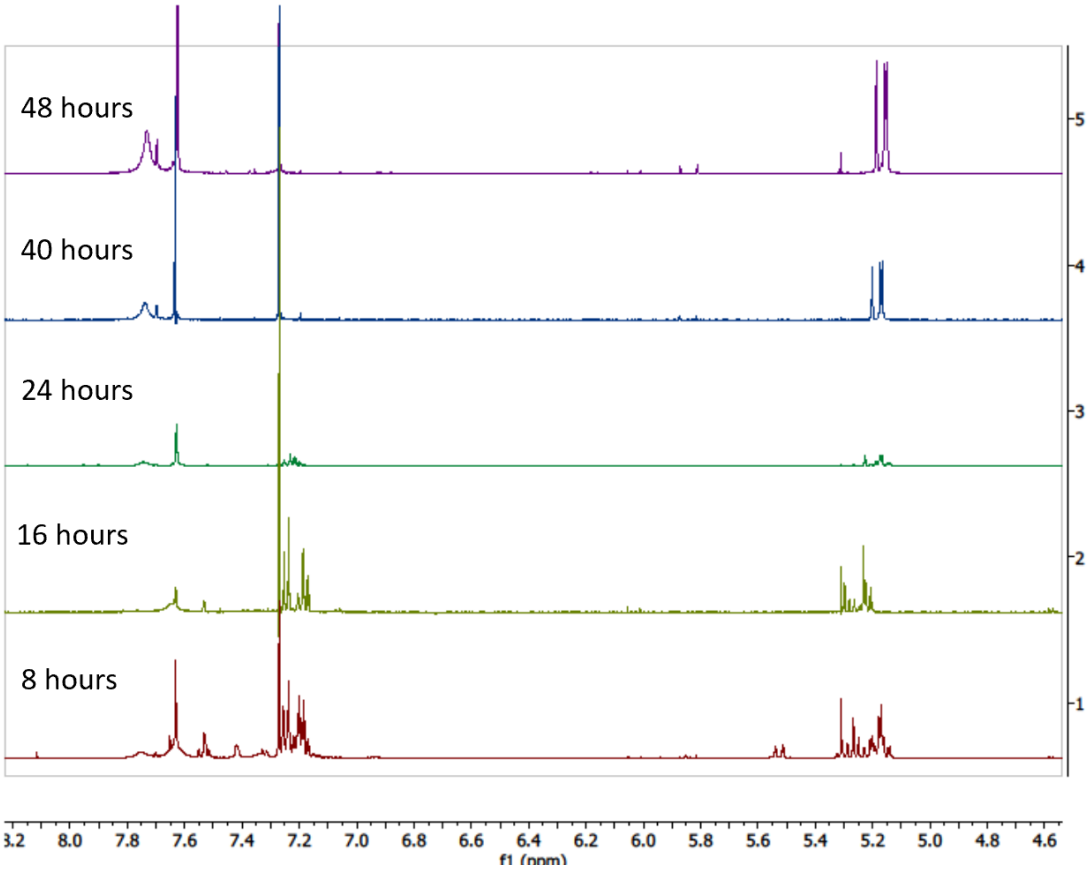

Figure 2.16 Stacked ^{1}H NMR hexabromo triptycene carbinol: Bromination of distal aromatic protons monitored as the reaction moved forward.

2.3.2 Synthesis of Fantrip Carbinol Precursor

In this process, *n*-BuLi generates the aryne in situ through lithium-halogen exchange of bromine and subsequent elimination at –30 °C. It is noteworthy that the reaction temperature significantly enhances the yields of the carbinol adduct. We experimented with temperatures as low as –78 °C but found that they resulted in lower yields. N-Methyltetrafluoroisoindole effectively traps the benzyne generated in this process, forming the trifold adduct (refer to Figure 2.17).

Similar to carboxy fantrip, hexabromo triptycene carbinol exhibits strong solvent retention properties. Water, acetic acid, acetone, CH_2Cl_2, and $CHCl_3$ cannot be effectively removed by vacuum at ambient temperature. Therefore, prior to aryne formation, it is necessary to apply high vacuum at elevated temperatures (110 °C) overnight and conduct solvent exchange with freshly distilled THF to remove any occluded solvents that could interfere with the *n*-BuLi-mediated aryne generation.

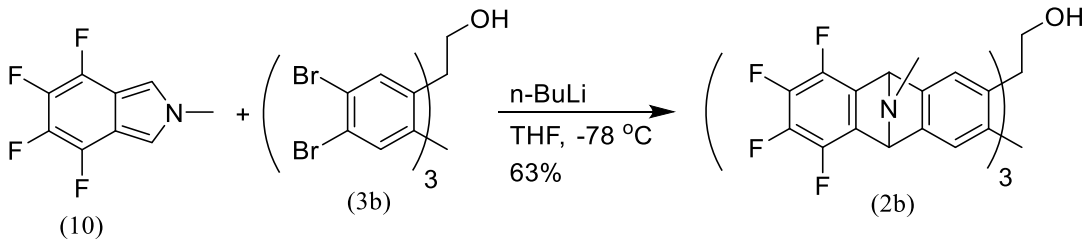

Figure 2.17 Reaction scheme of the triple benzyne: N-Methyltetrafluoroisoindole and the brominated triptycene react in a triple [4+2] Diels-Alder cycloaddition reaction to create the trifold adduct.

Chromatography posed challenges in purifying the trifold adduct due to anti and syn-isomeric confirmations and the spontaneous elimination of the N-methyl bridges on

the trifold adduct. To address the broad differences in R_f, we employed acid-base extraction to extract all stereoisomers. While acid-base extraction proved effective for the carbinol derivative, it did not work well for the carboxy acid analog. This extraction method removed excess N-methyltetrafluoroisoindole. In acidic aqueous conditions, the basic N-methyl bridges are protonated, and the resulting protonated trifold adduct is solubilize in water. Isoindole, on the other hand, is much less basic because protonation would disrupt the aromatic five-membered ring, and it is thus insoluble in acidic water (refer to Figure 2.18).

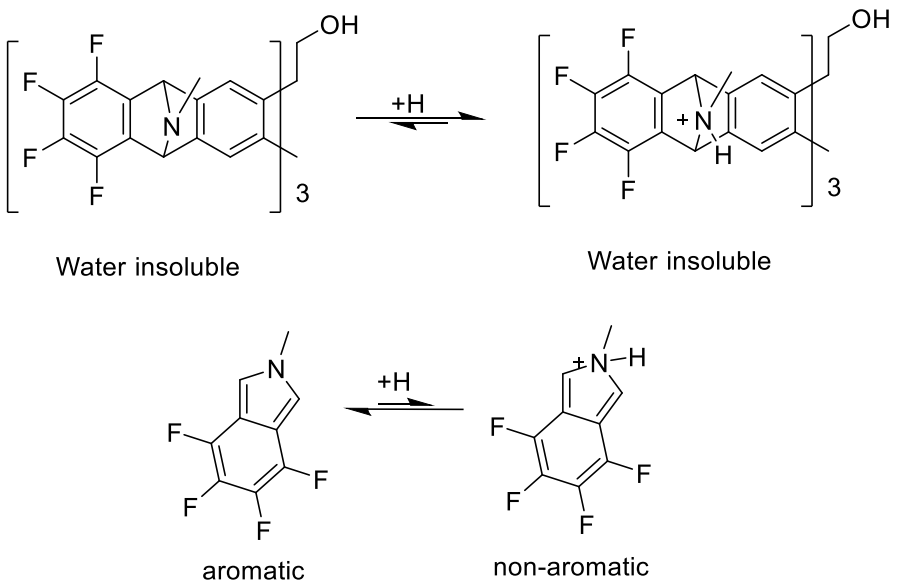

Figure 2.18 Solubility of fantrip precursor: The fantrip precursor's solubility in water is influenced by the protonation of N-methyl bridgeheads on the carboxy fantrip precursor, favoring acidic conditions (top). In contrast, isoindole favors aromaticity, leading to water insolubility (bottom).

2.3.3. Synthesis of Fantrip Carbinol

Elimination of N-methyl bridgeheads establishes aromaticity in the anthracene blades. Similar to the synthesis of carboxy fantrip, numerous oxidants were tested to induce elimination, encountering similar limitations. Benzyltriethylammonium chloride in a sodium hydroxide solution yielded trifold in poor yields (<10%). Aromaticity is introduces when chloroform is deprotonated and undergoes alpha-elimination to generate dichlorcarbene, which adds to the tertiary amines. Cheletropic elimination forms Cl_2CNCH_3, which is eliminated as a gas. Another method of elimination is by using meta-chloroperoxybenzoic acid (m-CPBA) facilitated effective elimination but resulted in a tedious separation of monomer and mCPBA or its reduced byproduct. Hydrogen peroxide (H_2O_2) proved to be the most effective, achieving N-methyl elimination and avoiding demanding purification of the monomer from reagents. This method increased the yield to an average of 41%, with the highest recorded yield reaching 63% over the two steps (the triple Diels-Alder reaction and the cheletropic elimination).

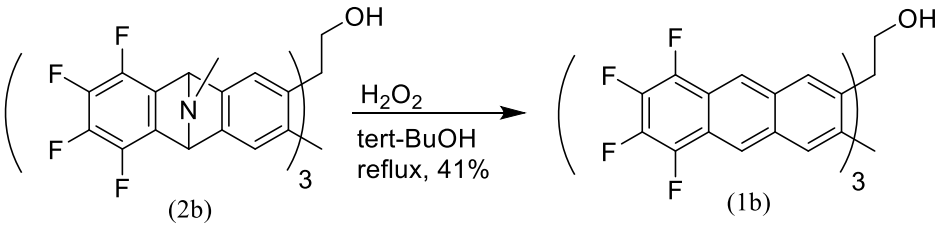

Figure 2.19 Cheletropic Elimination: Reaction scheme of the N-methyl bridgehead elimination affording three aromatic anthracene blades

Purifying fantrip carbinol proved to be easier compared to carboxy fantrip. By ensuring the purity and dryness of the starting materials before the triple benzyne and

carefully monitoring the elimination process with TLC, it becomes possible to completely avoid the use of silica. A straightforward recrystallization from chloroform is sufficient to achieve pure material, confirmed by NMR. In cases where the material doesn't recrystallize after complete dissolution in $CHCl_3$, a simple silica plug run in CH_2Cl_2 typically cleans the material enough to facilitate the crystallization of the product.

2.4 Oxidation of Fantrip Carbinol

Fantrip carbinol was originally synthesized as a secondary, possibly higher yielding route to carboxy fantrip. Initially, late-stage oxidation raised concerns due to the inherently harsh oxidative conditions. To address this transformation, the first reaction explored was a Corey-Schmidt oxidation using pyridinium dichromate (PDC) and dimethylformamide (DMF).[73] Despite attempting various conditions, such as raising the temperature (from room temperature to -50 °C) and using excess equivalents, oxidizing the carbinol proved unsuccessful. No product was formed when monitoring by TLC (refer to Figure 2.20).

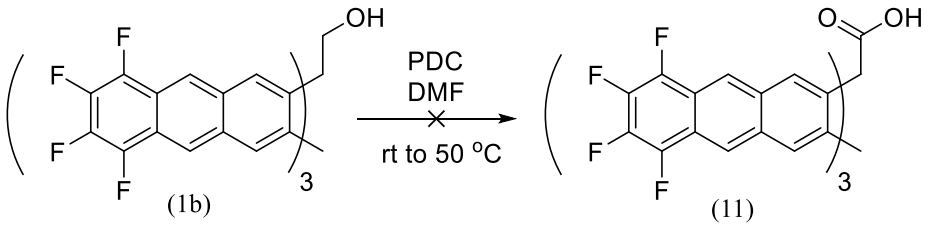

Figure 2.20 Oxidation of fantrip carbinol reaction scheme: Failed attempt using Corey-Schmidt conditions.

Attempts were made to oxidize the carbinol using Jones conditions: chromium trioxide (CrO_3) and sulfuric acid (H_2SO_4) at low temperatures (refer to Figure 2.21). However, the oxidation of the carbinol did not progress, indicated by TLC. Upon raising

the temperature to reflux, multiple polar products were observed through TLC. ^{1}H NMR of the crude material was conducted upon the disappearance of the starting material, revealing the formation of several bridgeheads during the reaction.

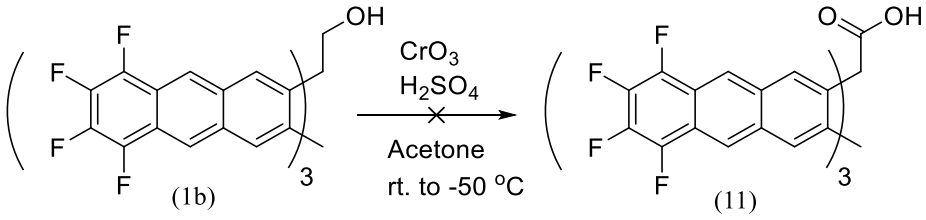

Figure 2. 21 Oxidation of fantrip carbinol reaction scheme: Failed attempt using Jones conditions.

Due to decomposition resulting from the harsh oxidation conditions, a milder approach was deemed necessary. Instead of a single-pot oxidation to the carboxylic acid, a two-step approach was pursued. This involved first oxidizing to the aldehyde and subsequently to the carboxylic acid. Swern conditions were explored using varying equivalents of oxidants and temperatures, but no aldehyde was extracted from the reaction mixture (refer to Figure 2.22).

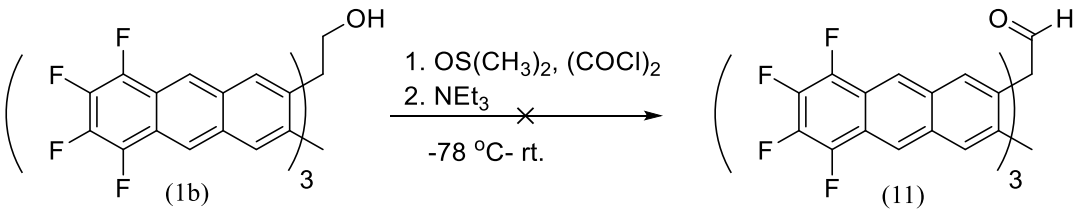

Figure 2.22 Oxidation of fantrip carbinol reaction scheme: Failed attempt using Swern conditions.

Daniel Swern (1976) reported a modified Swern-type reaction.[74] This method involves the reaction of acetic trifluoroacetic anhydride (TFAA) with dimethyl sulfoxide to oxidize primary alcohols to aldehydes through a trifluoroacetoxydimethylsulfonium trifluoroacetate intermediate (refer to Figure 2.23). The dimethylsulfonium intermediate is unstable and becomes violent or explosive at elevated temperatures. Therefore, it is absolutely critical for this reaction to remain cold. When kept at –78 °C, the primary alcohol on fantrip carbinol was successfully converted to an aldehyde with high yields and no side products. To maintain a low temperature, both the addition funnel and round-bottom flask were kept cold using an ice/acetone baths (–78 °C) during the addition process to ensure the stability of both the reaction solution and TFAA/DCM.

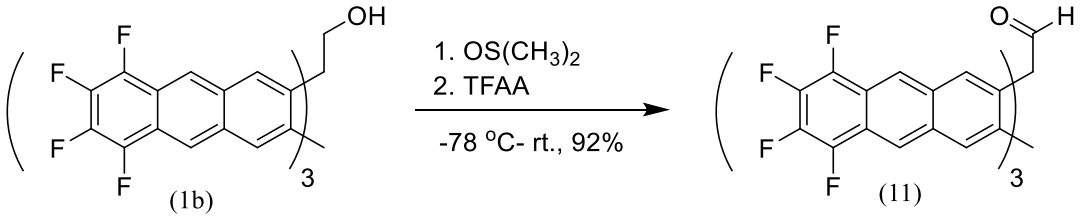

Figure 2.23 Oxidation of fantrip carbinol reaction scheme: Successful using Swern-type conditions.

Efforts were made to achieve a single-pot reaction for the synthesis of the carboxylic acid. A novel oxidation method reported by Zhao et al. involved using only two mol percent of CrO_3 and 2.5 equivalents of H_5IO_6 in wet acetonitrile (MeCN) to convert primary alcohols to carboxylic acids in excellent yield.[75] Under these reaction conditions, late-stage oxidation to carboxylic functionality was achieved in 37% yields. It's important to note that these yields are reported for small-scale reactions (under 100 mg), and there

might be an increase in yields with larger-scale reactions due to the inevitable loss of a small amount of product (refer to Figure 2.24).

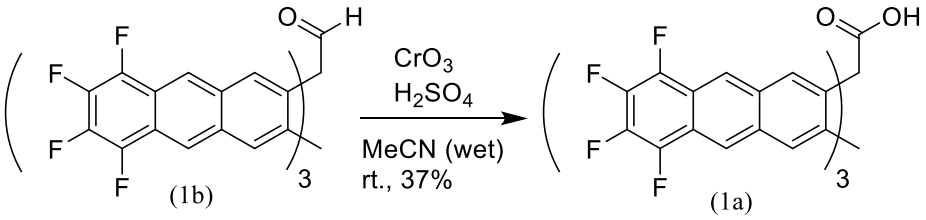

Figure 2.24 Oxidation of fantrip carbinol reaction scheme: Successful attempt using Jones-type conditions.

2.4.2 Amine Tether Synthesis

Achieving versatility at the air-water interface demands a diverse set of monomers with varying bridgehead functionality. Both carboxy fantrip and fantrip-DEG have demonstrated the capability to polymerize at the air-water interface. In order to enhance functionality at this interface, a primary amine tether was synthesized. The primary amine serves as a nucleophile in post-polymerization reactions and could be valuable when applications require coupling to an electrophile.

Because the carbaldehyde was readily available from the modified Swern conditions, reductive amination was used to functionalized the bridgehead. Initial experiments using mono Boc-protected ethylene diamine successfully synthesized a terminal primary amine tether. This work has laid the groundwork for a potential new monomer for polymerization at the air-water interface.

Refluxing in toluene with Boc-protected ethylene diamine yielded the imine in excellent yields (99%) (refer to Figure 2.25). The reaction can be concentrated and utilized

directly for the reduction without the need for purification. Monitoring the reaction through TLC is crucial to ensure complete conversion of all starting material to the imine. Specific TLC conditions are outlined in the experimental section.

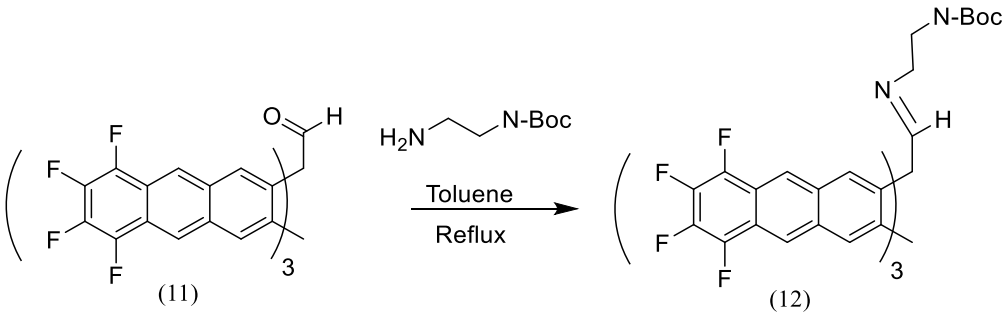

Figure 2.25 Imine formation reaction scheme: Successful using mono Boc-ethylene diamine.

The reduction of the imine is performed in a second step using $NaBH_4$ in methanol, initially cooled to 0 °C in an ice bath and then warmed to ambient temperature (refer to Figure 2.26). Monitoring the reaction through TLC is straightforward, and the reaction should be run to completion before workup to avoid unnecessary chromatography.

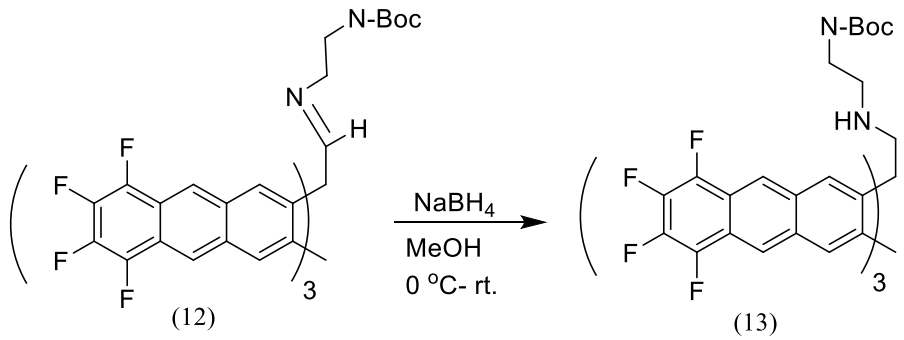

Figure 2.26 Imine reduction reaction scheme: Successful borohydride reductive conditions to form amine.

Boc-deprotection with trifluoroacetic acid (TFA) in dichloromethane yields the primary amine tether, which can be concentrated under reduced pressure and high vacuum to remove TFA (refer to Figure 2.27). Product degradation was observed when stored in d_6-DMSO for an extended period in the dark. For this reason, NMR analysis was conducted in deuterated methanol (d_4-CD_3OD).

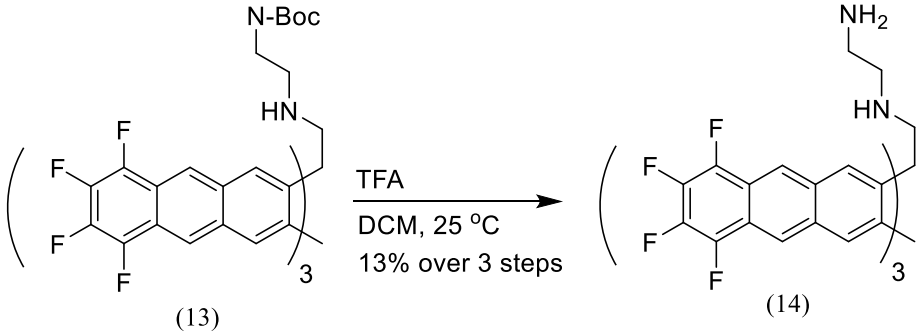

Figure 2.27 Deprotection of Boc-amine reaction scheme: Successful deprotection using TFA.

2.5 Experimental

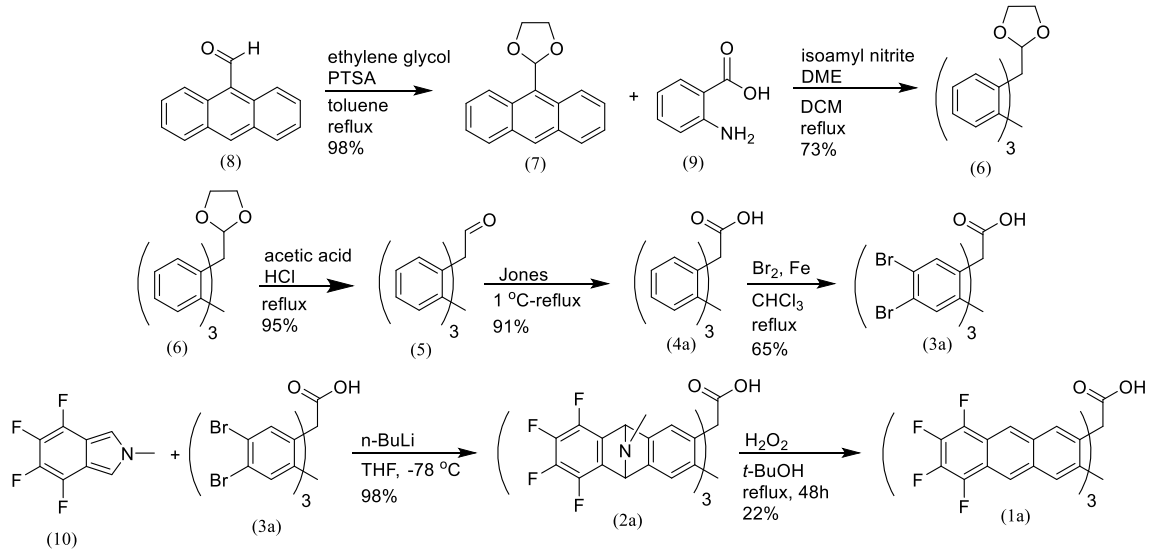

Figure 2. 28 Synthetic scheme of carboxy fantrip.

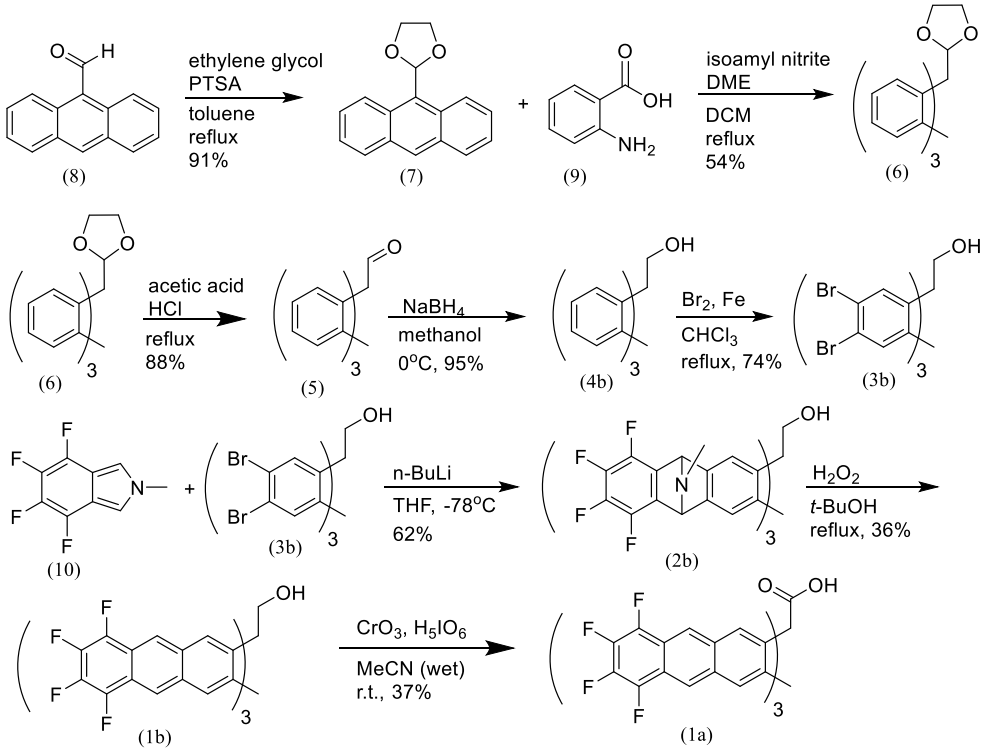

Figure 2. 29 Synthetic scheme of fantrip carbinol and carboxy fantrip.

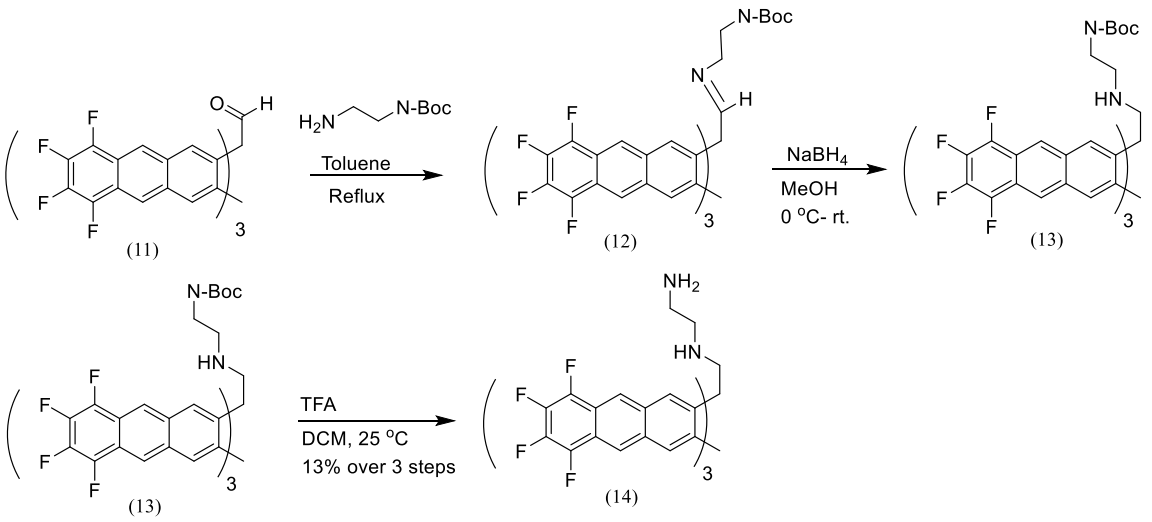

Figure 2. 30 Synthetic scheme of amine tether.

General Information:

^{1}H and ^{13}C NMR spectra were recorded on either a 400 or 500 MHz Agilent spectrometer and are reported in ppm. An Agilent TOFMS was used to record all mass spectrum data. IR data was recorded on a Bruker FTIR. NMR data are reported as follows: s = singlet, d = doublet, t = triplet, m = multiplet. Chloroform was distilled over activated 4A sieves before use. THF was freshly distilled over sodium before use. All other reagents or solvents were used as received by manufacturer.

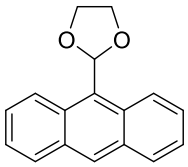

2-(antracene-9-yl)-1,3-dioxalane (7):

9-Anthraldehyde (**8**), ethylene glycol, and p-Toluenesulfonic acid were added to a round bottom flask and dissolved in toluene (300 mL). Flask was fitted with a dean stark trap and condenser and was heated to reflux for 16 h. Trapped H_2O was drained periodically. Molecular sieves (20 g, 4Å) were added to trap and reaction was allowed to reflux for an additional 24 h. Flask was cooled to 25 °C and 1M NaOH solutions (100 mL) was added. Flask was concentrated under reduced pressure to remove toluene. Product crashed out as pale yellow crystal. Solid was collected via vacuum filtration and washed with ample H_2O (300 mL) to give 9,10[1',2']-Benzenoanthracene-9(10H)-1,3-dioxalane (**7**) as a pale yellow crystal (98% yield).

^{1}H NMR data matched literature procedure[76]

^{1}H NMR (400 MHz, Chloroform-*d*) δ 8.65 – 8.46 (m, 3H), 8.01 (ddt, J = 8.2, 1.5, 0.7 Hz, 2H), 7.58 – 7.39 (m, 4H), 7.11 (s, 1H), 4.65 – 4.41 (m, 2H), 4.37 – 4.20 (m, 2H).

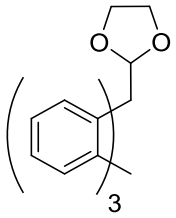

9,10[1',2']-Benzenoanthracene-9(10*H*)-1,3-dioxalane (6):

To a dry flask, 2-(antracene-9-yl)-1,3-dioxalane (**7**) (3.0 g, 11.3 mmol) and isoamyl nitrite (3.3 ml, 24.86 mmol) were added and dissolved in dry (3 Å sieves) CH_2Cl_2 (200 ml). The flask was degassed with N_2 (g) for five minutes and fitted with a reflux condenser followed by an addition funnel. The flask was brought to reflux with an oil bath set to 80 ^oC. Anthranilic acid (3.1 g, 22.6 mmol) was dissolved in dimethoxyethane (50 ml) and added to the addition funnel which was fitted with a N_2 (g) adapter. The anthranilic acid solution was added dropwise to the flask over the course of one hour. Upon the addition of anthranilic acid the solution within the flask turned a deep purple then a dark brown. After the addition of anthranilic acid, the flask was allowed to reflux for one hour. The flask was cooled to room temperature (20 ^oC) and concentrated under reduced pressure until a yellow solid crashed out of the solution. Cold (5 ^oC) MeOH was added to the flask and stirred within an ice bath at 0 ^oC for 30 min. The solution was filtered and washed with cold MeOH (5 x 15 ml) to reviel a pale yellow solid. The solid was collected and dried on high vacuum (200 mtorr) for two hours. (1.4 g, 4.3 mmol, 38% yield)

m.p. 287.1-287.4 ^{o} C; FT-IR: cm^{-1} 3070, 3036, 2965, 2956, 2897, 2866, 2844, 2764, 2159, 1459, 1397, 1211, 1172, 1156, 1141, 1108, 1089, 1044, 1030, 997, 946, 934, 921, 911, 882, 860, 765, 749, 740, 705, 683, 639, 618, 607, 595, 526, 514, 510, 502 ^{1}H NMR (500

MHz, Chloroform-*d*) δ 7.71 (dd, J = 7.1, 1.6 Hz, 2H), 7.61 (dd, J = 5.6, 3.3 Hz, 1H), 7.44 – 7.38 (m, 3H), 7.09 – 6.99 (m, 6H), 6.37 (s, 1H), 5.39 (s, 1H), 4.56 – 4.46 (m, 2H), 4.41 – 4.32 (m, 2H). ^{13}C NMR (126 MHz, chloroform-*d*) δ 146.52, 144.20, 141.66, 125.21, 124.97, 124.72, 124.64, 123.50, 123.36, 123.33, 104.19, 64.99, 56.20, 54.68.

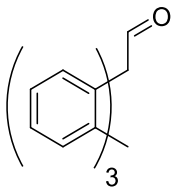

Synthesis of 9,10[1',2']-Benzenoanthracene-9(10*H*)-carboxaldehyde (5):

A solution of acetyl protected triptycene (3.50 g, 10.73 mmol) dissolved in glacial acetic acid (200 mL) and concentrated HCl (5 mL) was added to a flask fitted with a condenser and brought to reflux for 16 h. The flask was removed from heat and allowed to cool to 25 °C. To the solution, H_2O (200 mL) was added and the product precipitated out as a white solid. The solid was collected via vacuum filtration and washed with H_2O (200 mL) followed by cold ethanol (10 mL) to obtain a triptycene-9-aldehyde (2.88 g, 10.21 mmol, 95%) as a white powder.

m.p. 243.0-243.8 ^oC; FT-IR: cm^{-1} 3070, 3021, 2834, 2737, 1728, 1691, 1669, 1452, 1400, 1294, 1230, 1201, 1175, 1150, 1130, 1051, 1035, 942, 924, 874, 850, 801, 748, 709, 678, 655, 626, 611, 583, 519, 506. ^1H NMR (400 MHz, chloroform-*d*) δ 11.22 (s, 1H), 7.66 – 7.57 (m, 3H), 7.48 – 7.38 (m, 3H), 7.12 – 6.99 (m, 6H), 5.40 (s, 1H). ^{13}C NMR (126 MHz, chloroform-*d*) δ 201.0, 145.8, 142.6, 125.8, 125.2, 124.1, 122.4, 60.8, 54.2.

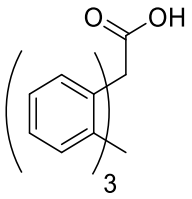

9,10[1',2']-Benzenoanthracene-9(10H)-carboxylic acid (4a):

To a round bottom flask, 9,10[1',2']-Benzenoanthracene-9(10H)-carboxaldehyde (4.93 g, 17.48 mmol) was added and dissolved in acetone (150 mL) then cooled to 0 ^{o}C. In a separate flask, concentrated sulfuric acid (2 mL) was diluted in H_2O (25 mL) and cooled to 0 ^{o}C. Chromium trioxide (2.62 g, 22.60 mmol) was slowly dissolved in the dilute sulfuric acid solution. The chromium solution was then slowly added to the round bottom flask containing the dissolved 9,10[1',2']-Benzenoanthracene-9(10H)-carboxaldehyde. The round bottom was fitted with a reflux condenser and heated to reflux for 2 h. The reaction was cooled to room temperature and 200 mL of ice cold water was added to the solution to precipitate out a white solid which was filtered and washed with an additional 300 mL of water to yield product (4.78 g, 15.93 mmol, 91%) as a white powder.

FT-IR: cm^{-1} 3066, 3037, 3034, 3018, 2950, 2910, 1710, 1456, 1404, 1393, 1262, 1216, 1167, 925, 901, 869, 748, 684, 655, 644, 620, 607, 526 ^{1}H NMR (500 MHz, chloroform-*d*) δ 7.96 – 7.84 (m, 3H), 7.50 – 7.38 (m, 3H), 7.16 – 6.99 (m, 6H), 5.42 (s, 1H). ^{13}C NMR (126 MHz, chloroform-*d*) δ 172.94, 145.44, 142.55, 125.87, 125.22, 123.67, 123.63, 54.55, 29.72. HRMS (ESI-TOF) m/z: [M - H] Calcd for 297.0975; Found 297.0972.

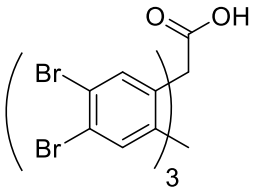

Carboxy hexabromo-triptycene (3a):

To a round bottom flask 9,10[1',2']-Benzenoanthracene-9(10*H*)-carboxylic acid (2.50 g, 8.38 mmol) was dissolved in chloroform (1500 mL). The flask was then charged with iron flakes (0.23 g, 4.12 mmol) and Br_2 (3.10 mL, 60.33 mmol) under a flow of N_2 (g). The reaction was then stirred under N_2 (g) at reflux for 16 h. ^{1}H NMR analysis of an aliquot indicated the reaction was not complete. Additional bromine (0.86 ml, 16.76 mmol) and iron flakes (20 mg, 0.36 mmol) were charged into the flask and allowed to stir at reflux for 6 more hours. Reaction progress by ^{1}H NMR still showed signs of starting material so additional bromine (0.86 mL, 16.76 mmol) and iron flakes (20 mg, 0.36 mmol) were added to flask and reaction was allowed to reflux for 16 h. Reaction progress showed completion by ^{1}H NMR so reaction flask was taken off heat and allowed to cool to 25 ^{o}C. Flask was concentrated under reduced pressure to obtain a red/brown solid. Product was ran through a plug of silica with a mobile phase of 100% THF. The first 500 mL were collected, concentrated under reduced pressure and high vacuum to give a brown powered. Recrystallization from acetone reviled product (3.0 g, 3.89 mmol, 46%) as white crystals.

m.p. >300 ^{o}C; FT-IR: cm^{-1} 2509, 2503, 1716, 1682, 1436, 1355, 1267, 1245, 1207, 1177, 1160, 1142, 1107, 1089, 1012, 946, 901, 879, 855, 802, 733, 666, 543, 527, 520. ^{1}H NMR (500 MHz, DMSO-d_6) δ 8.04 (s, 2H), 7.89 (s, 2H), 5.82 (s, 1H). 13C NMR (126 MHz,

DMSO-d_6) δ 169.33, 145.73, 143.28, 129.81, 129.80, 121.91, 121.16, 60.00, 49.79. HRMS (ESI-TOF) m/z: [M - H] Calcd for 770.5565; Found 770.5587.

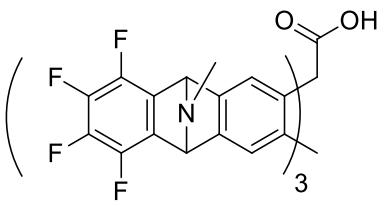

Fantrip precursor (2a):

Carboxy hexabromo-triptycene (1.08 g, 1.40 mmol) and 4,5,6,7-tetrafluoro-4,5-dihydro-2H-isoindole (1.28 g, 6.30 mmol) were added to a flask and dissolved in freshly distilled THF (20 mL), then concentrated under reduced pressure. The previous step was repeated 3x to exchange occluded solvents in starting materials with THF. The resulting mixture was then dissolved in freshly distilled THF (290 mL) and carefully cooled in an isopropyl slushy to -78 ^{o}C under N_2 (g) atmosphere. n-BuLi (1.26 mL, 2.5 M) was added dropwise via syringe over 10 min. The flask was allowed to stir at -78 ^{o}C for 2 hours, then slowly warm up to 25 ^{o}C over 1 h. The reaction was quenched with H_2O (1 mL) and concentrated under reduced pressure and high vacuum. The remaining tan solid was dissolved in CH_2Cl_2 (15 mL) and ran through a plug of silica, mobile phase 100% CH_2Cl_2 to remove excess 4,5,6,7-tetrafluoro-4,5-dihydro-2H-isoindole then gradient changed to 90:10 CH_2Cl_2:MeOH to extract product on baseline. Baseline fractions were collected and concentrated to obtain trifold adduct (1.24 g, 1.38 mmol, 98%) as a tan powder.

m.p. >300 ^{o}C; FT-IR: cm^{-1} 3392, 3361, 1727, 1513, 1492, 906, 729, 677, 649, 633, 610, 596, 589, 583, 575, 569, 553, 507. ^{1}H NMR (500 MHz, chloroform-*d*) δ 8.77 – 7.26 (m, 7H), 5.54 – 4.66 (m, 7H), 2.52 – 2.02 (m, 7H).

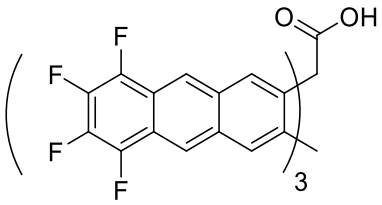

Carboxy Fantrip Trifold (1a):

Carboxy fantrip trifold adduct (1.30 g, 1.44 mmol) was added to a round bottom flask and dissolved in tert-butyl alcohol (250 mL) and heated to a reflux. To the refluxing solution 30% H_2O_2 (1 mL) was added and refluxed for 1 h. Reaction progress was monitored by TLC (mobile phase: 7:3 EtOAc:Hex with 0.1% AcOH). No product for formed so additional H_2O_2 (20 mL) was added and reaction was allowed to reflux for 2 h. Reaction progress stalled after 2 hrs so H_2O_2 (20 mL) was added to flask and allowed to heat for 4 h. Reaction appeared finished by TLC and flask was cooled to room temp followed by the addition of H_2O (100 mL). Flask was concentrated under reduced pressure to remove tert-butyl alcohol. Product was extracted in ethyl acetate (3x 100 mL), dried with $MgSO_4$, filtered, and concentrated under reduced pressure and high vacuum. Silica column was ran using TLC conditions and the top three bands were collected, combine, and dried to give a yellow/orange solid. The solid was recrystallized from chloroform (10 mL) at -18 ^oC followed by trituration of the yellow solid in chloroform (20 ml) to give carboxy fantrip monomer (250 mg, 0.310 mmol, 22%) as a pale yellow powder.

m.p. >300 ^oC; FT-IR: cm^{-1} 2962, 1680, 1591, 1493, 1459, 1358, 1260, 1091, 1018, 1007, 996, 944, 902, 865, 799, 740, 723, 720, 703, 686, 676, 668, 636, 632, 557, 539, 534, 528, 514, 508, 50. ^1H NMR (500 MHz, d_6-acetone) δ 8.95 (s, 3H), 8.80 (s, 3H), 8.74 (s, 3H),

8.49 (s, 3H), 6.37 (s, 1H). HRMS (APPI-TOF) m/z: [M - H] Calcd for 814.0729; Found 813.0731.

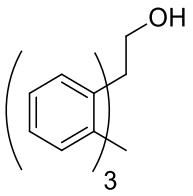

Triptycene-9-carbinol (4b):

Triptycene aldehyde (16.0 mmol, 4.5 g) was dissolved in methanol (300 mL) in a flask. The solution was stirred and cooled using an ice bath to 0 ^{o}C. $NaBH_4$ (48.0 mmol, 1.8 g) was slowly added to the solution over 1 h. The reaction mixture was allowed to warm to 25 ^{o}C over the course of 1 h. The reaction was quenched by addition of H_2O (700 mL) which precipitated a white solid. The solid was collected via vacuum filtration. The filtrate was dissolved in dichloromethane (100 mL), dried with $MgSO_4$, concentrated under reduced pressure and evaporated to dryness in vacuum, to afford triptycene-9-carbinol (4.3 g, 15.2 mmol, 95%) a white power.

mp. 240.0 - 241.4 ^{o}C; FT-IR: cm^{-1} 3300, 3070, 3060, 2944, 1457, 1303, 1284, 1190, 1135, 1070, 1036, 1025, 923, 798, 748, 743, 737, 711, 674, 647, 627, 611, 603, 578. ^{1}H NMR (400 MHz, chloroform-*d*) δ 7.48 (s, 3H), 7.42 – 7.32 (m, 3H), 7.14 – 6.88 (m, 6H), 5.38 (s, 1H), 5.27 (d, 2H). ^{13}C NMR (101 MHz, chloroform-*d*) δ 146.8, 144.4, 125.2, 125.1, 123.7, 122.0, 61.1, 54.4, 54.3. HRMS (APPI-TOF) m/z: [M - H] Calcd for $C_{21}H_{16}OH$ 284.1274; Found 284.1248.

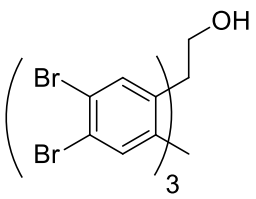

2,3,7,6,14,15-hexabromotriptacene-9-carbinol (3b):

Triptycene-9-carbinol (8.1 mmol, 2.3 g), iron flakes (0.8 mmol, 45.3 mg), and chloroform (300 mL) were added to an oven-dried flask fitted with a condenser under N_2 atmosphere. The mixture was heated to using an oil bath at 80 °C. Bromine (51.9 mmol, 2.7 mL), diluted in chloroform (20 mL) was added to an addition funnel fitted on top of the condenser. The bromine solution was added dropwise to the flask over 4 h. The flask was allowed to reflux for 16 hours. ^{1}H NMR analysis of an aliquot indicated the reaction was not complete (NMR analysis reported in SI). Additional bromine (5.7 mmol, 0.3 mL) was diluted in chloroform (10 mL) and added dropwise to the flask over 1 hour. The flask was allowed to react for an additional 16 h. After the second addition of bromine, NMR analysis showed that the reaction progression was not complete. Bromine (5.7 mmol, 0.3 mL) was diluted in 10 mL of chloroform and added dropwise over 1 hour. The flask was allowed to reflux for 16 hours. The reaction was allowed to cool to 25 °C and washed with an aqueous KOH solution (25 mL, 1 M). The organic solution was extracted with dichloromethane (3x, 20 mL), dried under $MgSO_4$, and concentrated under reduced pressure to afford a tan powder. The tan powder was ran through a plug of silica (mobile phase: 100% dichloromethane), concentrated under reduced pressure and evaporated to dryness in vacuum to obtain 2,3,7,6,14,15-hexabromo-9-triptycenecarbinol (4.5 g, 6.0 mmol, 74%) as a tan powder.

mp. decomposition at 378.2 ^{o}C; FT-IR: cm^{-1} 3450, 1698, 1439, 1435, 1414, 1357, 1227, 1180, 1104, 1088, 1072, 1044, 1037, 900, 883, 849, 801, 782, 609, 563, 554, 548, 527. ^{1}H NMR (400 MHz, chloroform-*d*) δ 7.80 – 7.66 (m, 3H), 7.62 (s, 3H), 5.18 (s, 1H), 5.15 (d, J = 3.2 Hz, 2H). ^{13}C NMR (101 MHz, chloroform-*d*) δ 145.3, 143.6, 128.7, 128.2, 121.9, 121.8, 59.7, 52.9, 51.2. HRMS (APPI-TOF) m/z: [M - H] Calcd. for $C_{21}H_{10}Br_6OH$ 757.5845; Found 757.5815.

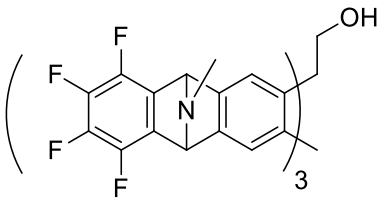

Trifold carbinol precursor (2b):

2,3,7,6,14,15-hexabromotriptacene-9-carbinol (3.6 g, 4.71 mmol) and 4,5,6,7-tetrafluoro-4,5-dihydro-2H-isoindole (3.3 g, 16.8 mmol) were added to a flask and dissolved in freshly distilled THF (20 mL), then concentrated under reduced pressure. The previous step was repeated 3x to exchange occluded solvents in starting materials with THF. The resulting mixture was then dissolved in THF (200 mL) and carefully cooled in an isopropyl slushy to -30 ^{o}C under N_2 atmosphere. n-BuLi (3.5 mL, 1.5M) was added dropwise via syringe over 1 h. The flask was allowed to slowly warm up to 25 ^{o}C over 4 hours. To the flask, an aqueous HCl solution was added (300 mL, 1 M). The solution was gently washed with ethyl acetate (3x, 20 mL). Aqueous KOH (200 mL, 2 M) was added to the solution causing a white solid to precipitate. The precipitated solid was extracted with ethyl acetate (3x, 100 mL). The organic fractions were combine, dried with $MgSO_4$, concentrated under reduced pressure, and evaporated to dryness in vacuum to obtain the precursor (2.64 g, 2.9 mmol, 62%) as a tan oil.

FT-IR cm^{-1} 2958, 2953, 2870, 1679, 1495, 1482, 1450, 1415, 1397, 1385, 1316, 1266, 1222, 1201, 1184, 1113, 1092, 1048, 997, 958, 924, 907, 866, 848, 832, 804, 773, 730, 686, 668, 646, 619, 615, 608, 605, 599, 587, 564, 550, 540. ^{1}H NMR (400 MHz, chloroform-d) δ 7.65 – 7.24 (m, 4H), 5.21 – 4.96 (m, 7H), 2.25 – 1.96 (m, 7H). HRMS (APPI-TOF) m/z: [M - H] Calcd for $C_{48}H_{25}F_{12}N_3O$ 888.1879; Found 888.1892.

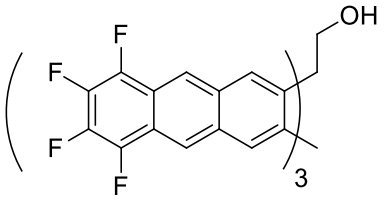

Fantrip Carbinol (1b):

Fantrip precursor (0.4g, 0.451 mmol) was dissolved in tert-butanol (50 mL) and added to a flask fitted with a condenser and heated in an oil bath at 110 ^{o}C. To the flask was added H_2O_2 (30% solution, 1 mL) and allowed to reflux for 1 h. Reaction was not complete by TLC (100% CH_2Cl_2: S.M. Rf. 0.3, Product Rf. 0.9). Additional H_2O_2 (30% solution, 4 mL) was added to the flask over the course of two days in 2 mL increments until the reaction was complete via TLC. The flask was allowed to cool to room temperature and a pale yellow solid crashed out of solution. To the flask was added H_2O (5 mL), and the tert-butanol was removed under reduced pressure. The remaining oil was dissolved in ethyl acetate (100 mL) and washed with H_2O (3x 50 mL). The organic phase was collected, dried with $MgSO_4$ and concentrated under reduced pressure. The solid was ran through a plug of silica (mobile phase 100% CH_2Cl_2). The top band was collected and concentrated under reduced pressure and evaporated to dryness in vacuum to revile a yellow powder which was recrystallized in chloroform to obtain fantrip carbinol (0.130 g, 0.16 mmol, 36%) as a pale yellow crystal.

FT-IR cm^{-1} 3655, 3643, 3635, 3626, 3617, 3608, 3602, 3594, 2958, 2931, 1680, 1609, 1591, 1490, 1458, 1427, 1400, 1355, 1317, 1280, 1173, 1150, 1121, 1055, 1003, 992, 900, 864, 840, 822, 801, 797, 757, 738, 665, 632, 589, 581, 572, 557, 546, 540, 534. ^{1}H NMR

(400 MHz, chloroform-*d*) δ 8.57 (s, 3H), 8.52 (s, 3H), 8.24 (s, 3H), 8.13 (s, 3H), 5.89 (s, 1H), 5.74 (d, J = 4.1 Hz, 2H). HRMS (APPI-TOF) m/z: [M - H] Calcd for $C_{45}H_{16}F_{12}O$ 800.1010; Found 888.1046.

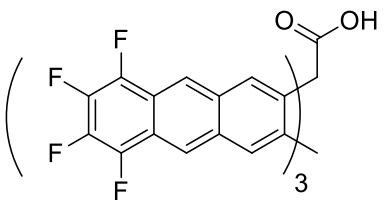

Carboxy Fantrip (1a):

Fantrip carbinol was dissolved in a flask containing wet MeCN (0.75 v % water, 50 mL). A solution of H_5IO_6/CrO_3 was prepared by dissolving H_5IO_6 (6.8 mg, 0.003 mmol) and CrO_3 (1.5 mg, 0.00144 mmol) in wet MeCN (0.75 v % water, 10 mL) and was added dropwise to the flask over 30 min. The reaction was allowed to stir for an additional 30 min until the complete disappearance of starting material shown by TLC (100% DCM: S.M. Rf. 0.9, Product Rf. 0.0). To the flask H_2O (10 mL) was added and then concentrated under reduced pressure to remove MeCN. The product was extracted into ethyl acetate (3x, 50 mL) and then washed with H_2O (3x 20 mL). The organic phase was dried with $MgSO_4$, filtered, concentrated under reduced pressure, and evaporated to dryness in vacuum to obtain a white solid. The product was recrystallized in chloroform followed by trituration in pentane to obtain carboxy fantrip (38 mg, 0.047 mmol, 37%) as a white crystal.

^{1}H NMR (400 MHz, chloroform-*d*) δ 8.62 (s, 3H), 8.60 (s, 3H), 8.53 (s, 3H), 8.15 (s, 3H), 5.87 (s, 1H). HRMS (APPI-TOF) m/z: [M - H] Calcd for $C_{45}H_{14}F_{12}O_2$ 813.0729; Found 813.0731.

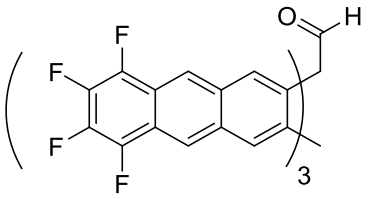

Fantrip Aldehyde (11):

To a round bottom dimethyl sulfoxide (0.261 ml, 3.68 mmol) and CH_2Cl_2 (70 ml) were added and cooled to –78 ºC with a acetone dry ice bath. To a jacketed addition funnel cooled to -78 ºC TFAA (0.38 mL, 2.27 mmol) was added and diluted with CH_2Cl_2 (75 ml). Once the solution was cooled it was added dropwise to the round bottom flask slowely over 15 min. Fantrip carbinol (98 mg, 0.122 mmol) was dissolved in CH_2Cl_2 (200 ml) and added to jacketed addition funnel and cooled to -78 ºC. This cooled solution was added dropwise over 1 hour. Once added, the solution was allawed to stir for an additional 20 min. TEA (2.8 ml) was diluted in CH_2Cl_2 (50 ml) and cooled to -78 ºC and added dropwise over the course of 20 min. the flask was allowed to stir for 20 min then allawed to warm to room temp naturally over 2 hours. The solution was quenched with water (100 ml) and extracted with ethyl acetate (3x 100 ml). Organic was dried with $MgSO_4$, filtered and concentrated under reduced pressure and high vacuum to recover fantrip aldehyde as a white/yellow solid (90 mg, 0.113 mmol, 92%)

^{1}H NMR (500 MHz, Chloroform-*d*) δ 11.57 (s, 1H), 8.58 (s, 3H), 8.54 (s, 3H), 8.38 (s, 3H), 8.19 (s, 3H), 5.92 (s, 1H).

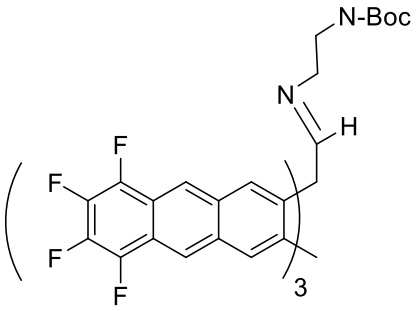

Fantrip Imine (12):

To a round bottom flask fantrip aldehyde (0.13g, 0.163 mmol) and boc-ethylene diamine (0.261g, 1.628 mmol) was added and dissolved in toluene (250 ml). The flask was fitted with a dean stark trap and refluxed (1.5 hours). Solution was taken off heat and concentrated under reduced pressure. ^{1}H NMR of crude material was taken and 100% of starting material was converted to the imine. This product was used without further purification.

Possible ^{1}H NMR spectra:

^{1}H NMR (500 MHz, Chloroform-*d*) δ 9.47 (s, 1H), 8.60 (s, 3H), 8.55 (s, 3H), 8.43 (s, 3H), 8.18 (s, 3H), 5.93 (s, 1H), 4.45 (s, 2H), 3.98 (s, 2H), 1.53 (s, 9H).

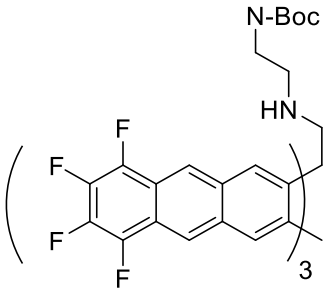

Fantrip Boc-Amine(13):

Fantrip imine was used as is from previous step. This solid was dissolved in MeOH (500 mL) then cooled to 0 ^{o}C with an ice bath. $NaBH_4$ (0.54 g, 14.3 mmol) was slowly added to the flask over the course of 10 min. The flask was allowed to warm to room temp over 30 min, then stirred for an additional 1 hour. Reaction was monitored by TLC (mobile phase 100% DCM) top dot R_f: 0.6 was starting material, dot below R_f: 0.45 was product. Solution was allowed to stir until the disappearance of starting material by TLC. Once reaction was complete, H_2O (100 ml) was added and mixture was concentrated to remove MeOH. Product was extracted with ethyl acetate (3x 100 ml) concentrated under reduced pressure and high vacuum. Silica plug was used to purify mixture mobile phase 100% DCM. Yield was not acquired as it was used directly in the next reaction.

Possible ^{1}H NMR spectra:

^{1}H NMR (500 MHz, Chloroform-*d*) δ 8.60 (s, 3H), 8.53 (s, 3H), 8.25 (s, 3H), 8.14 (s, 3H), 5.90 (s, 1H), 3.69 (d, *J* = 14.6 Hz, 2H), 3.52 (s, 2H), 1.27 (d, *J* = 2.1 Hz, 9H).

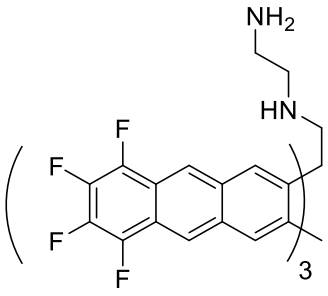

Fantrip Amine (14):

Fantrip used from last step was dissolved in DCM (5 ml) and equal amount of TFA. The reaction was allowed to stir in the dark for 4 hours. The reaction mixture was concentrated under reduced pressure then dissolved in ethyl acetate (100 ml) and washed with H_2O (2x 30 ml). The organic phase was collected and dried with $MgSO_4$, filtered and concentrated under reduced pressure and high vacuum. White/yellow solid was purified by gradient silica plug (100% DCM) to run any impurities through. Mobile phase was changed to (8:2 DCM: Ethyl Acetate) to move baseline. Baseline fractions were combine, concentrated under reduced pressure and high vacuum to afford a white/yellow solid of fantrip amine tether (19 mg, 0.0223 mmol, 13% yield over 3 steps).

Possible ^{1}H NMR spectra:

^{1}H NMR (500 MHz, Acetone-d_6) δ 8.71 (s, 2H), 8.62 (s, 9H), 8.39 (s, 3H), 6.30 (s, 1H), 3.73 (s, 1H), 3.59 (t, J = 5.6 Hz, 1H).

^{1}H NMR of 2-(antracene-9-yl)-1,3-dioxalane (7):

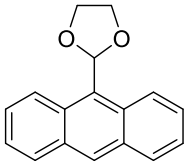

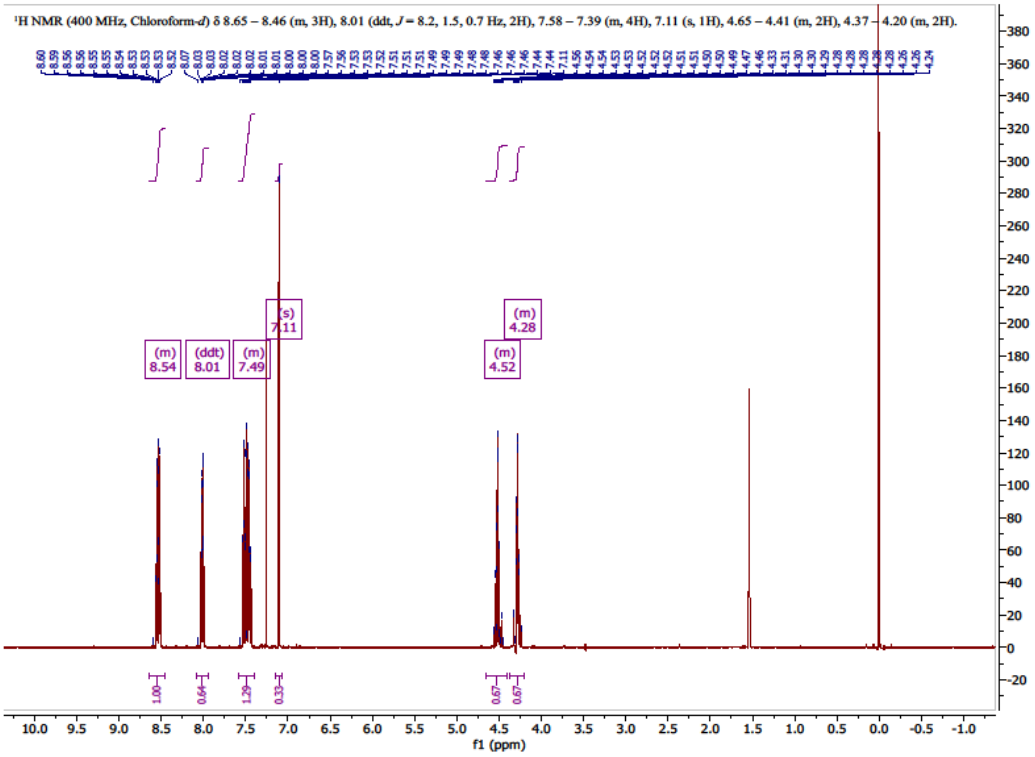

^{1}H NMR of 9,10[1',2']-Benzenoanthracene-9(10H)-1,3-dioxalane: (6)

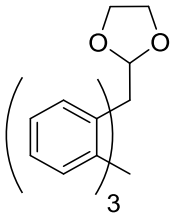

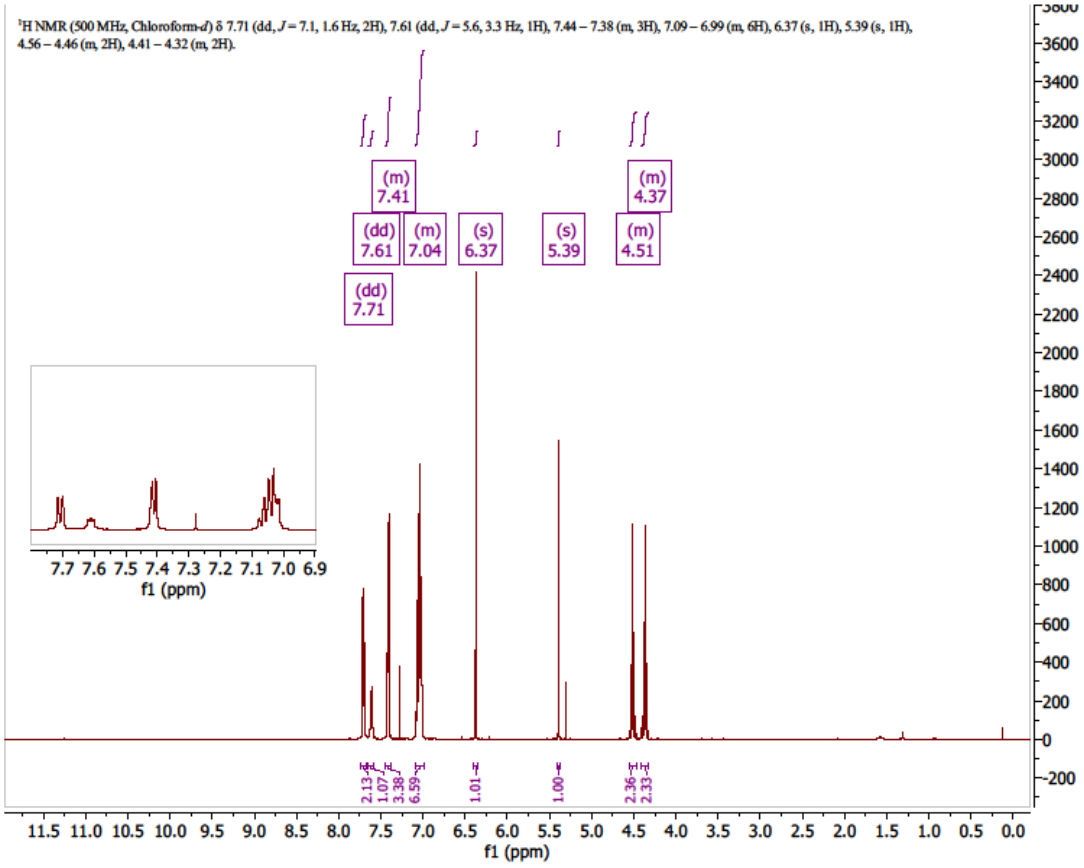

^{13}C NMR of 9,10[1',2']-Benzenoanthracene-9(10H)-1,3-dioxalane: (6)

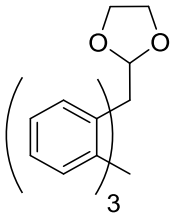

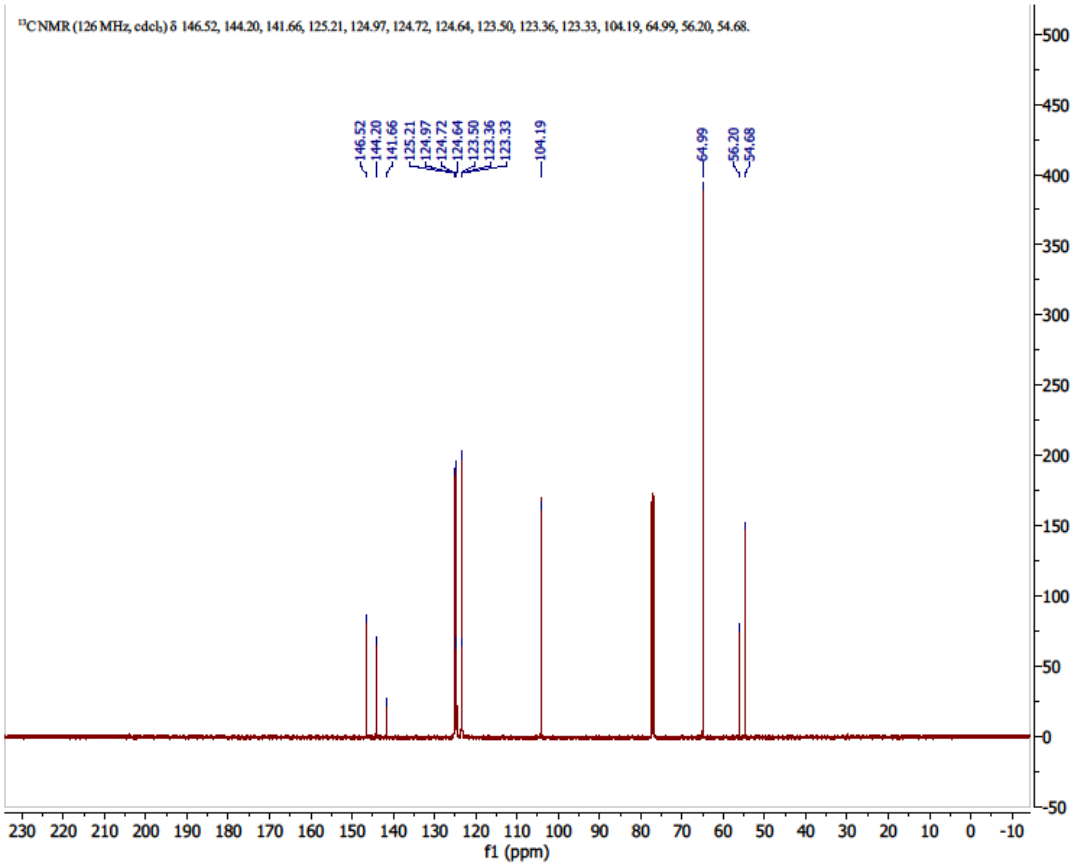

^{1}H NMR of 9,10[1',2']-Benzenoanthracene-9(10H)-carboxaldehyde (5):

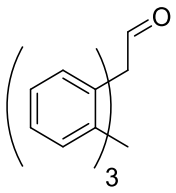

^{1}H NMR (400 MHz, Chloroform-*d*) δ 11.22 (s, 1H), 7.66 – 7.57 (m, 3H), 7.48 – 7.38 (m, 3H), 7.12 – 6.99 (m, 6H), 5.40 (s, 1H).

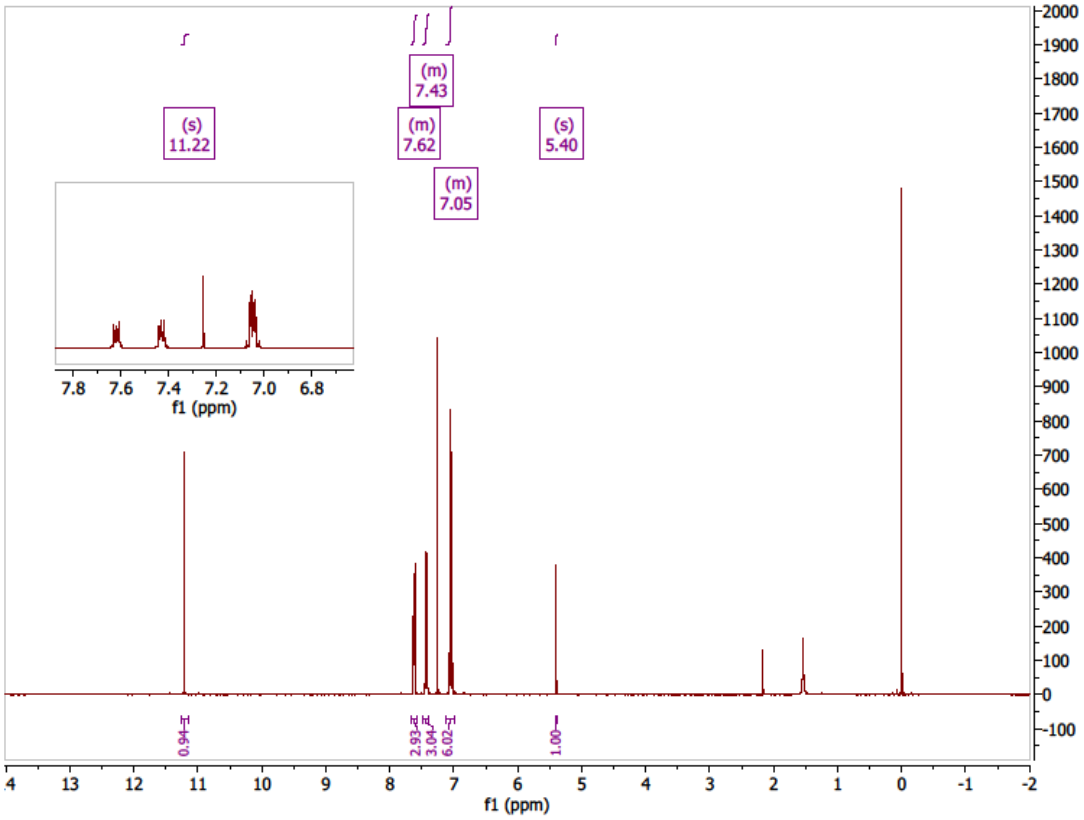

^{13}C NMR of 9,10[1',2']-Benzenoanthracene-9(10H)-carboxaldehyde (5):

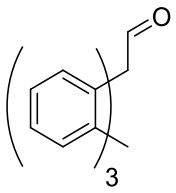

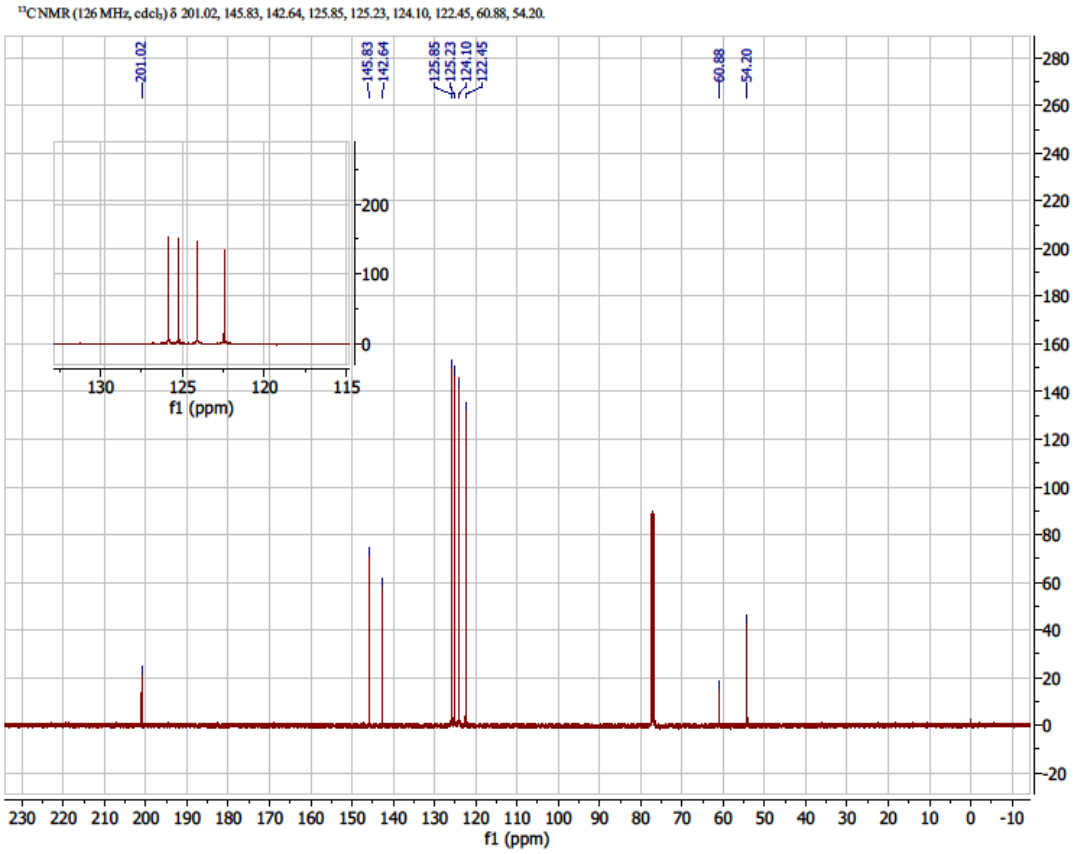

^{1}H NMR of 9,10[1',2']-Benzenoanthracene-9(10H)-carboxylic acid: (4a):

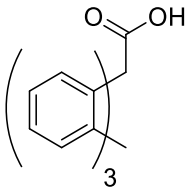

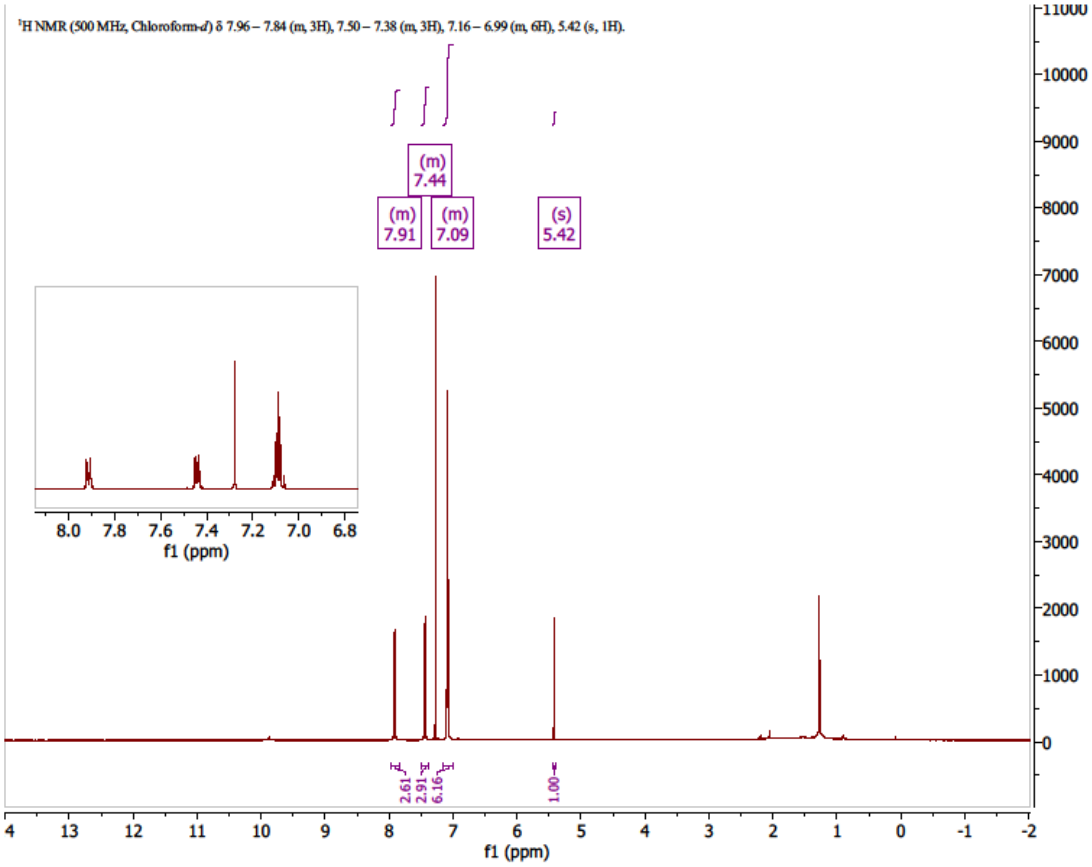

^{13}C NMR of 9,10[1',2']-Benzenoanthracene-9(10H)-carboxylic acid (4a):

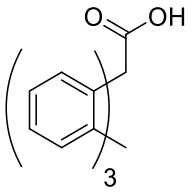

^{13}C NMR (126 MHz, cdcl$_3$) δ 172.94, 145.44, 142.55, 125.87, 125.22, 123.67, 123.63, 54.55, 29.72.

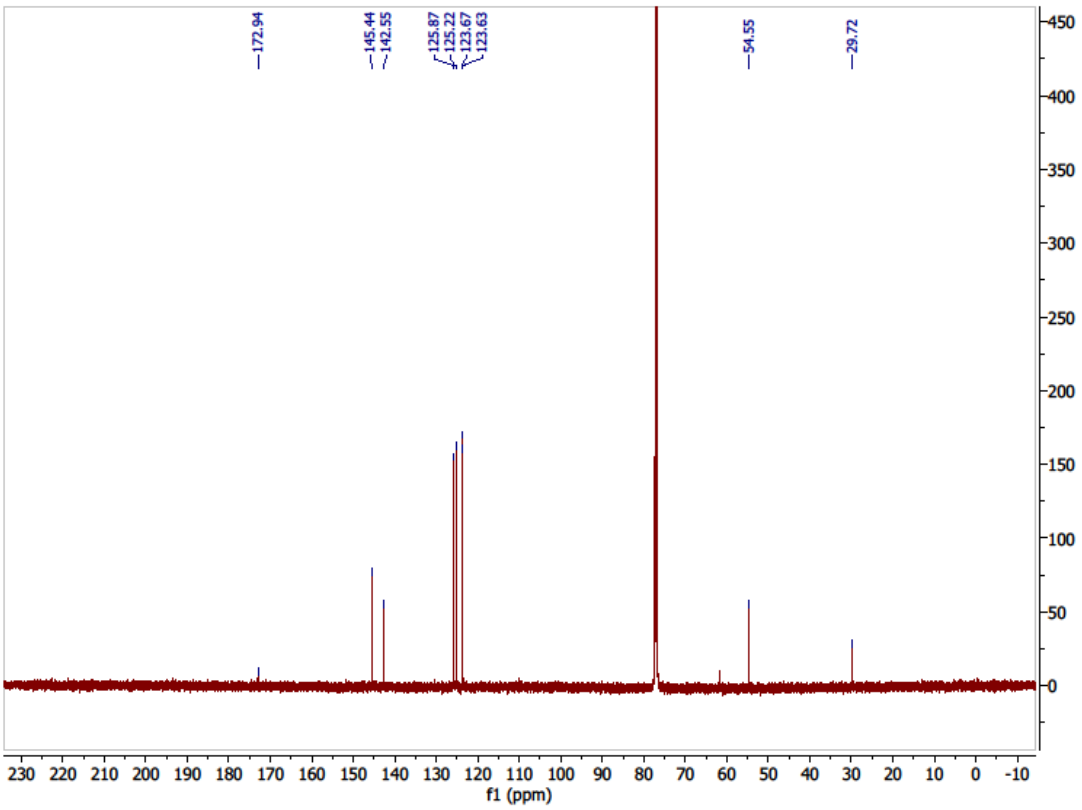

^{1}H NMR of 2,3,7,6,14,15-hexabromotriptoic acid (3a):

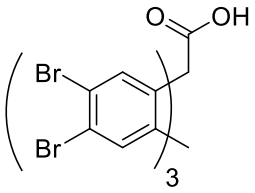

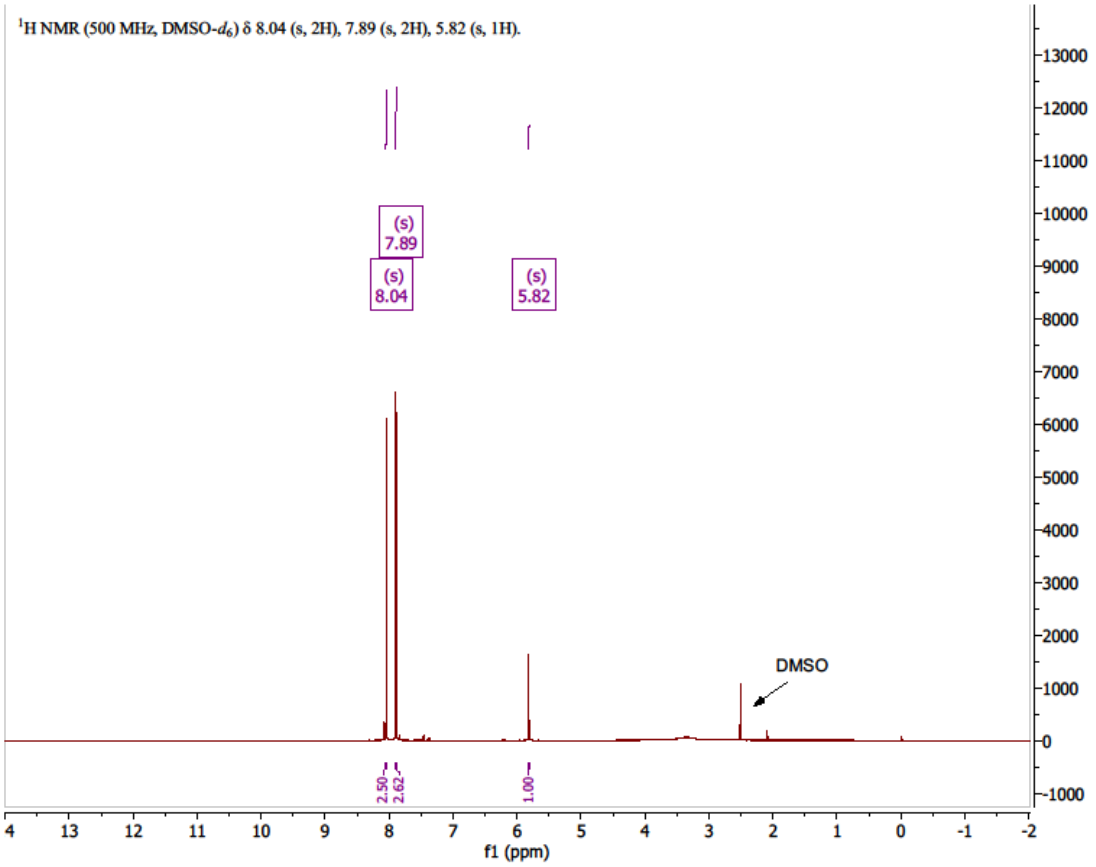

^{13}C NMR of 2,3,7,6,14,15-hexabromotriptoic acid (3a):

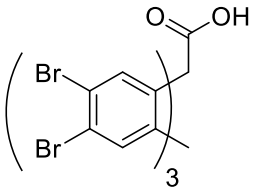

^{13}C NMR (126 MHz, dmso) δ 169.33, 145.73, 143.28, 129.81, 129.80, 121.91, 121.16, 60.00, 49.79.

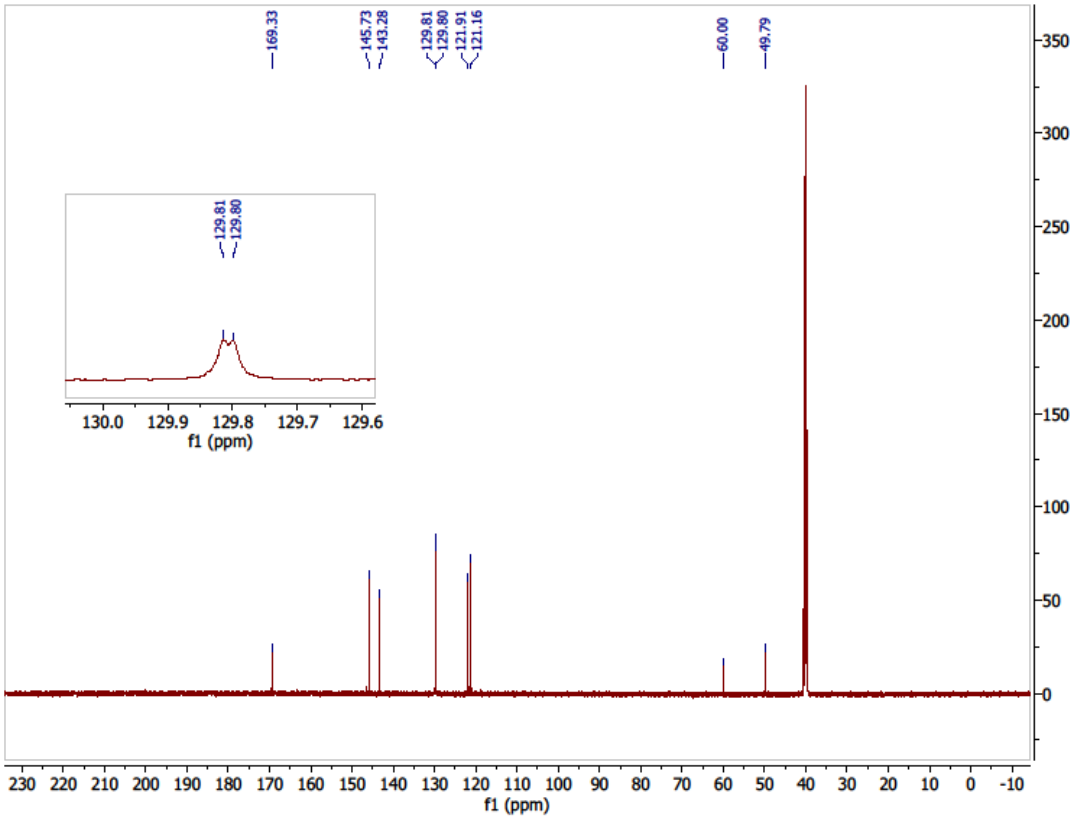

^{1}H NMR of fantrip trifold adduct (2a):

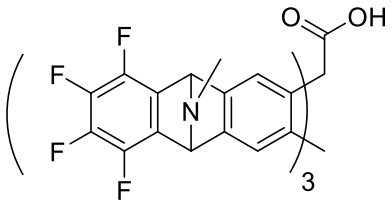

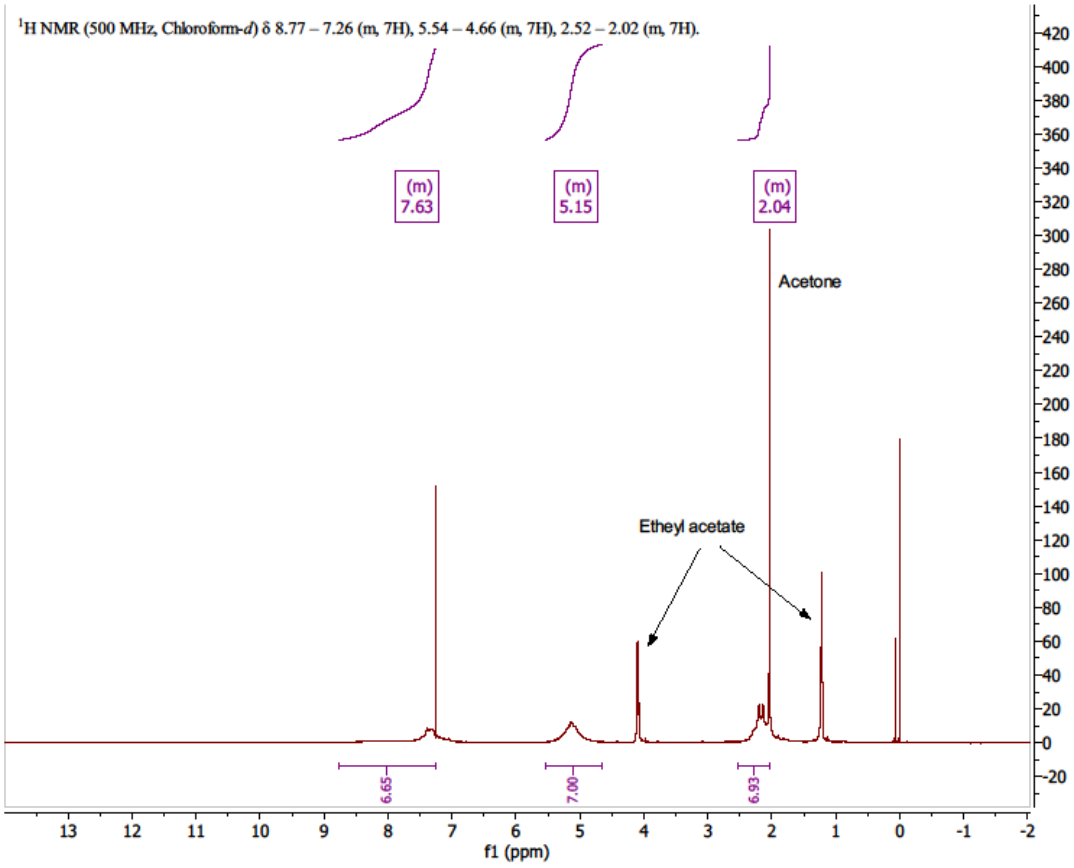

^{1}H NMR of carboxy fantrip (1a):

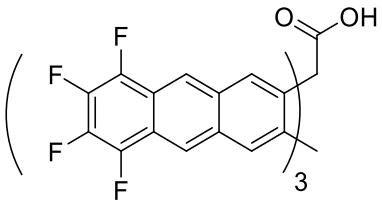

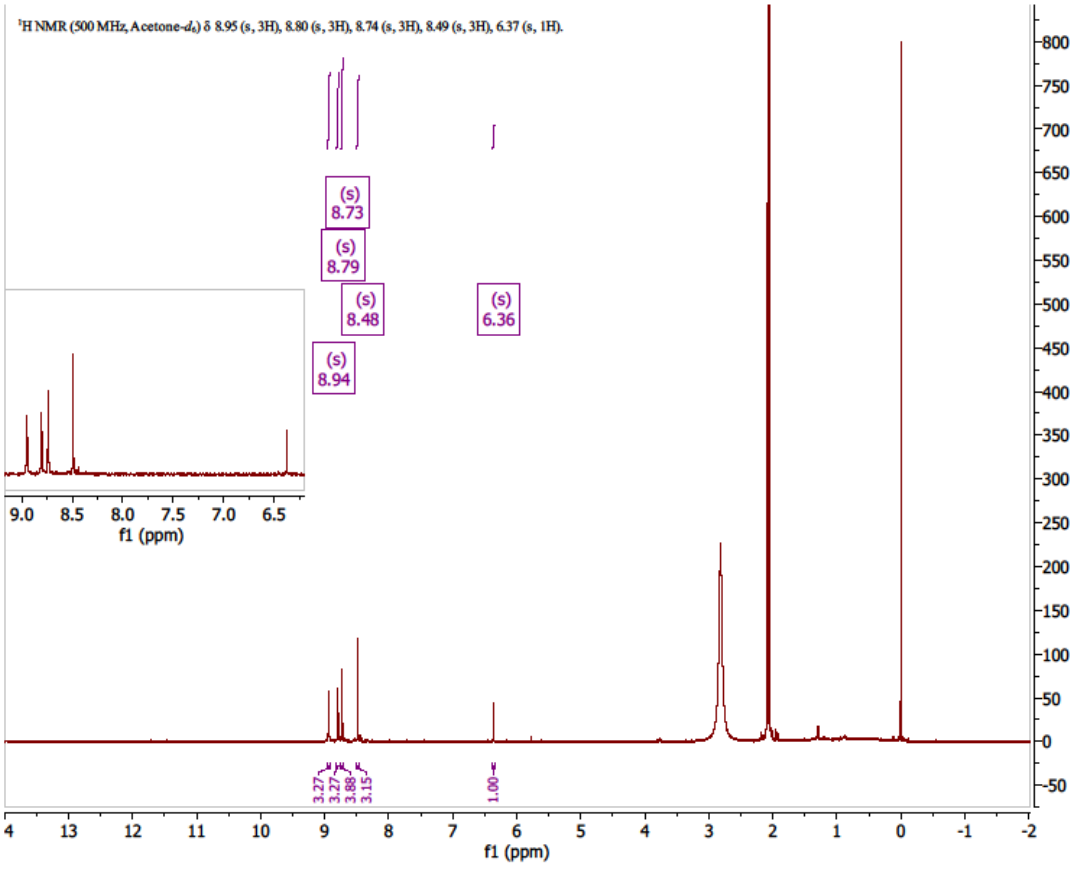

carboxy fantrip d-DMSO

^{1}H NMR (500 MHz, DMSO-d_6) δ 8.81 (s, 3H), 8.77 (s, 3H), 8.75 (s, 3H), 8.46 (s, 3H), 6.26 (s, 1H).

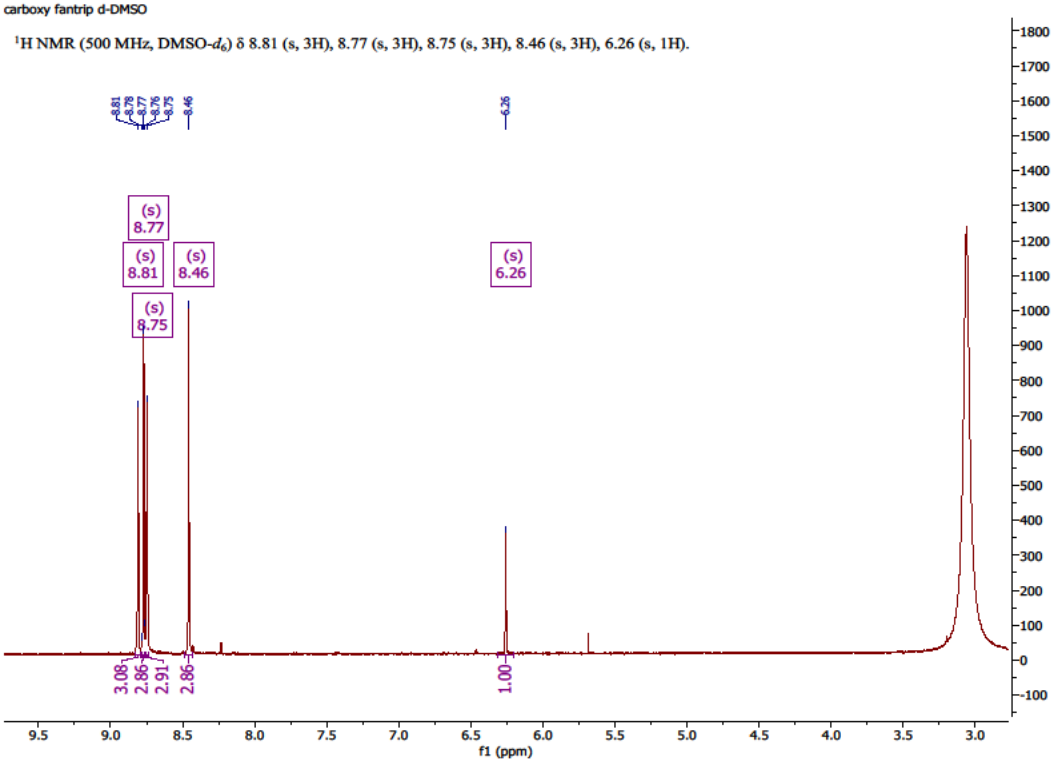

^{1}H NMR of 9,10[1',2']-Benzenoanthracene-9(10H)-carbinol (4b):

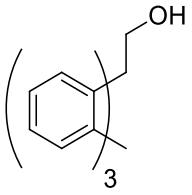

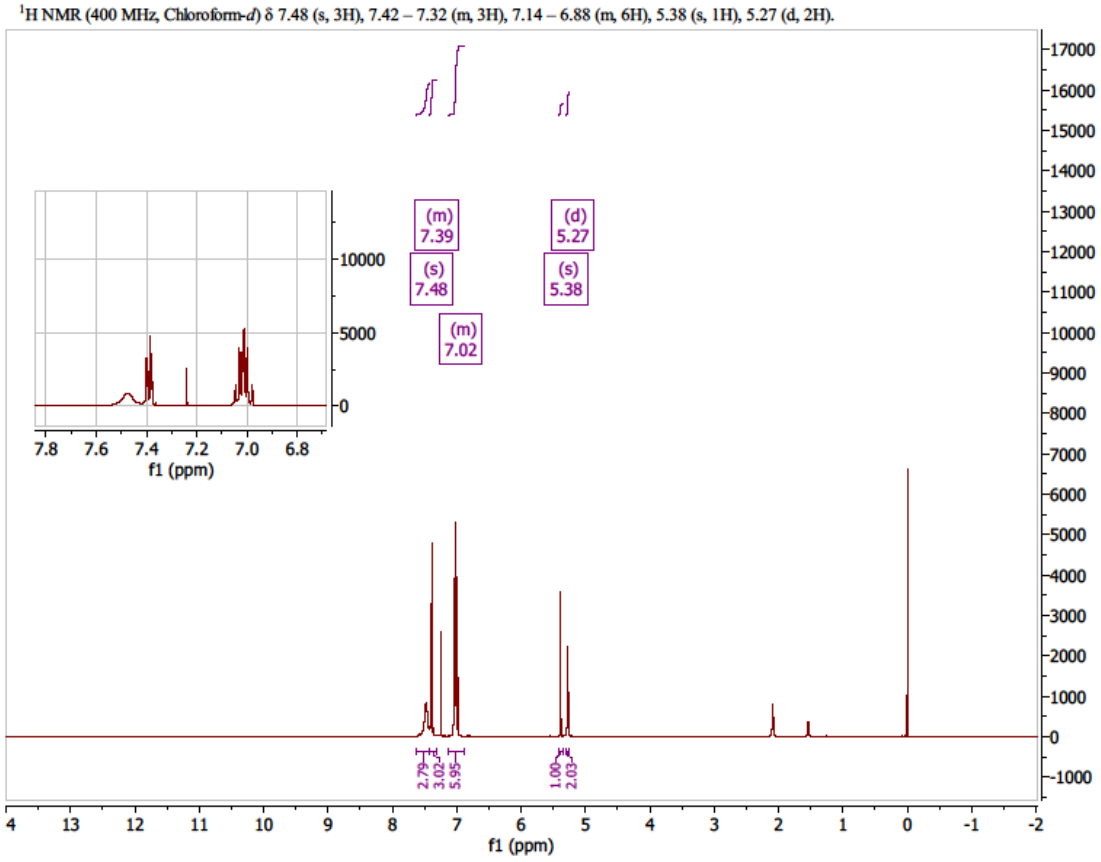

^{13}C NMR of 9,10[1',2']-Benzenoanthracene-9(10H)-carbinol (4b):

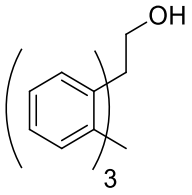

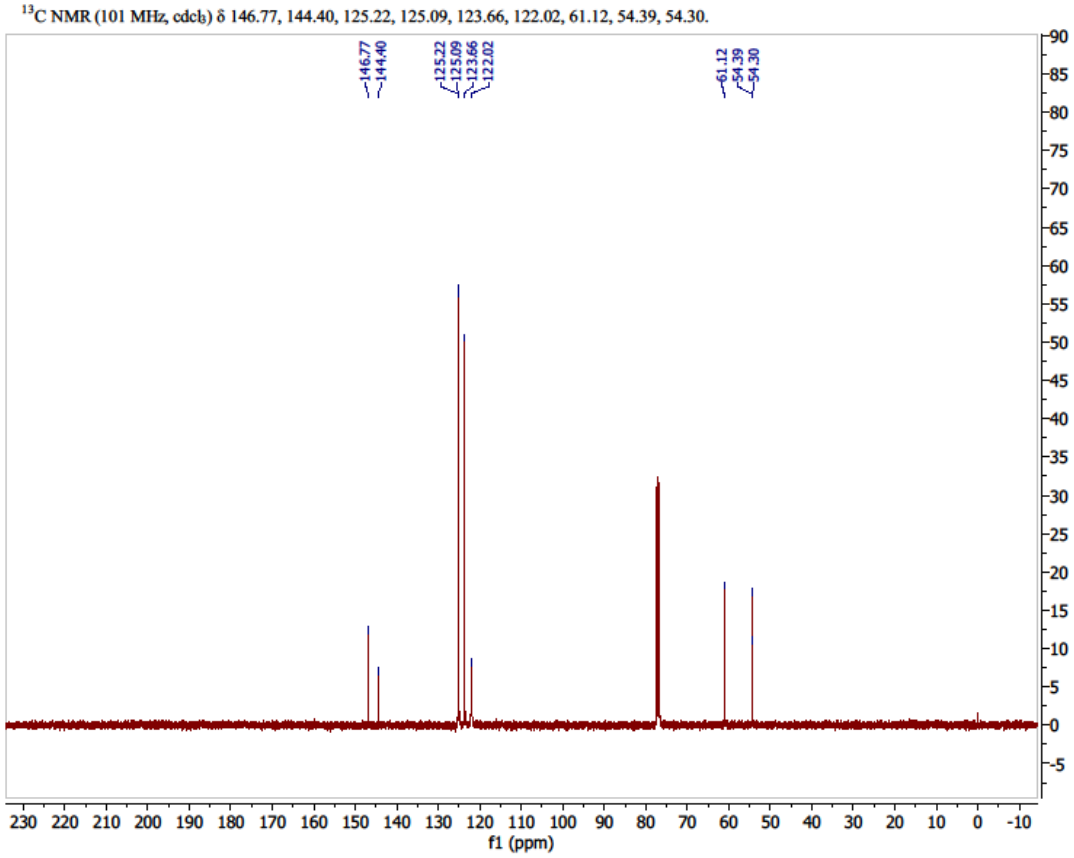

^{1}H NMR of Carboxy hexabromo-triptycene (3b):

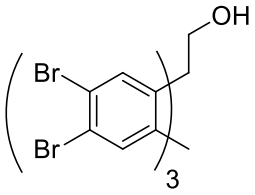

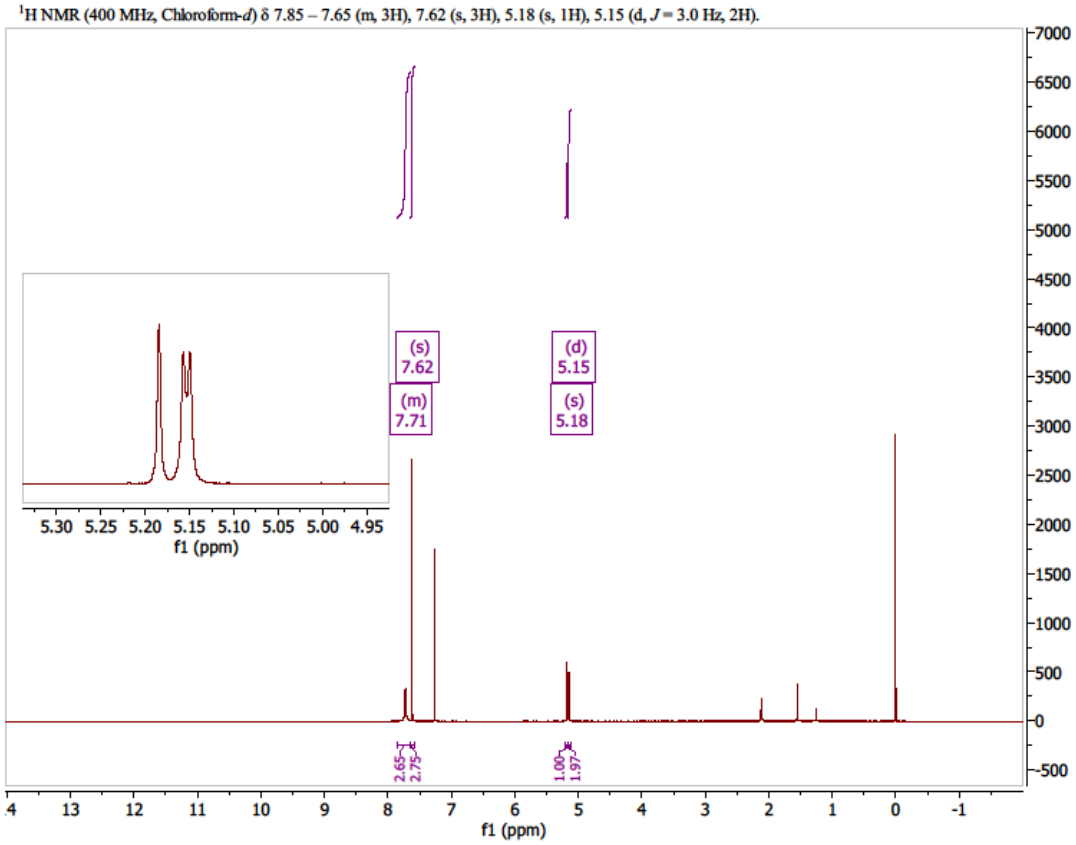

^{13}C NMR of Carboxy hexabromo-triptycene (3b):

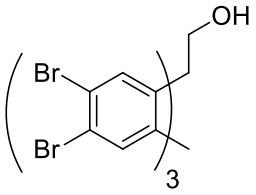

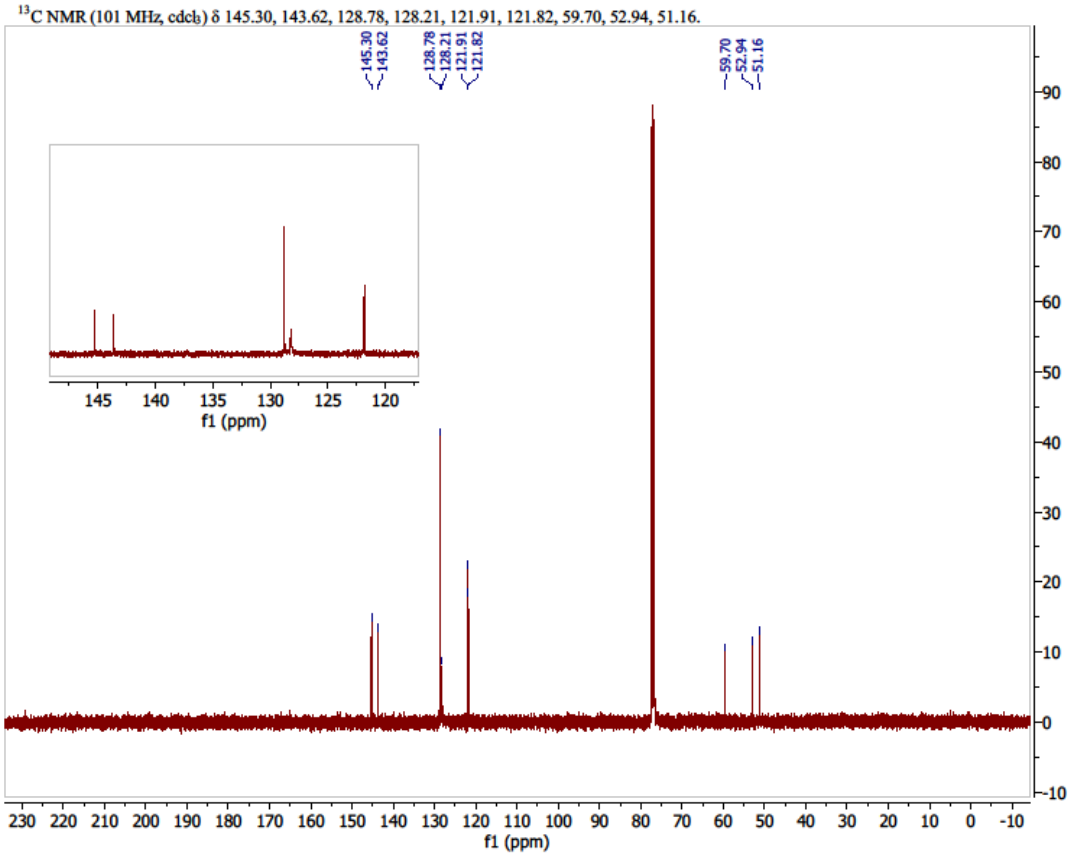

^{1}H NMR of Trifold carbinol precursor (2b):

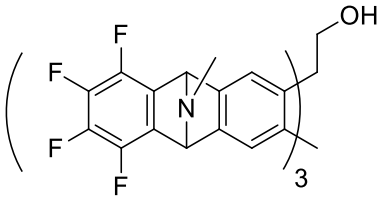

^{1}H NMR (400 MHz, Chloroform-*d*) δ 7.65 – 7.24 (m, 4H), 5.21 – 4.96 (m, 7H), 2.25 – 1.96 (m, 7H).

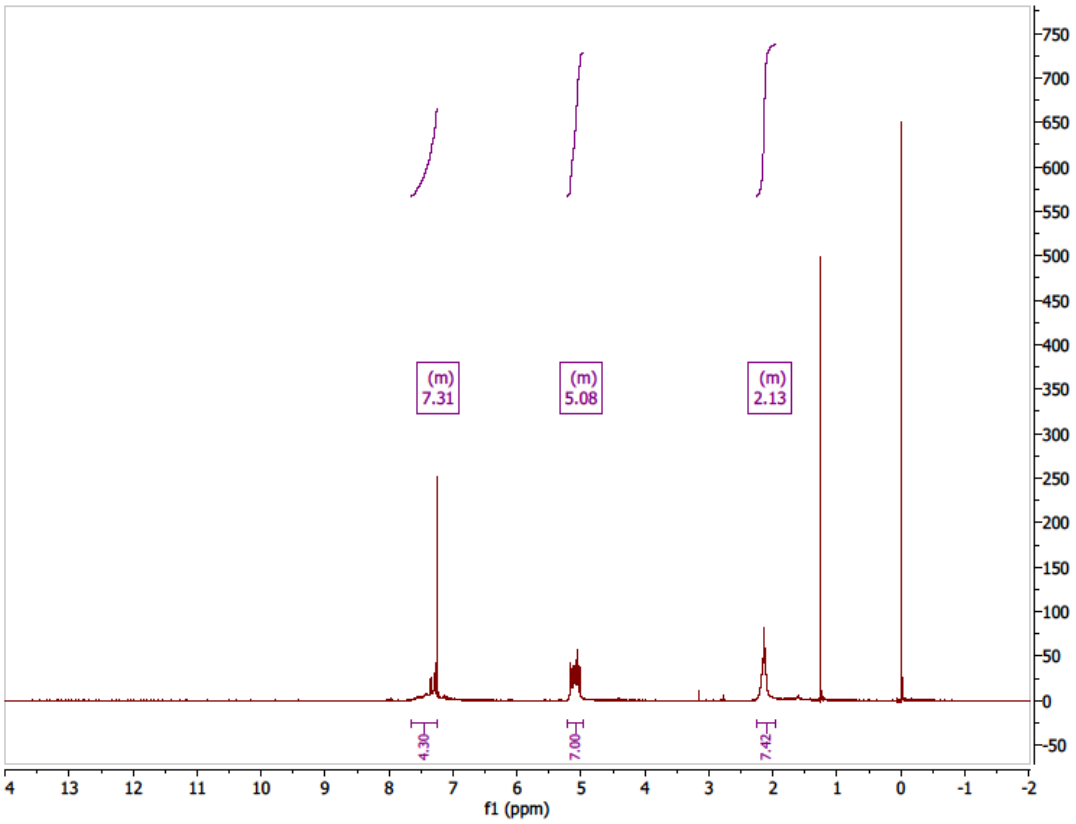

^{13}C NMR of Trifold carbinol precursor (2b):

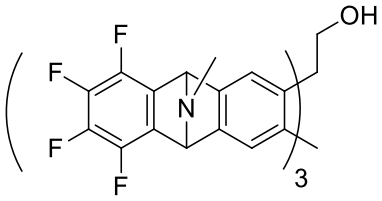

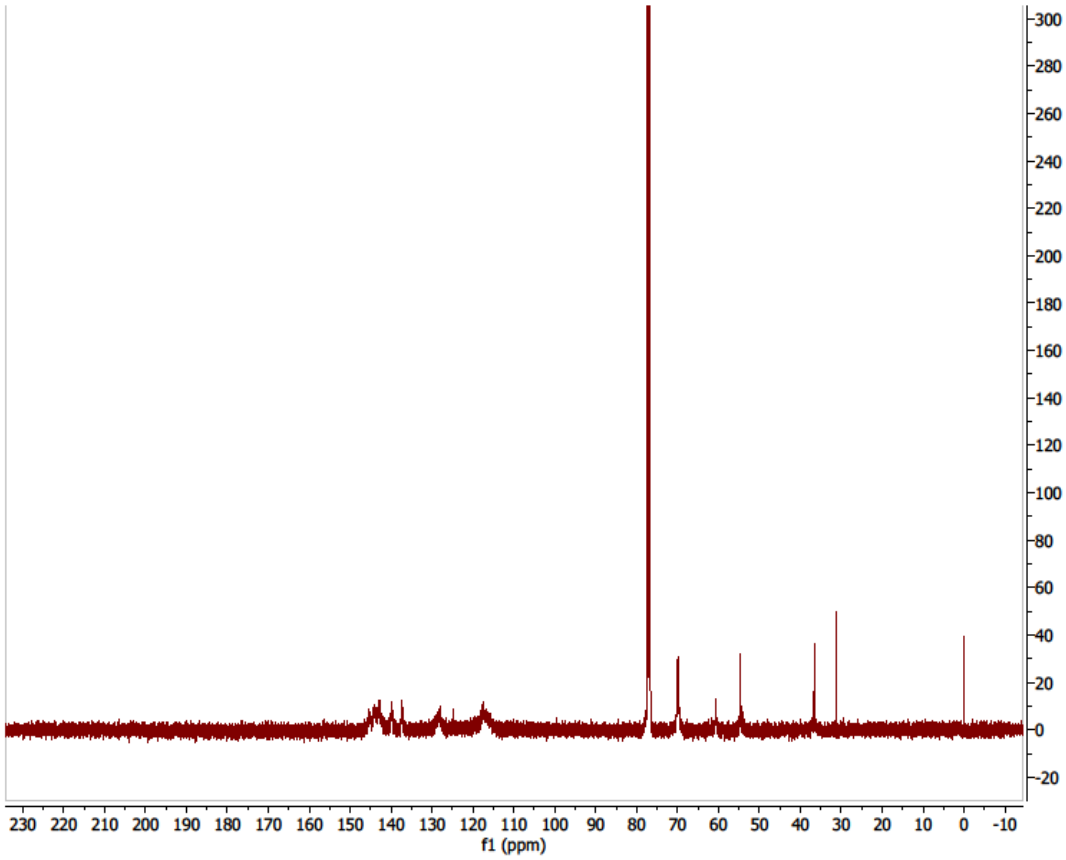

^{1}H NMR of Fantrip Carbinol (1b):

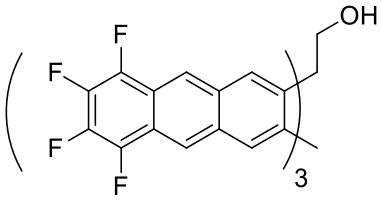

^{1}H NMR (400 MHz, Chloroform-*d*) δ 8.57 (s, 3H), 8.52 (s, 3H), 8.24 (s, 3H), 8.13 (s, 3H), 5.89 (s, 1H), 5.74 (d, *J* = 4.1 Hz, 2H).

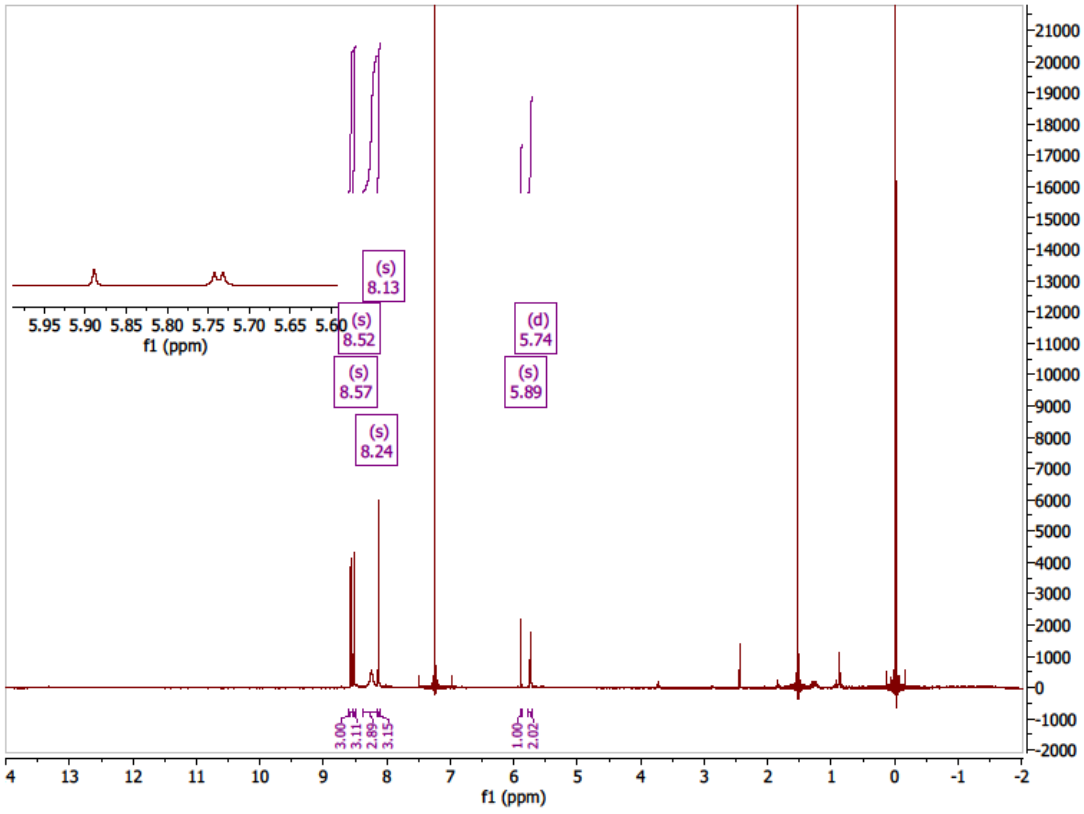

^{1}H NMR of Fantrip aldehyde:

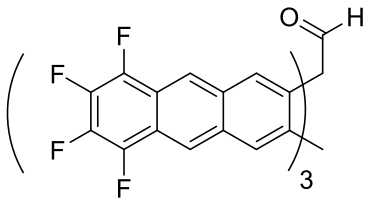

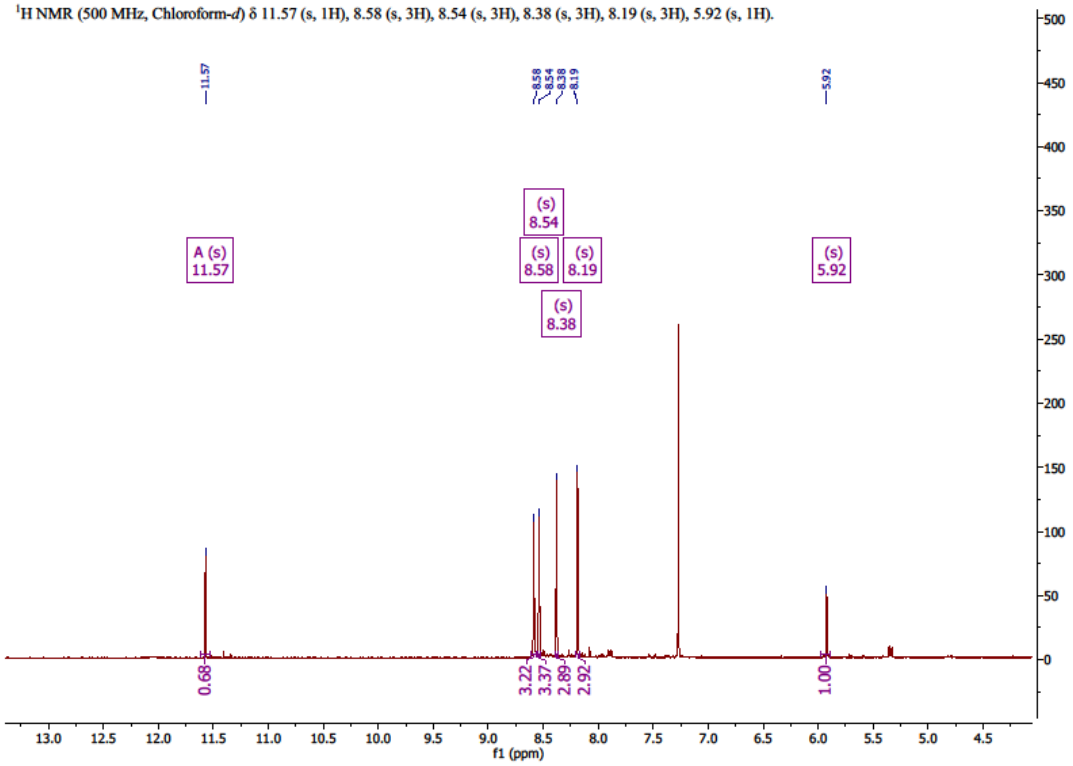

^{1}H NMR of Fantrip Imine (12):

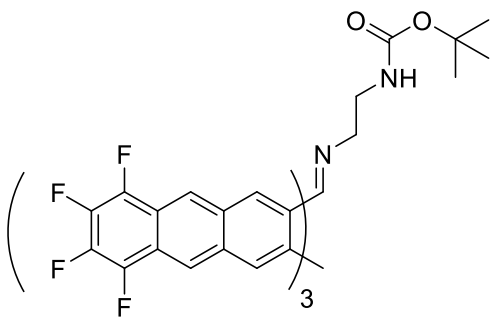

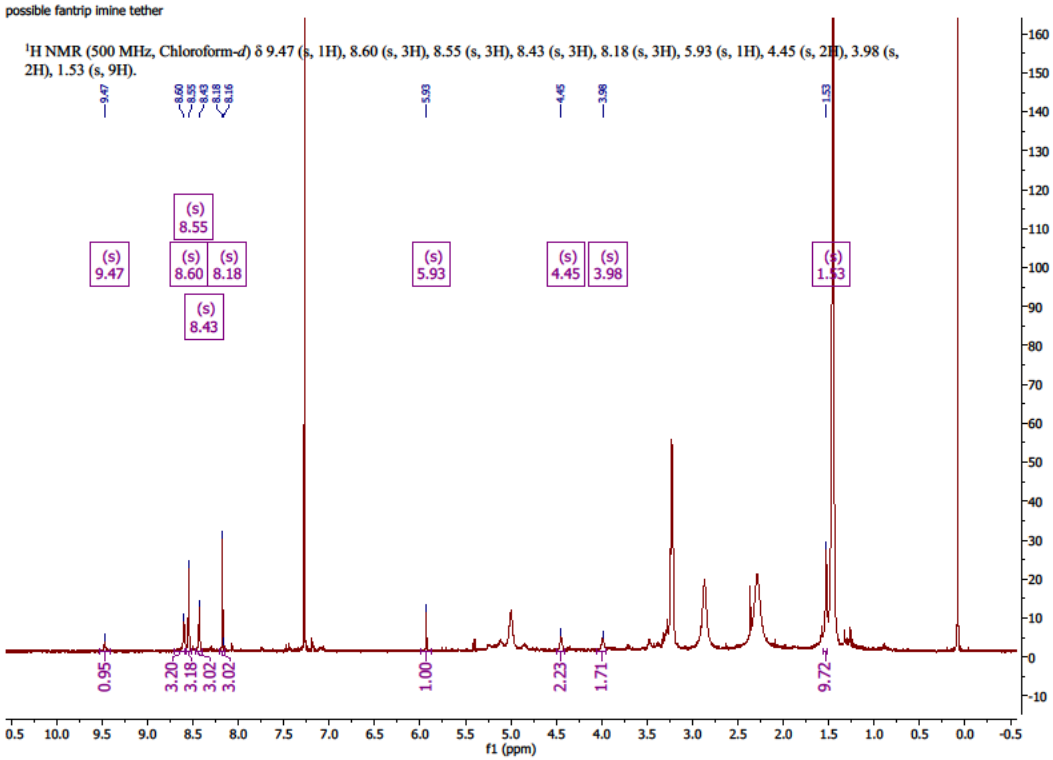

Fantrip Boc-Amine(13):

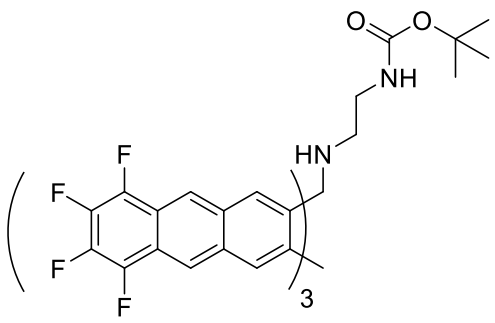

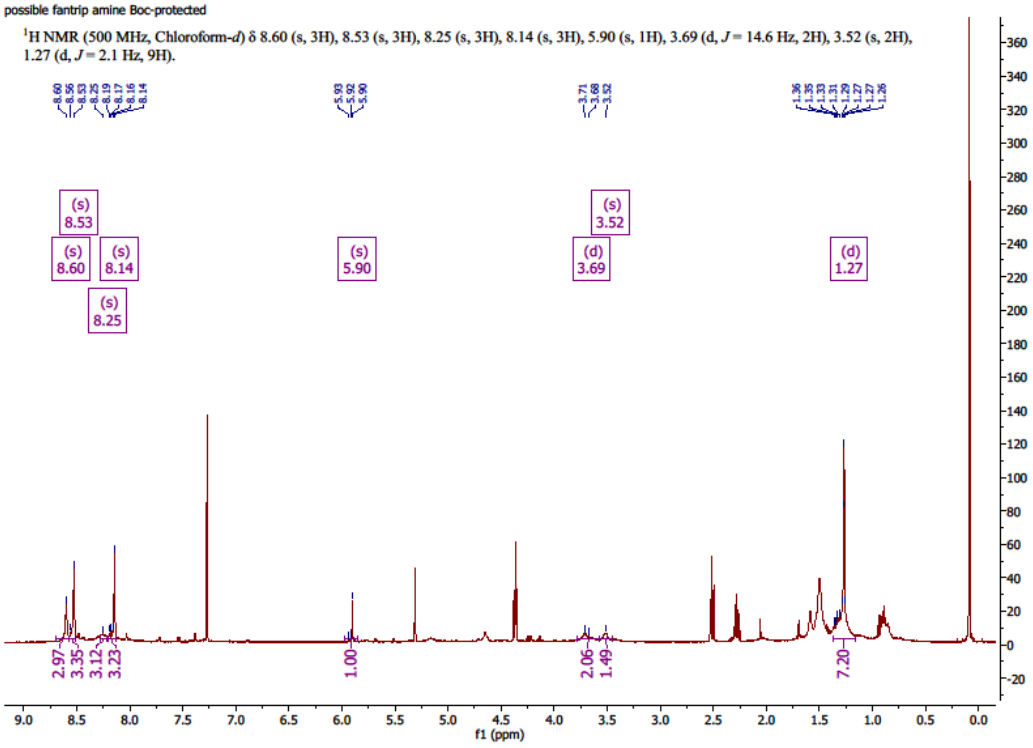

Fantrip Amine (14):

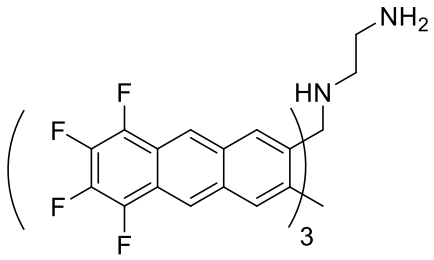

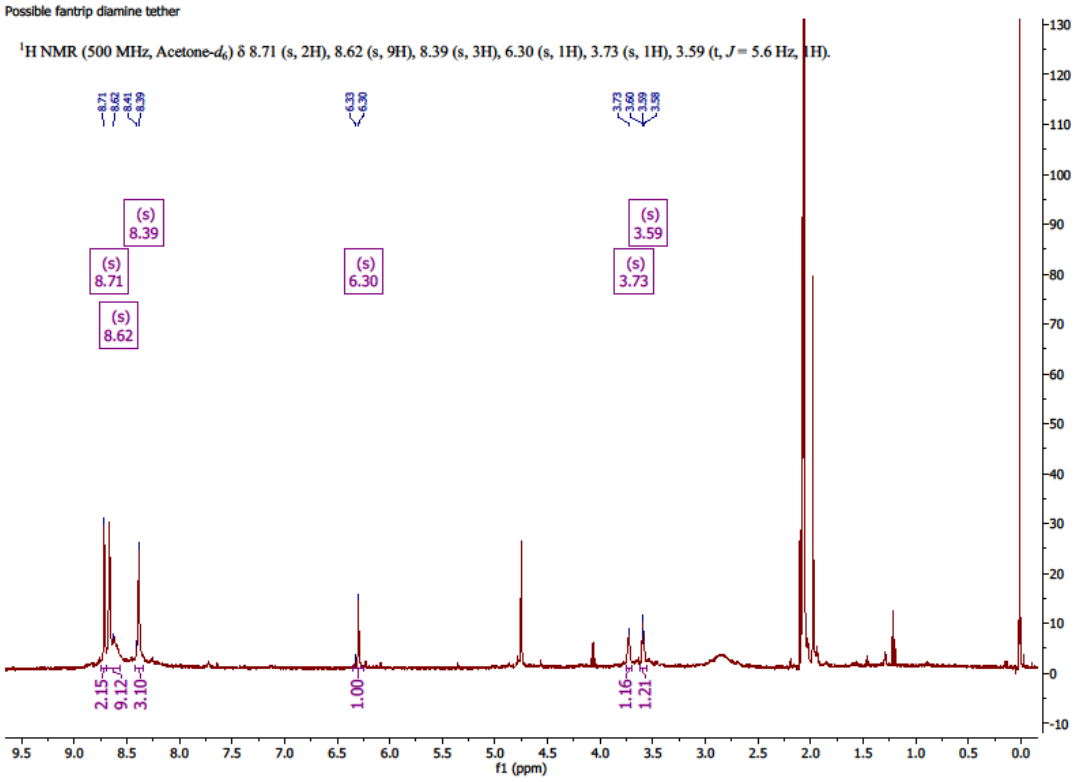

IR:

9,10[1',2']-Benzenoanthracene-9(10H)-1,3-dioxalane (6):

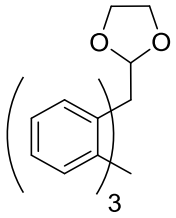

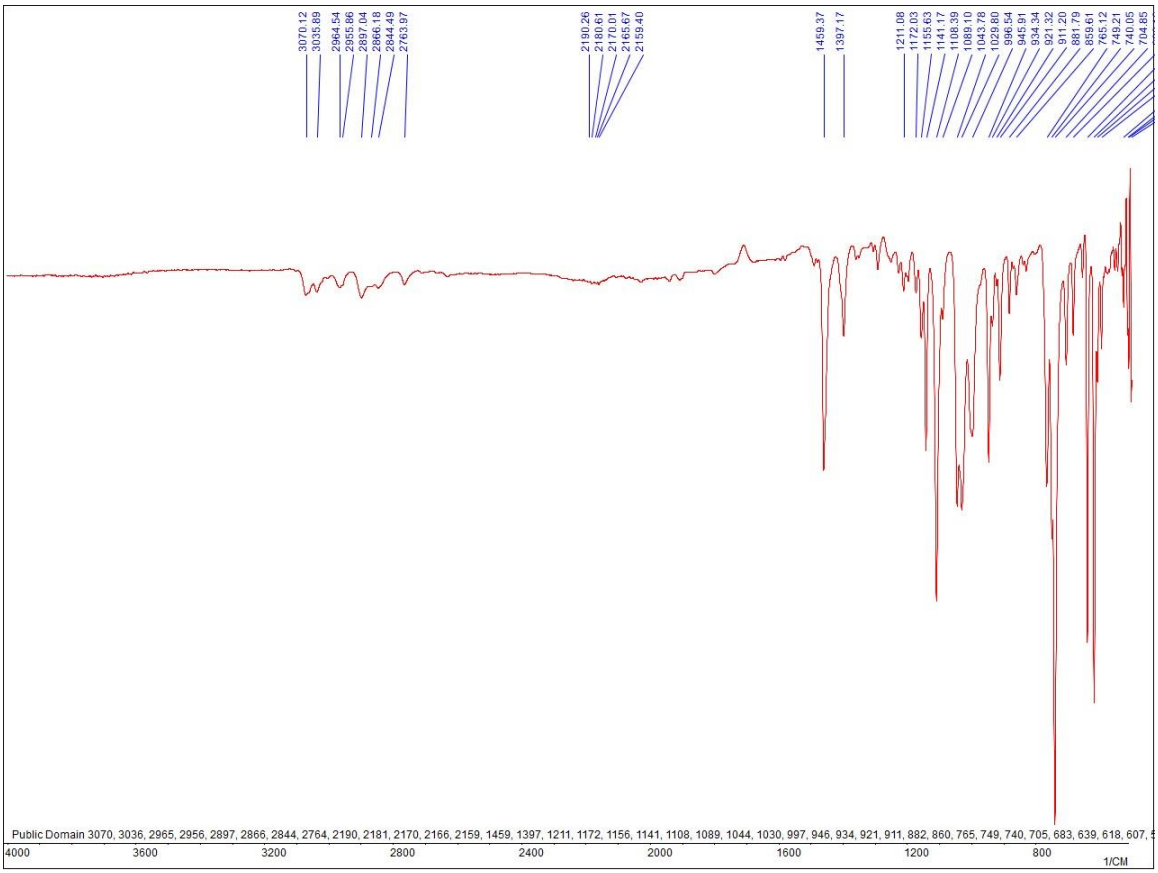

9,10[1',2']-Benzenoanthracene-9(10H)-carboxaldehyde (5):

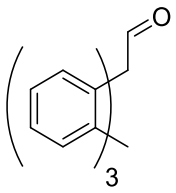

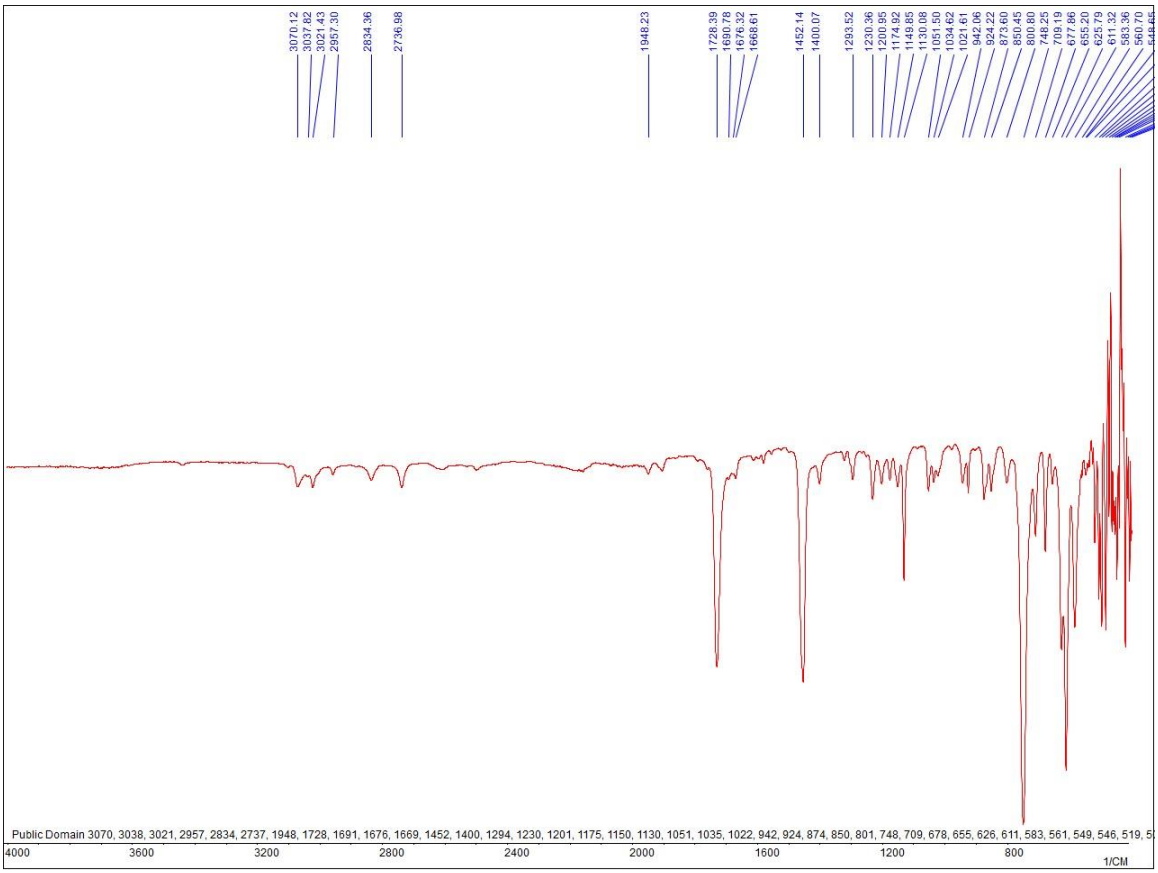

9,10[1',2']-Benzenoanthracene-9(10H)-carboxylic acid (4a):

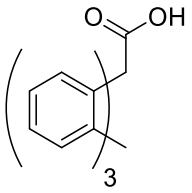

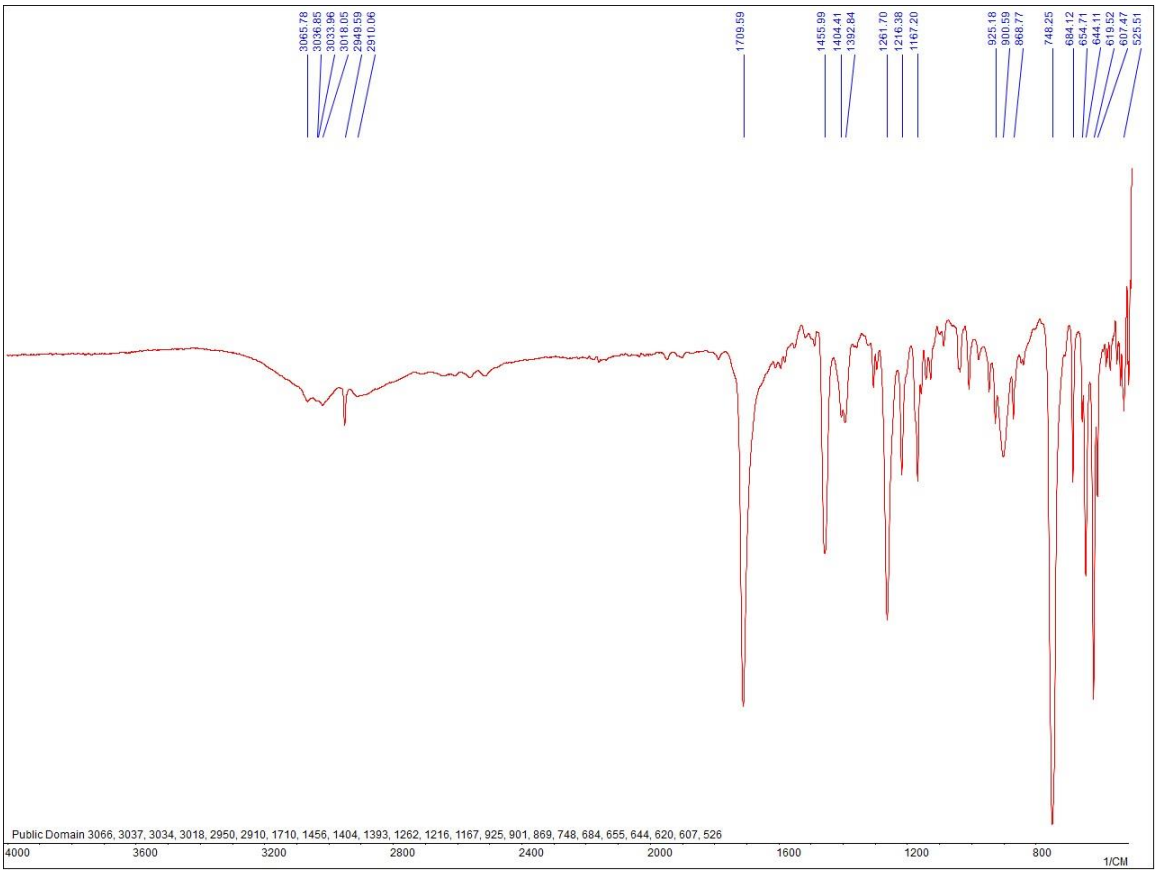

2,3,7,6,14,15-hexabromotriptoic acid (3a):

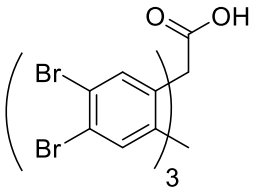

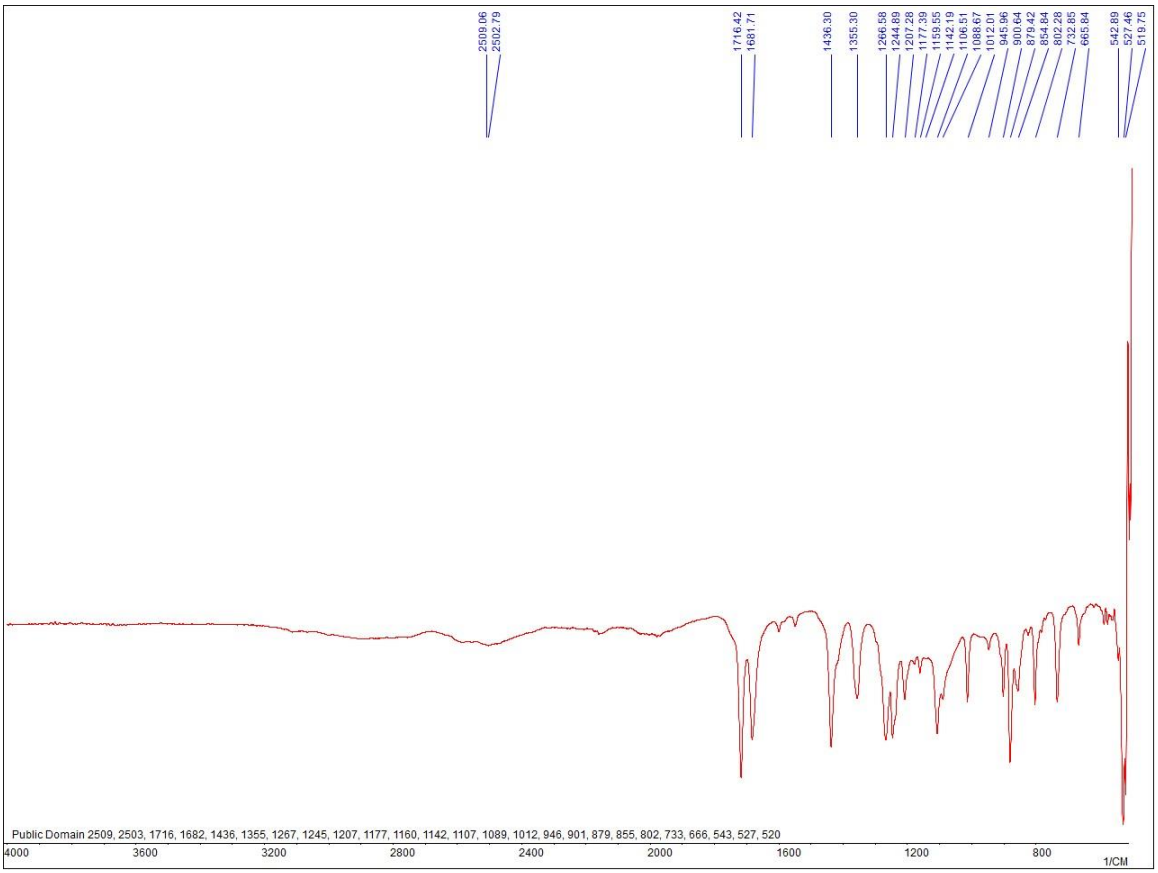

Carboxy fantrip trifold adduct (2a):

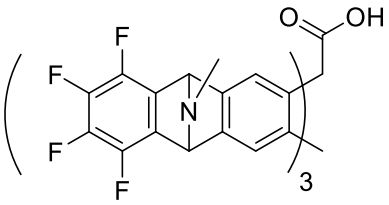

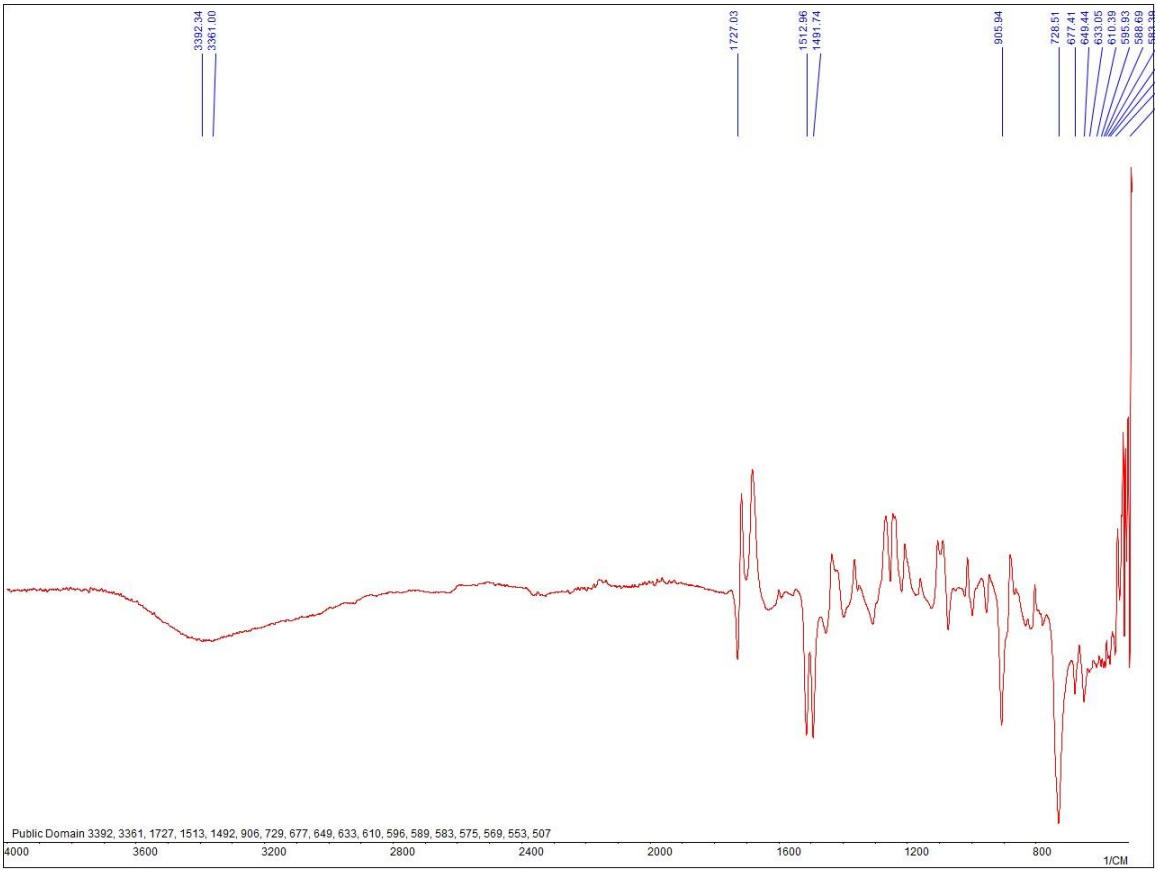

Carboxy Fantrip (1a):

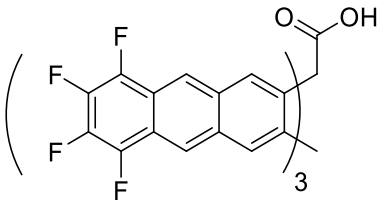

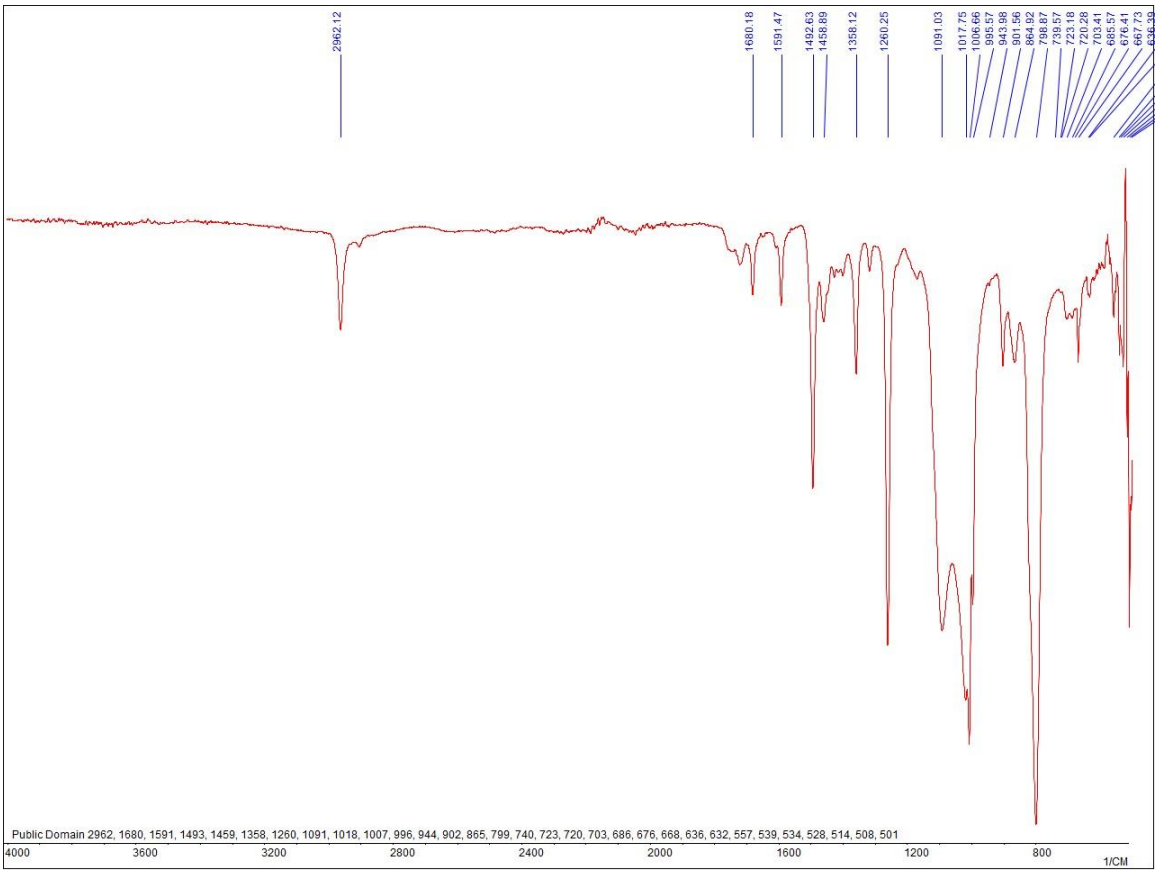

9,10[1',2']-Benzenoanthracene-9(10H)-carbinol (4b):

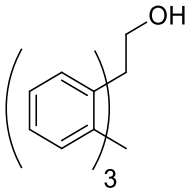

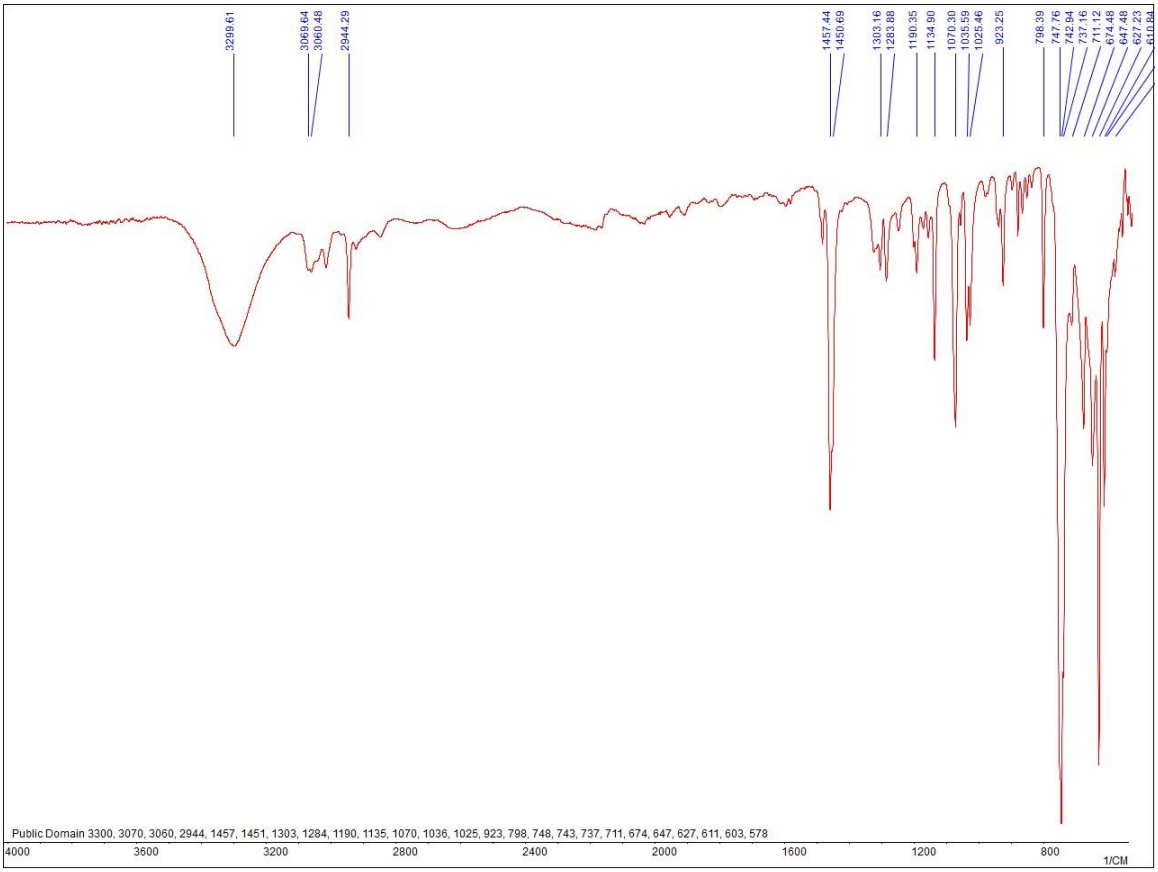

Carboxy hexabromo-triptycene (3b):

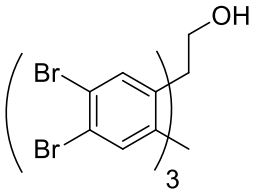

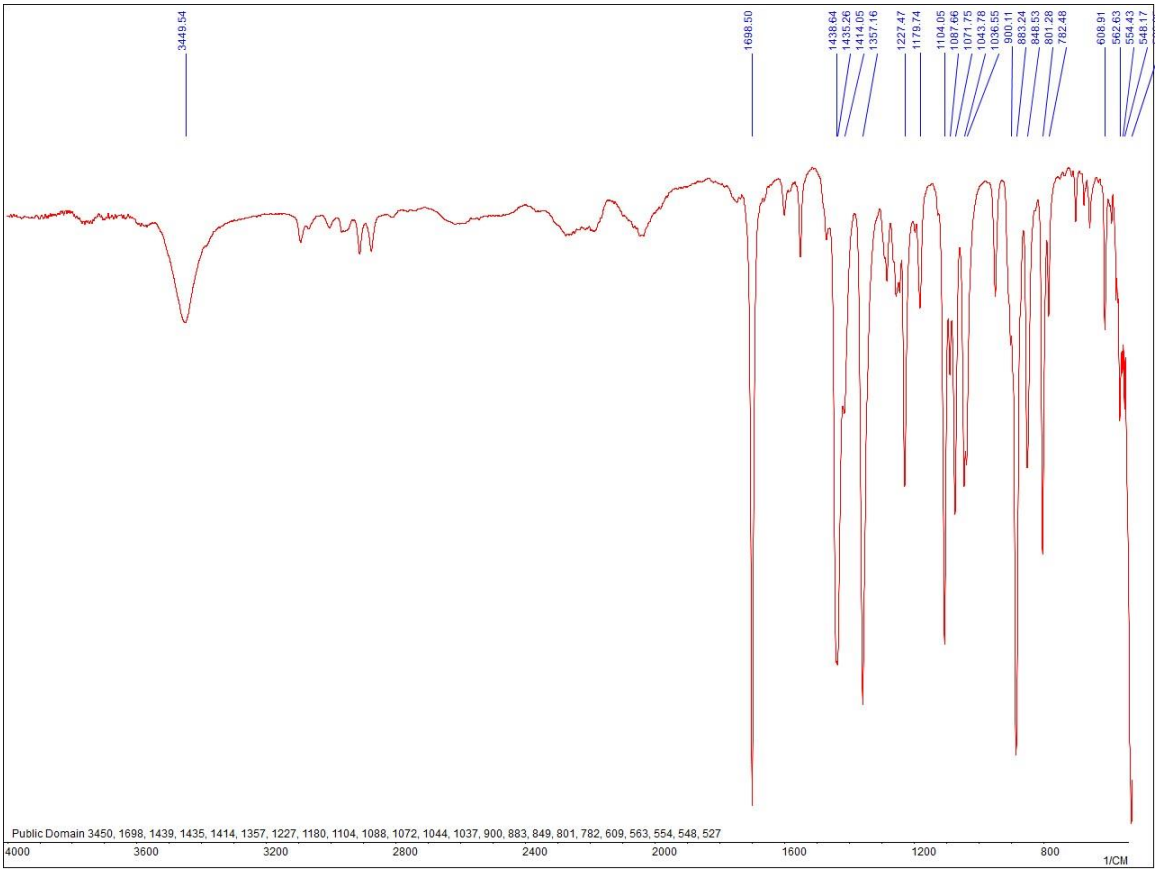

Trifold carbinol precursor (2b):

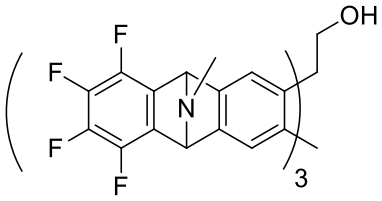

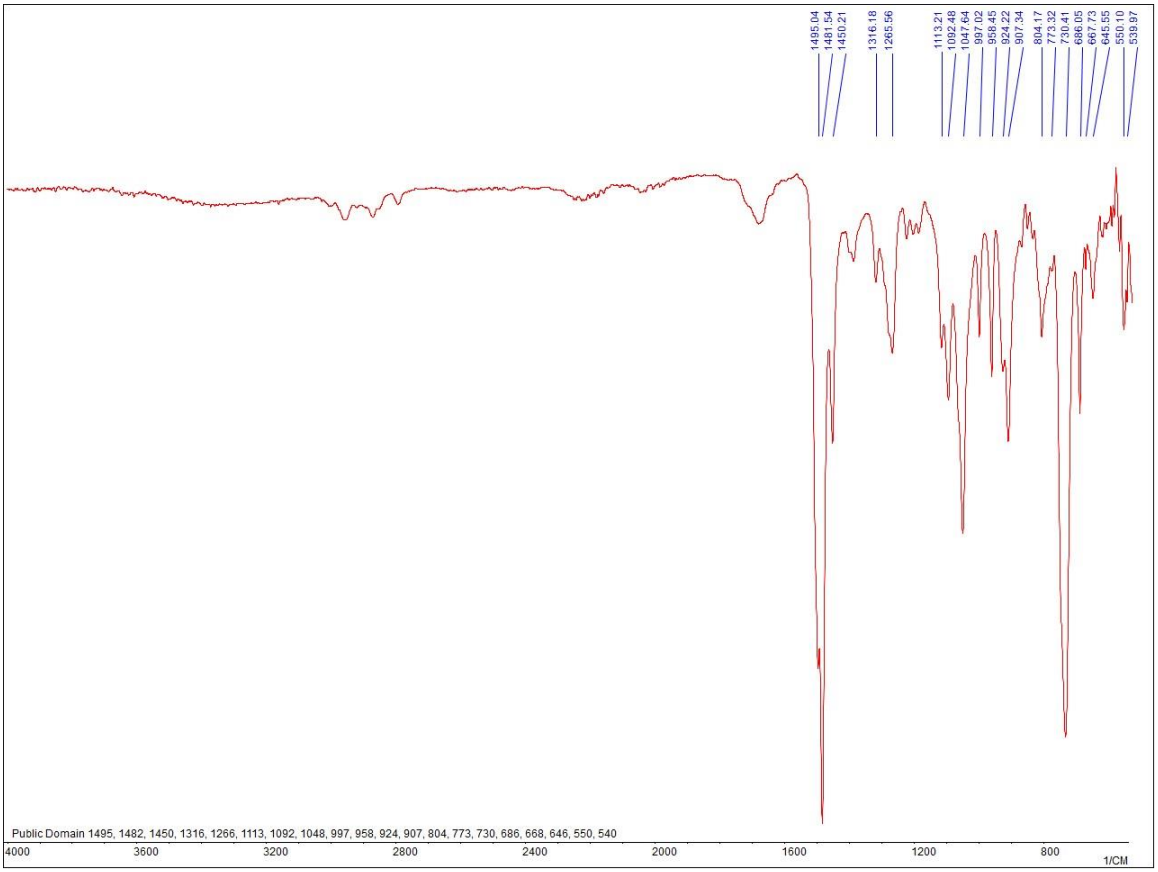

Fantrip Carbinol (1b):

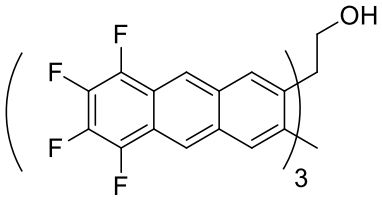

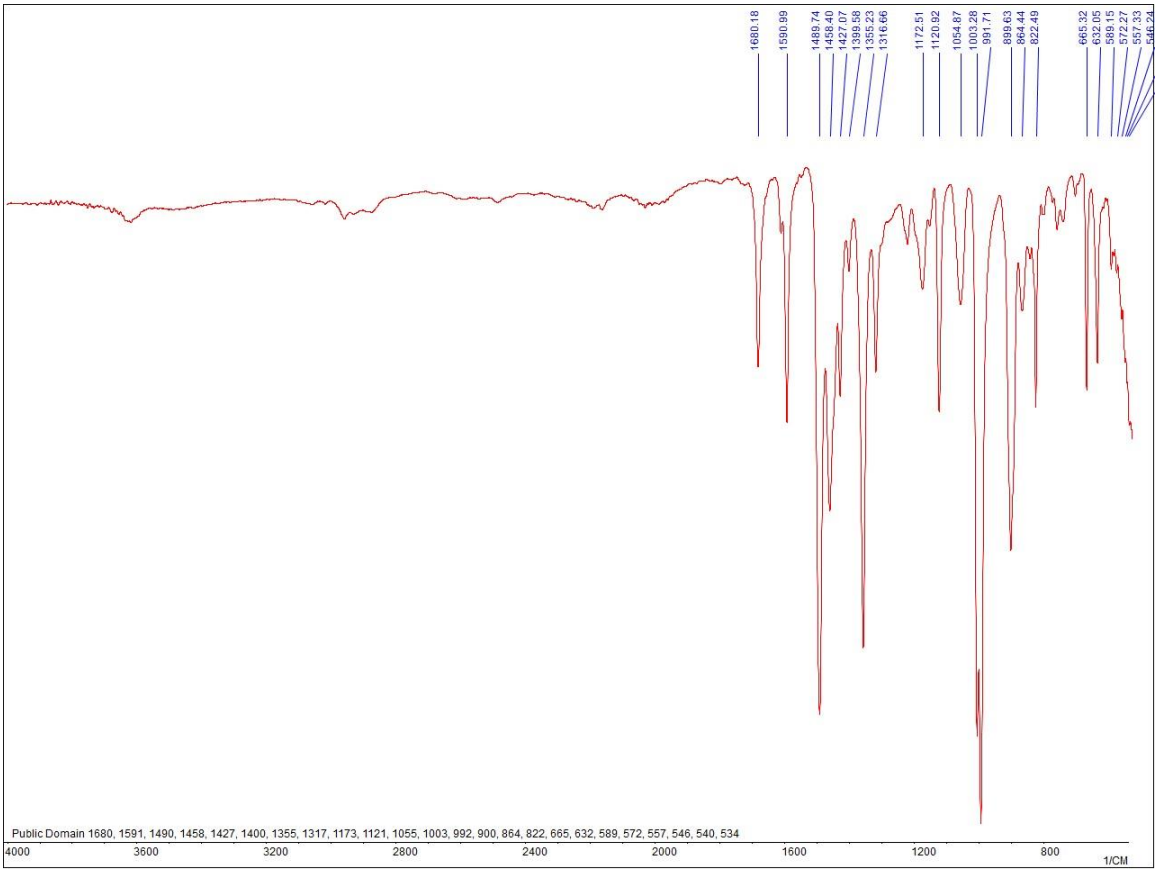

9,10[1',2']-Benzenoanthracene-9(10H)-carboxylic acid (4a):

Chemical Formula: $C_{21}H_{14}O_2$

Exact Mass (M-H): 297.0975

Found: 297.0972

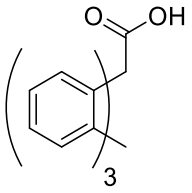

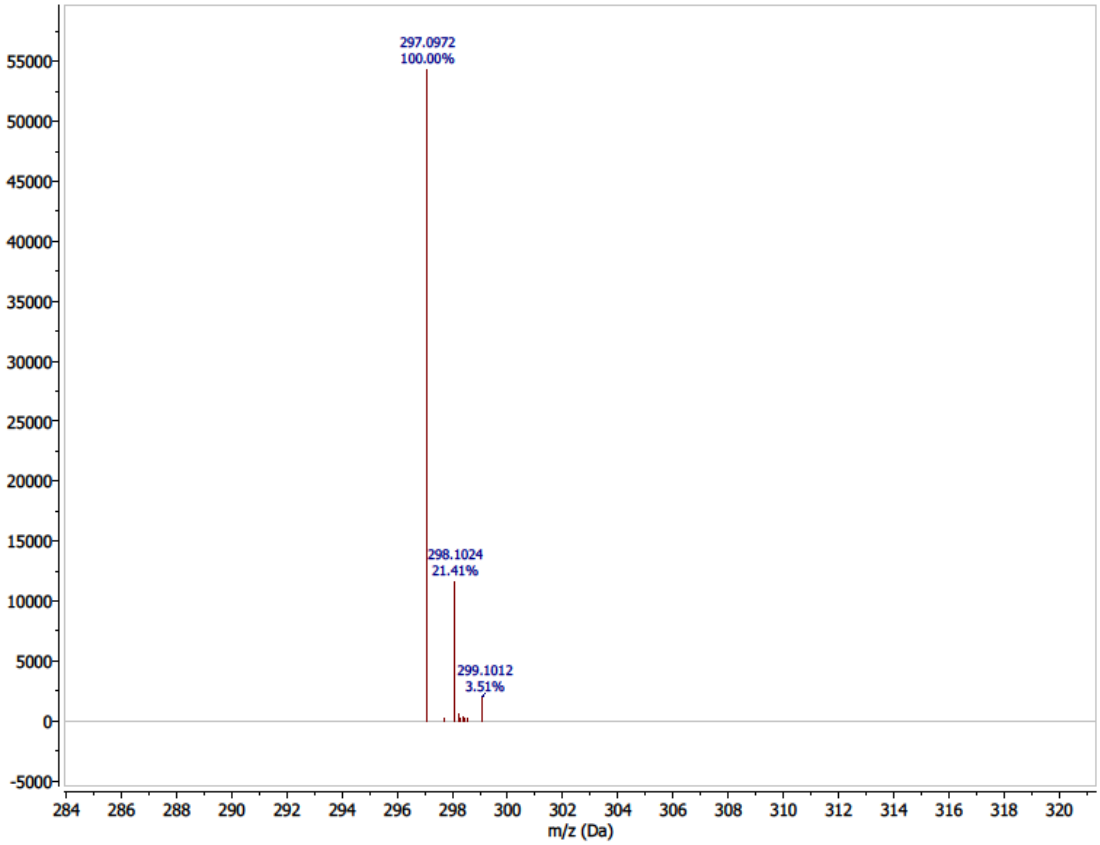

2,3,7,6,14,15-hexabromotriptoic acid (3a):

Chemical Formula: $C_{21}H_8Br_6O_2$

Exact Mass (M-H): 770.5565

Found: 770.5587

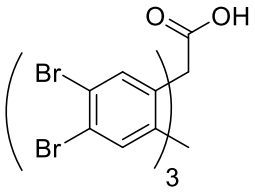

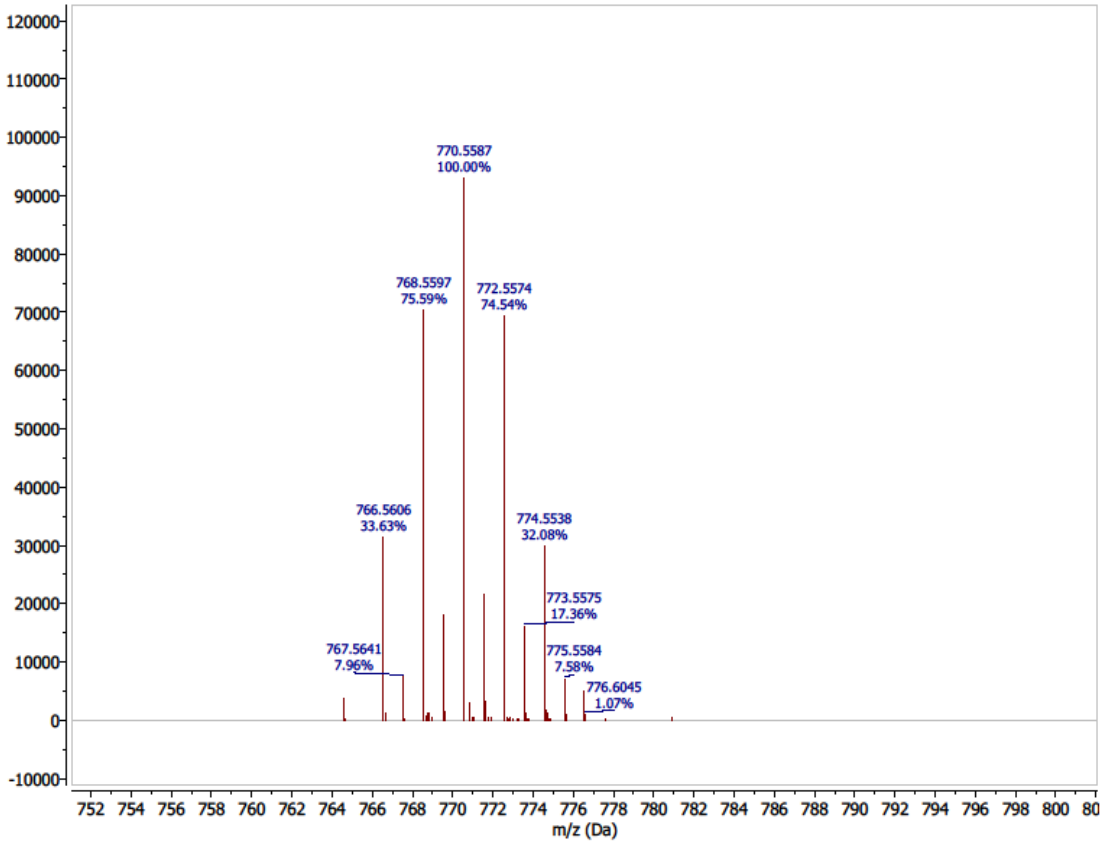

Carboxy Fantrip (1a):

Chemical Formula: $C_{45}H_{14}F_{12}O_2$

Exact Mass: 814.0729

Found: 813.0731

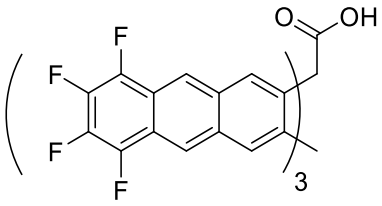

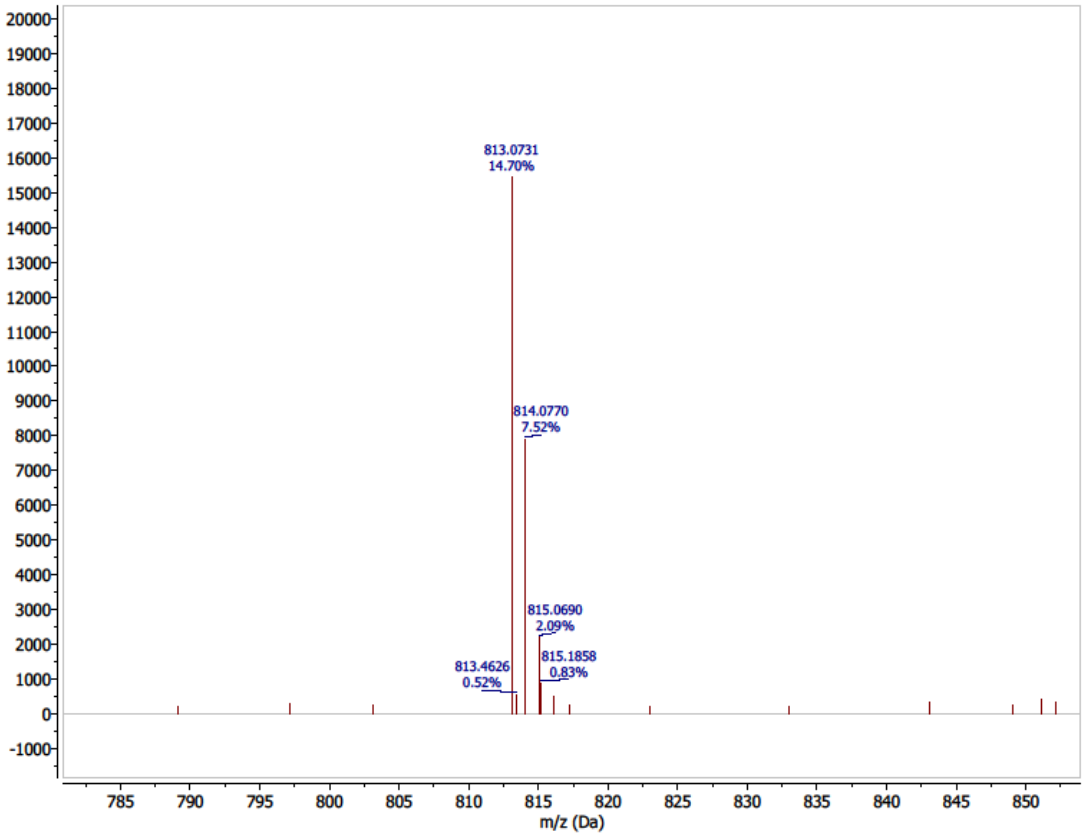

9,10[1',2']-Benzenoanthracene-9(10H)-carbinol (4b):

Chemical Formula: $C_{21}H_{16}O$

Exact Mass: 285.1274

Found: 284.1248

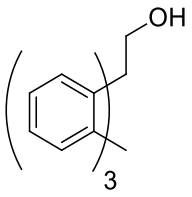

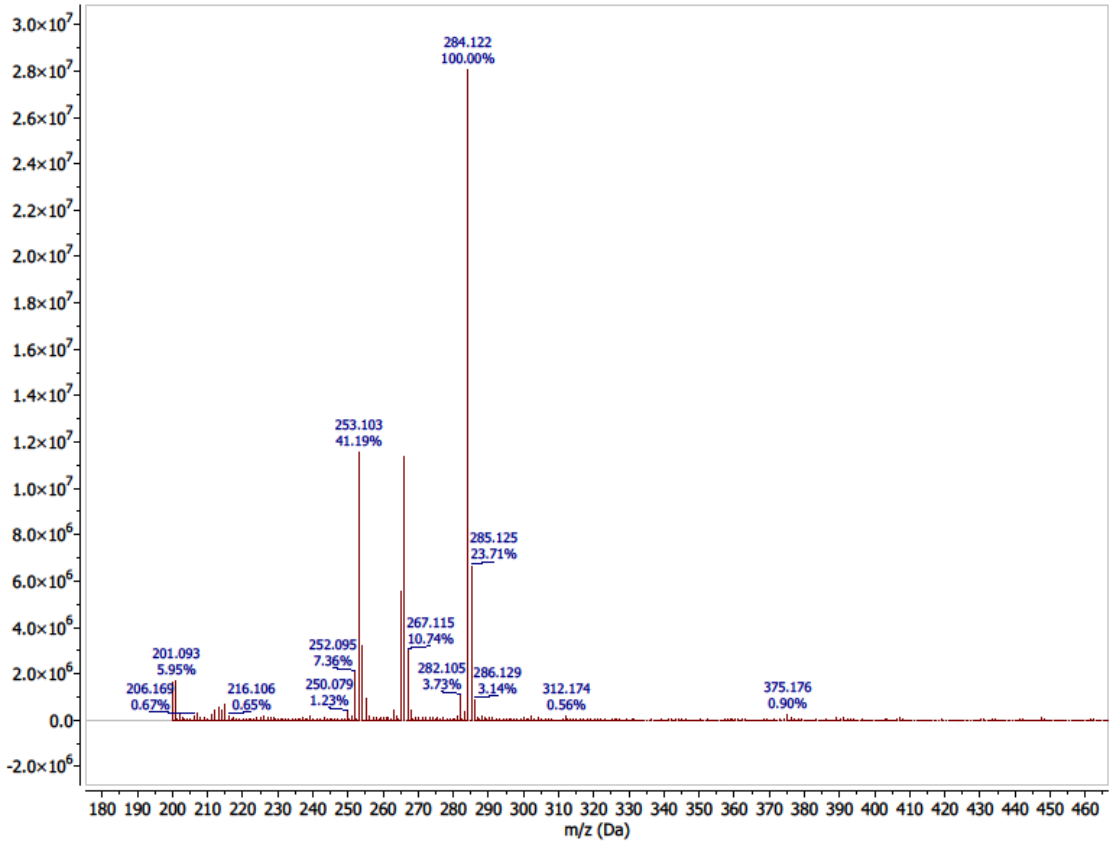

2,3,7,6,14,15-Hexabromotriptycene-carbinol (3b):

Chemical Formula: $C_{21}H_{10}Br_6O$

Exact Mass: 757.5845

Found: 757.5815

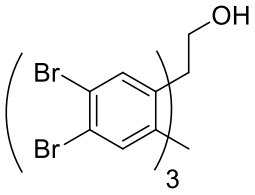

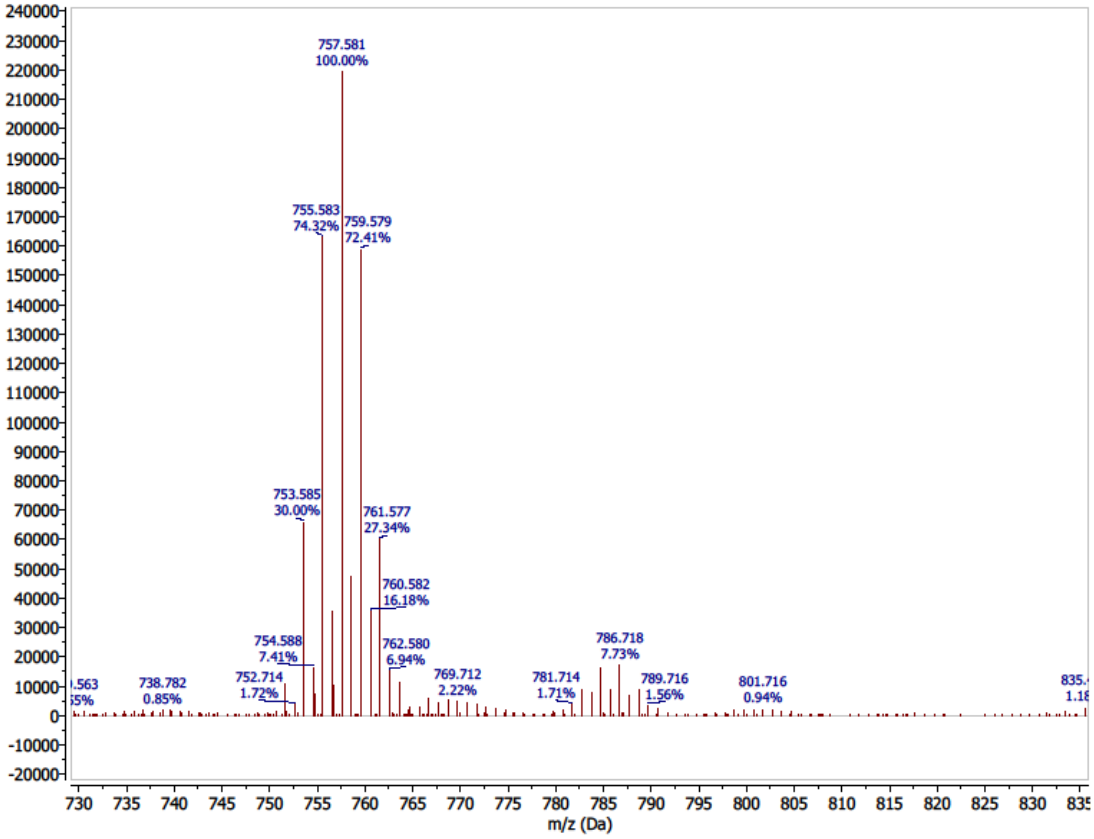

Trifold carbinol precursor (2b):

Chemical Formula: $C_{48}H_{25}F_{12}N_3O$

Exact Mass: 888.1879

Found: 888.1892

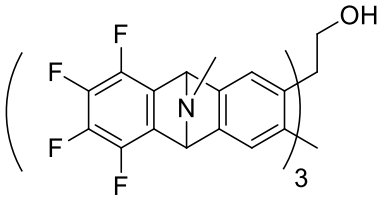

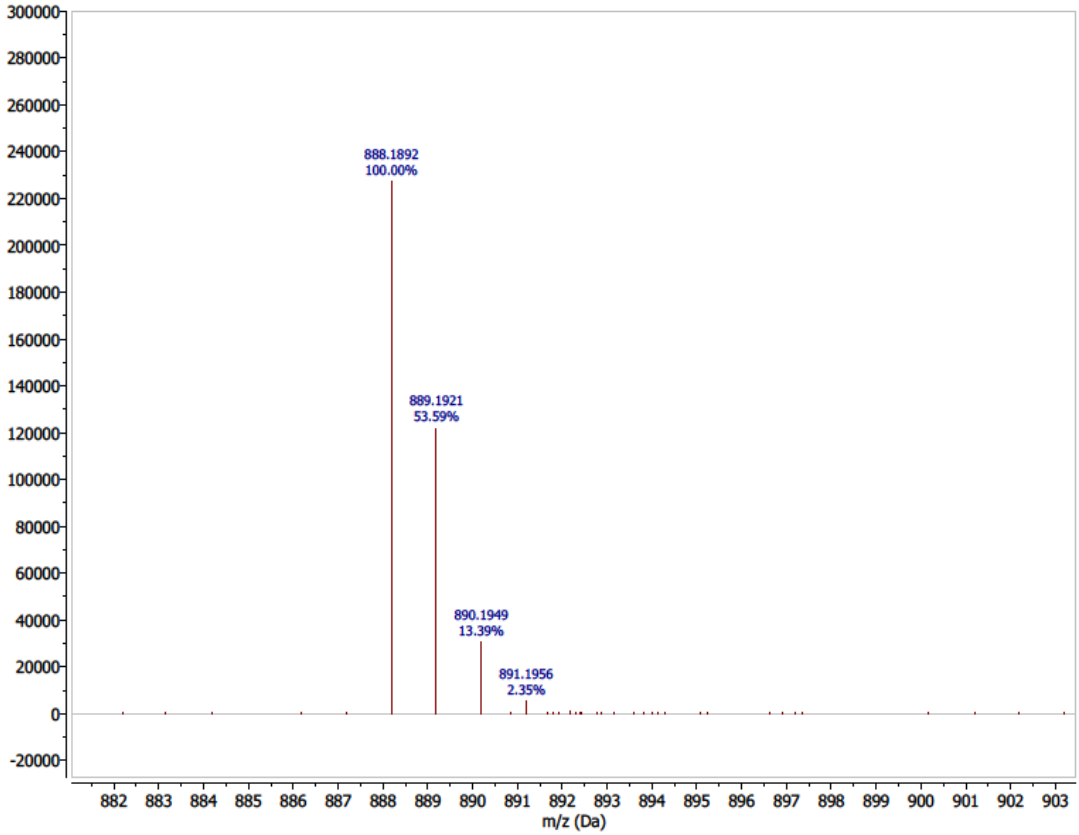

Fantrip carbinol (1b):

Chemical Formula: $C_{45}H_{16}F_{12}O$

Exact Mass: 800.1010

Found: 800.1046

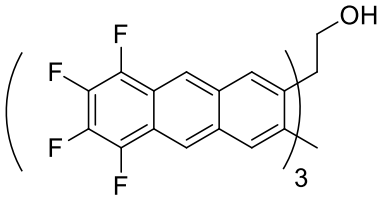

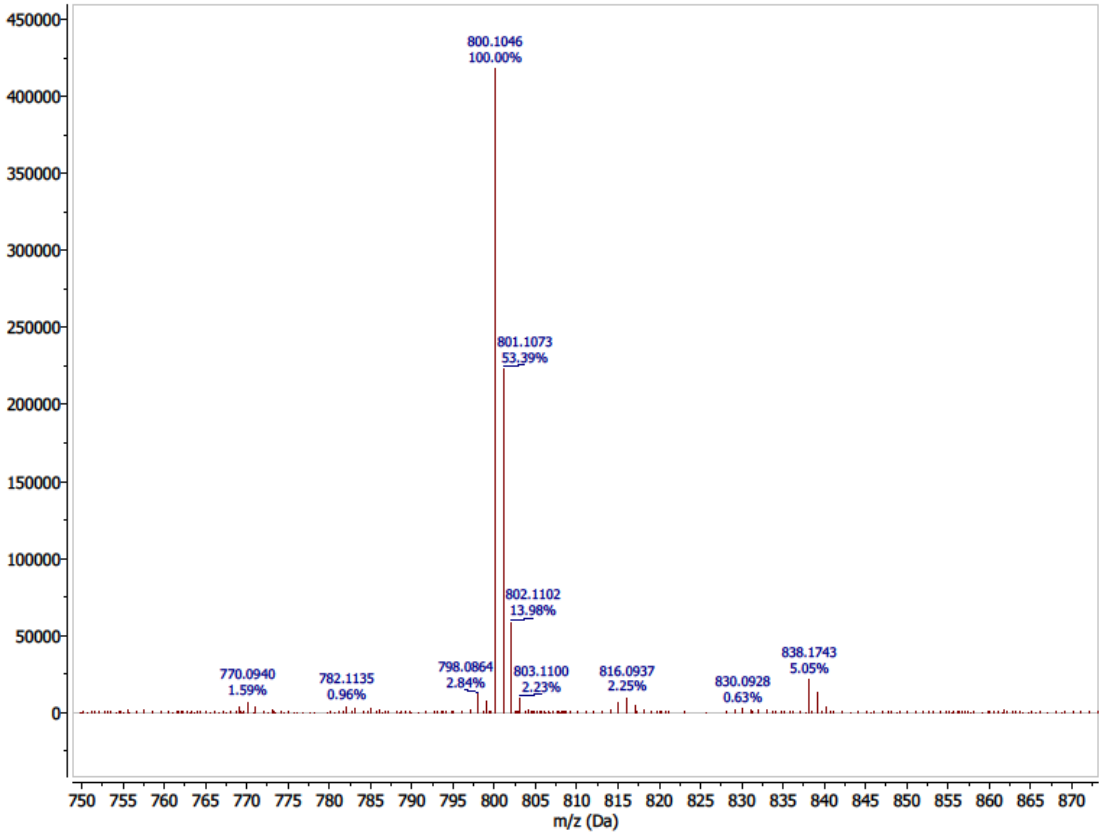

UV-Vis Carboxy Fantrip Monomer (1a):

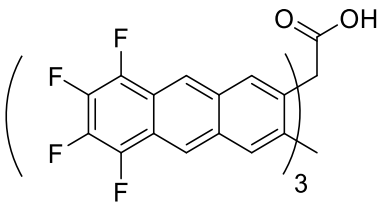

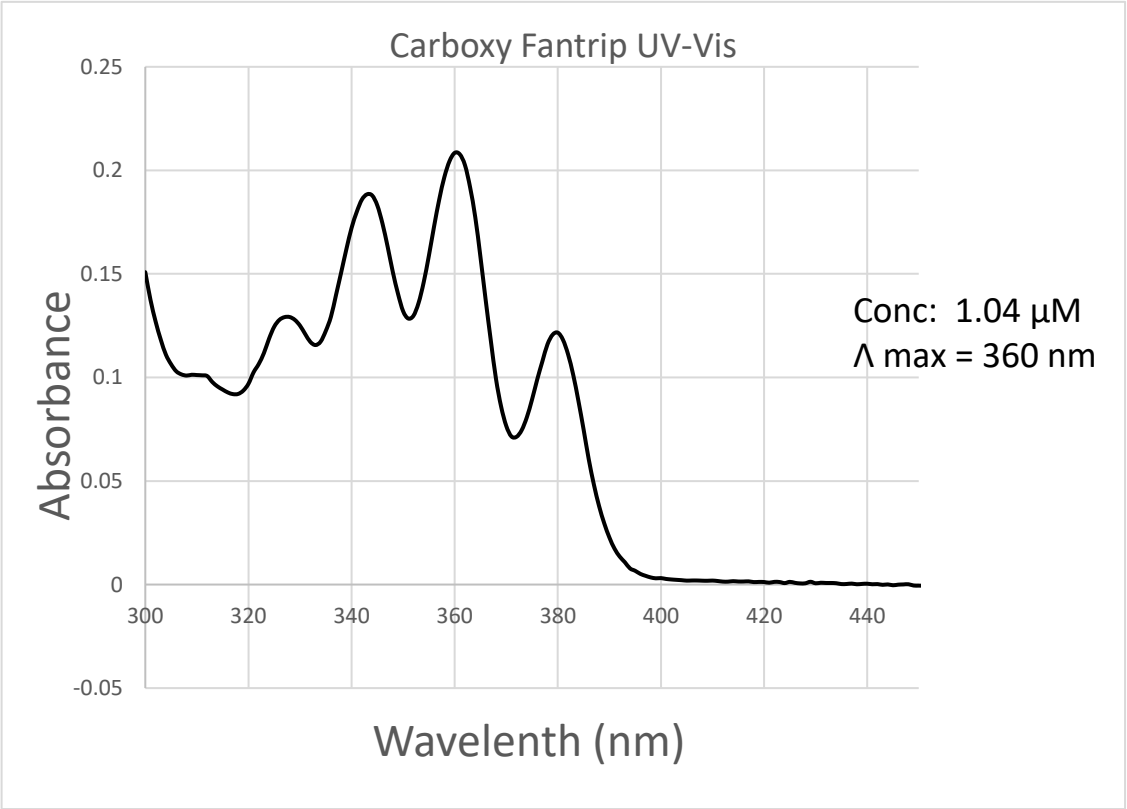

Chapter 3: Poly(Carboxy Fantrip) Langmuir Method

The Langmuir-Blodgett method is widely utilized for depositing monolayer films on solid substrates while maintaining precise control over thickness and monomer organization. Traditionally, two-dimensional films on the air/water interface involve self-assembled monolayers (SAMs) comprising a polar anchor and a hydrophobic tail bonded together by intermolecular forces (IMFs). Amphiphilic units densely pack into highly ordered structures, allowing for the creation of predictable lattices with applications in sensors, optoelectronic devices, or as ultra-thin membranes for surface modification.[77] Recent advancements in our monomer synthesis have extended this technique to fabricate covalently bonded two-dimensional polymers (2DPs).

As reported in Chapter Two, our monomer, carboxy fantrip, is singularly functionalized with a carboxylic bridgehead at the central position of the [2.2.2] bicyclic core, serving as a polar anchor. The hydrophobic end is composed of three tetrafluoroanthraceno blades. The carboxylic acid causes three anthraceno blades to float perpendicular to the water (i.e., with the bridgehead-bridgehead vector normal to the water surface), promoting a hexagonal monomer packing with blades of adjacent monomers cofacially aligned. This packing is conducive to photodimerization under UV irradiation via a [4+4] cycloaddition (refer to Figure 3.1).

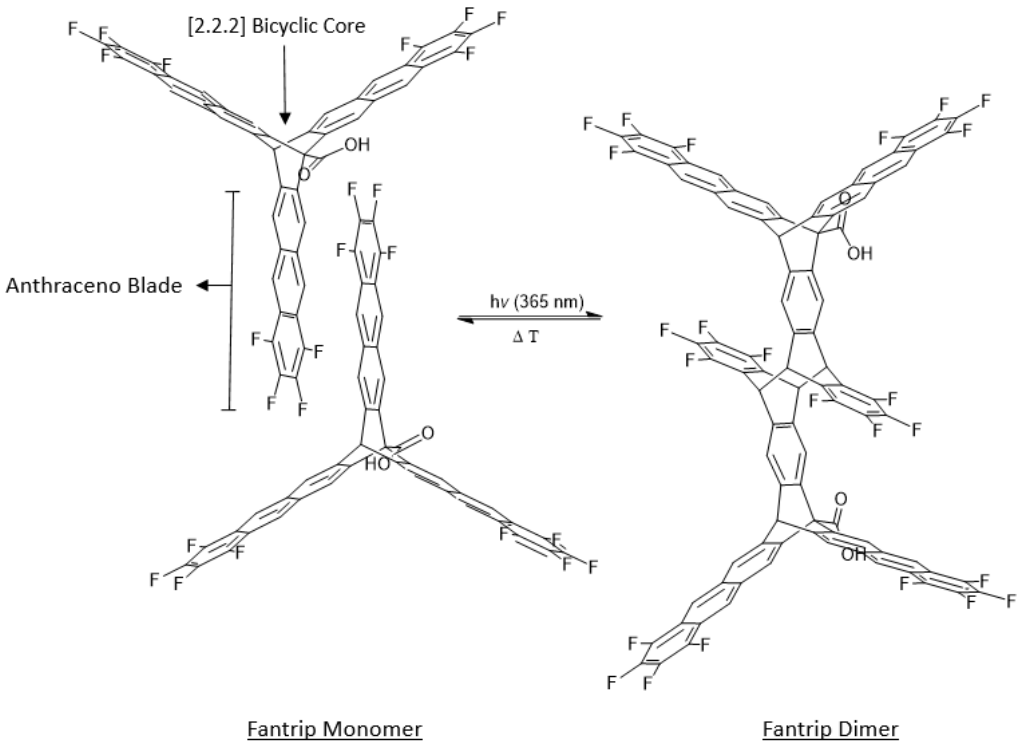

Figure 3.1 Fantrip monomer anti-parallel packing (left) Fantrip dimerization (right).

The polymerized carboxy fantrip films transferred onto SiO_2/Si wafers are molecularly thin (~1.5 nm) and possess a rigid trigonal star structure with monodisperse pores. Unfunctionalized fantrip, as reported, exhibited monodispersed pores of ~9 Å with a high pore density of ~3.3×10^{13} pores cm^{-1} (Refer to figure 3.2).[70]

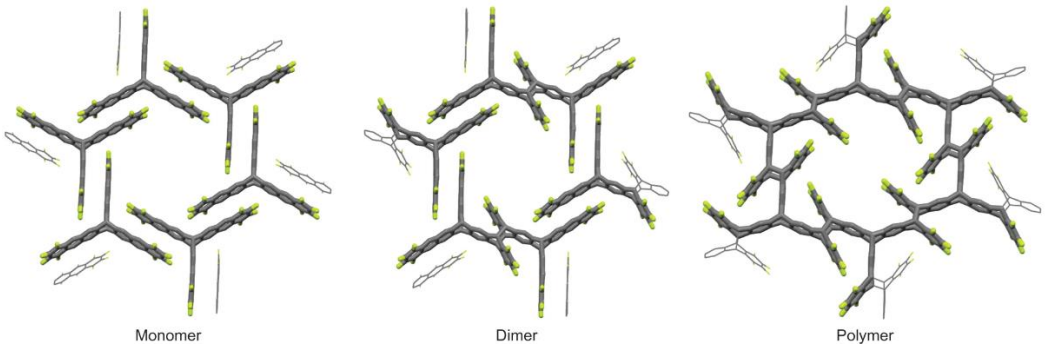

Figure 3.2 Fantrip polymerization: Fantrip monomers preorganized in a honeycomb lattice (left). Two fantrip blades intermolecularly dimerize forming dimer (center). Complete dimerization of all neighboring anthracene blades (right).

Producing a highly ordered film through photo-polymerization critically hinges on understanding the packing of monomers on the air/water surface. Brewster angle microscopy (BAM) is employed to visualize monomer spreading, compression, and annealing, thereby monitoring the self-assembled monolayer (SAM) to gain insight into proper dimerization. After to photopolymerization and transfer to substrate, optical microscopy could reveal the morphology of the resulting polymer.

3.1 Spreading of Monomer to the Subphase

Achieving homogeneous monolayers relies on specific spreading techniques for monomers on the air/water interface. The adsorption of monomers at the interface is influenced by the spreadability of the solvent, the concentration of monomer in the dropping solvent, and the time taken for solvent evaporation from the air/water interface. All these factors collectively contribute to the effective spreading of the molecule on the subphase.

The choice of organic solvent is crucial to ensure full dissolution of the monomer in the solution, suppressing the formation of aggregates. The presence of aggregates interfere with the formation of monolayers and impact the isothermal compression process. A volatile and water-immiscible spreading solvent, chloroform plays a crucial role in the adsorption process of carboxy fantrip monomer on the air/liquid interface. Although a relatively dilute concentration (0.07 mg/ml) is required for effective spreading on the trough, prolonged storage can result in the formation of crystals. Due to the propensity of carboxy fantrip to readily recrystallize from chloroform, it becomes necessary to undertake frequent solution preparations to prevent unwanted monomer aggregation.

Water-miscible solvents, such as methanol, ethanol, and isopropanol, have been utilized in a range of applications to alleviate colloidal aggregation in polymers and graphene oxides (GO).[78–80] Although colloidal dispersion and lower solvent toxicity make these solvents appealing, the miscibility alcohols and water induces turbulence within the subphase, causing a significant loss of spreading materials as the applied droplet intermixes (refer to Figure 3.3).[81]

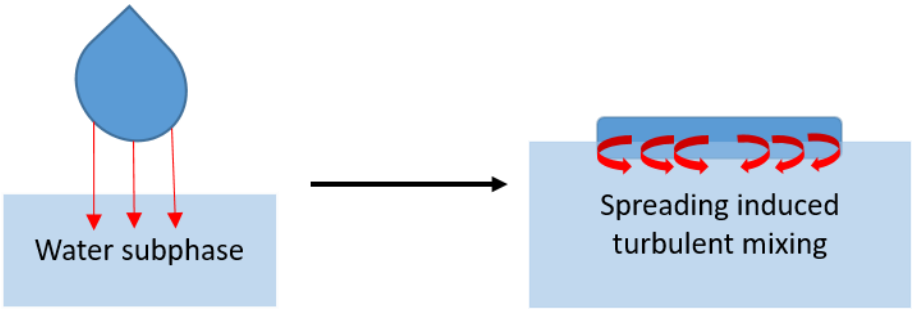

Figure 3.3 Water miscible spreading: Application of a water miscible droplet to a subphase (left). Spreading of a water-miscible droplet induces turbulence to water causing intermixing of analyte and subphase.

To spread the carboxy fantrip monomer on the air/water interface, a small droplet of dissolved monomer is drawn from the tip of the needle and gently pressed onto the air/liquid interface. Upon contact, the chloroform solution rapidly spreads across the subphase surface, ensuring homogeneous spreading of monomers. The hexagonal packing of monomers, crucial for complete polymerization, is highly dependent on the gentle deposition of the monomer solution. Given that chloroform has a greater density than water, it requires careful deposition of the solution to the surface. Haphazard introduction of the solution may result in the droplet submerging below the water's interface, causing an undefined loss of monomer to the subphase (refer to Figure 3.4).

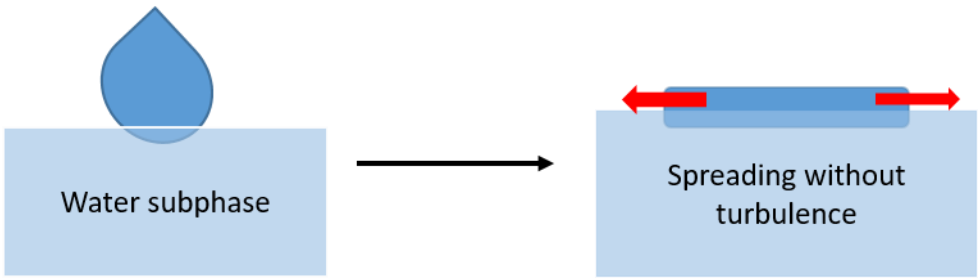

Figure 3.4 Water immiscible spreading: Gentle application of a droplet to a subphase. Immiscible solvent spreads over subphase surface without turbulent mixing or depression of solvent below the air/water surface.

To avoid overloading the subphase surface with solvent, it is crucial to ensure complete evaporation of the solvent between droplets. A waiting period of thirty seconds should be observed before adding each consecutive droplet to the subphase. Once the total amount of solution is loaded onto the surface, a resting time of 10-15 minutes should be allowed for the film to equilibrate. Failure to correctly blanket the monomer on the surface may result in blotchy domains upon photo-polymerization.

3.2 Isothermal Compression of Carboxy Fantrip

Langmuir-Blodgett troughs can be assembled in multiple ways, depending on the required application. The simplest setup involves a single barrier, where the monomer is adsorbed between a barrier and one side of the trough. This setup, previously utilized for the polymerization of poly(antrip-DEG), introduces large defects in polymerized films due to significant Wilhelmy plate deflection during compression (refer to Figure 3.5).

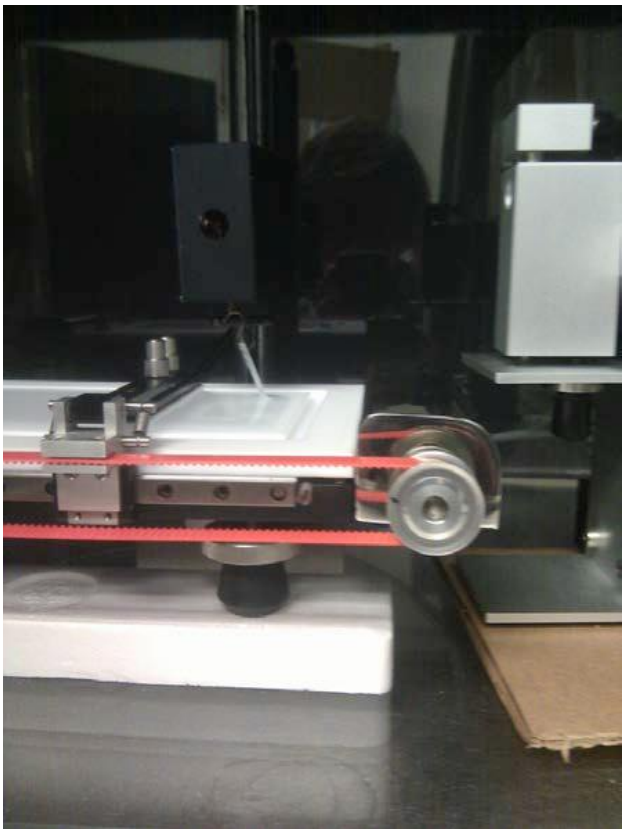

Figure 3.5 Single Barrier Trough: Image depicting large deflection of the Wilhelmy plate during compression of antrip-DEG. Upon relaxation of barrier, Wilhelmy plate falls back to a vertical position. Image taken by Daniel Murray.

The Wilhelmy plate, connected to a microbalance, serves to measure changes in surface pressure during the compression of monomers at the air/liquid interface. During polymerization, neighboring monomers dimerize, reducing the effective mean molecular area (MMA) and consequently decreasing surface tension—an event observed during dimerization. The decrease in MMA during polymerization results in the Wilhelmy plate falling back to a vertical position and consequently damaging the ridged polymer leading to large defects.

Another common Langmuir-Blodgett trough configuration is the dual-barrier setup, which was employed for the polymerization of carboxy fantrip. In this setup, the monomer is spread between two barriers of the trough. Both barriers move toward the center in tandem, thereby eliminating the drastic deflection experienced by the Wilhelmy plate.

Figure 3.6 Langmuir Blodgett trough: Dual barrier trough design with microbalance sensor, dipping arm and temperature probe. Image of a Kibron Microtrough G2 from Kibron.com.

Upon compressing carboxy fantrip at 1 °C, three distinct phase transitions are observed. Before compression, monomers begin by floating on the surface, considered to be in a pseudo gaseous state (G), where the surface pressure is at 0 mm^2/mm. As the barriers slowly compress, noncovalent interactions occur between molecules, leading to a liquid condensed state (L1) between 0-4 mN/M. Surface pressures above 4 mN/m result in the

formation of a 2D crystal lattice of the monomer, representing the solid state (S) (refer to Figure 3.7).

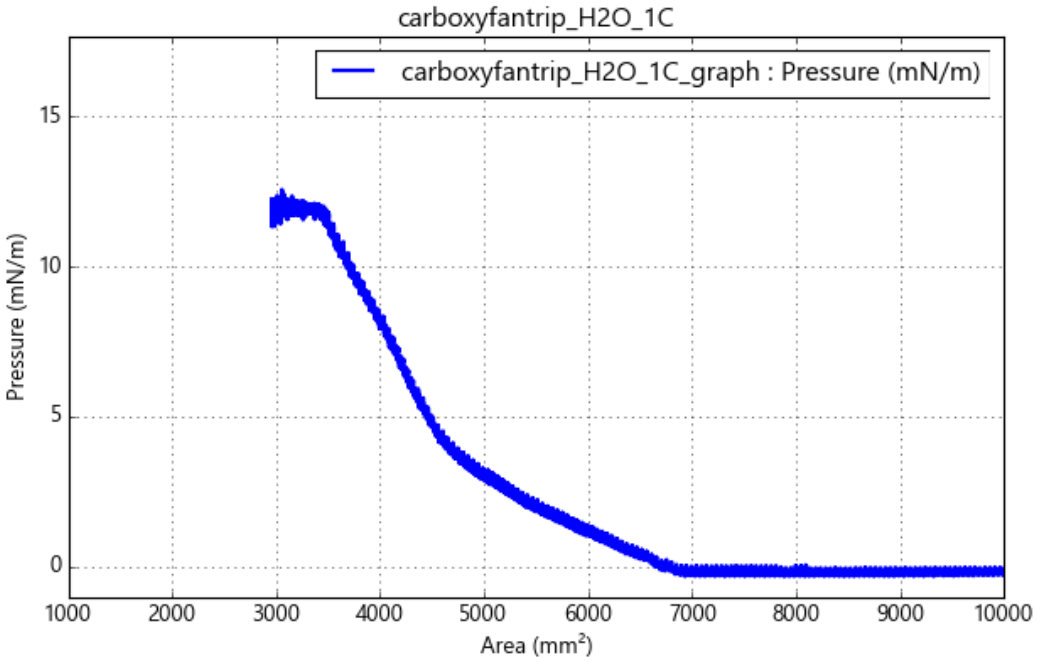

Figure 3.7 Pressure vs area plot of carboxy fantrip: Isothermal compression of carboxy fantrip monomer. Monomer concentration 0.08 mg/mL: 80 μL adsorbed on trough.

Brewster angle microscopy (BAM) played a critical role in visualizing surface morphology and the distribution of monomers. BAM is an imaging technique that utilizes the Brewster angle, where polarized light incident on a surface is perfectly transmitted. By exploiting this angle, imaging of thin films and interfaces are greatly enhanced allowing for visualization of monolayers on the surface of water.[82,83] During the initial adsorption of the monomer (0 mN/m), island-like features exhibiting sharp edges and acute angles were visualized on the surface, suggesting the ordered aggregate formation of monomers prior

to compression. Barrier compression coalesced these islands into a homogeneous film (refer to Figure 3.8, images 1-6).

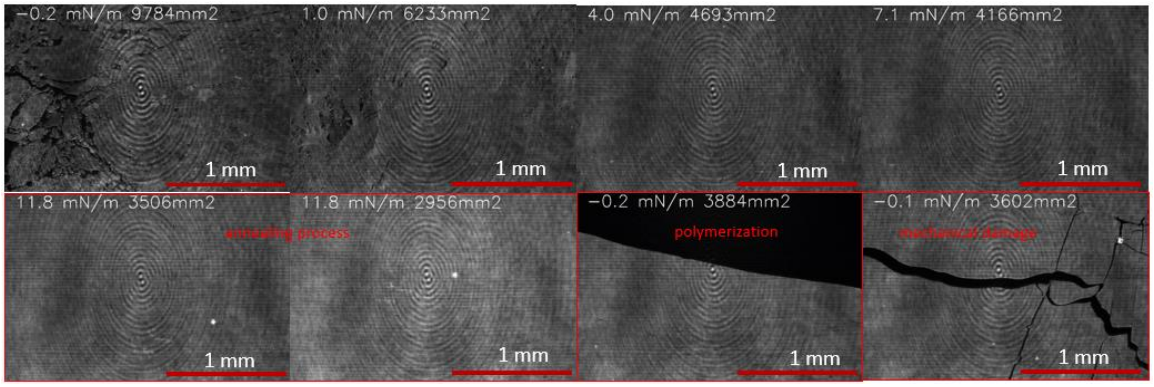

Figure 3.8 Brewster angle microscope images: Carboxy fantrip monomer compression images 1-6. Polymerization and mechanical destruction of 2DP images 7-8.

Annealing is essential to achieve the 2D crystalline packing of the monomers and, subsequently, large, homogenous domains of 2D polymer. Additional packing of the monomer prior to polymerization was observed as a steady decrease in surface pressure at the solid-state phase after the barriers were stopped (refer to Figure 3.7). Monitoring the compression by BAM microscopy confirmed this observation. A series of images taken during compression displayed non-homogeneous aggregation at the beginning of the solid-state phase (Figure 3.7, image 3). As pressure is held constant, the domains become tightly packed and may merge, effectively reducing the area of the trough. This is evident (refer to Figure 3.7, image 6) where the surface pressure remains at 12 mN/m, but the area is decreased by 550 mm^2 from the start of annealing (refer to Figure 3.7, image 7). Once barrier compression is halted and pressure remains constant, the monomer film is likely annealed.

Annealing significantly enhances the quality of transferred films after polymerization. Films polymerized without the annealing process tend to resemble the gas phase monomer aggregation, as observed by BAM, and exhibit the same morphology when transferred onto SiO2 substrates and imaged optically (refer to Figure 3.9).

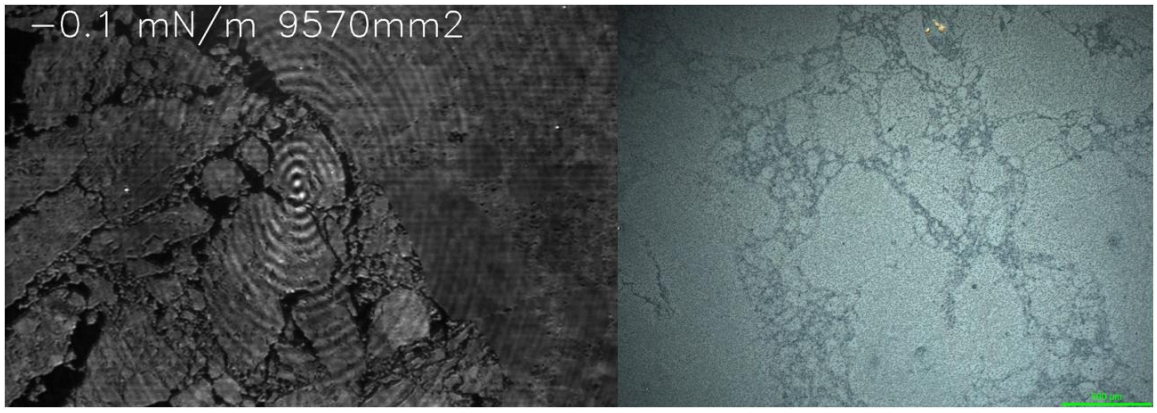

Figure 3.9 Incomplete polymerization of carboxy fantrip: Low packing density of monomer before compression (left). Transfer of polymer with many defects resembling low packing density (right)

3.3 Polymer Transfer onto Solid Substrates

The cumbersome nature of LB film fabrication limits its use in industry due to challenges in automation and a lack of reproducibility in defect-free films. [84] The success of polymer transfers at the air/water interface to a solid support is influenced by multiple factors, including polymer structure (bridgehead functionalization and rigidity), subphase composition (pH and temperature), dipping speed and angle, substrate surface chemistry, and surface pressure of deposition.[42] Difficulties in monolayer transfer necessitate meticulous experimental tuning of conditions, which is not straightforward. The surface

polarity of the film and substrate plays a significant role in adhesion during the transfer process and greatly affects the chosen method (adhesion through upstroke or downstroke).

3.3.1 Solid Support Surface Chemistry

Poly(carboxy fantrip) is a rigid polymer containing a polar carboxylic acid at the center of each monomer facing downward into the liquid subphase (refer to Figure 3.10). The transfer method used will determine the orientation of the carboxylic acid substituents. Two methods—1) a vertical upstroke deposition and 2) a bottom-up Langmuir-Schaefer approach—will result in the carboxylic acid of poly(carboxy fantrip) facing the solid support. This can be imagined as an egg prepared sunny-side-down. Polar substrates, e.g., SiO_2, work well for these methods as the polar carboxylic acid adheres to the polar surface of the substrate through hydrogen bond forces.

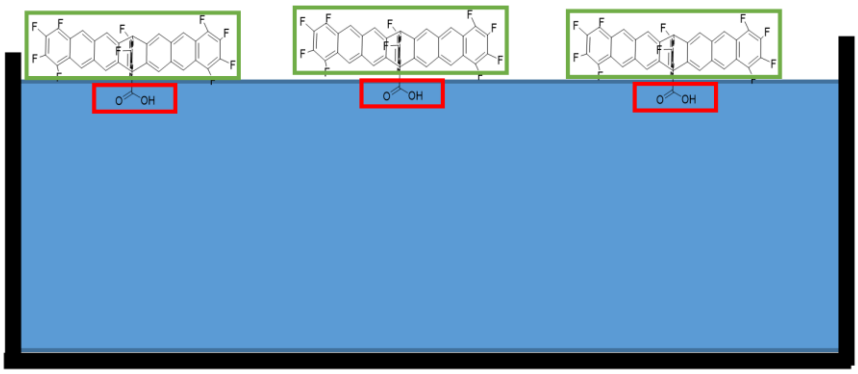

Figure 3.10 Carboxy fantrip monomer floating on the air water interface: Anthracene blades float perpendicular to the water's surface (within green box). Carboxylic acid acts as a polar anchor which stays submerged in water (red box).

To achieve a transfer where the carboxylic acid groups of the polymer face upward (away from the substrates surface), a non-polar substrate is essential for securing the 2DP

to the substrate through Van der Waals forces. The process involves trialkyl silylation of SiO_2 surfaces to create a hydrophobic monolayer of alkyl chains. Employing a top-down approach, the substrate is brought parallel to the interface and lowered onto the film. Upon contact, the substrate is carefully pulled away from the water's surface. Successful organofunctionalization of SiO_2 using silanes facilitates the sunny-side-up transfer of poly(carboxy fantrip). Additionally, gold (Au) metal substrates prove effective towards this approach with no organofunctionalization and can serve as conductive platforms for scanning tunneling microscopy (STM).

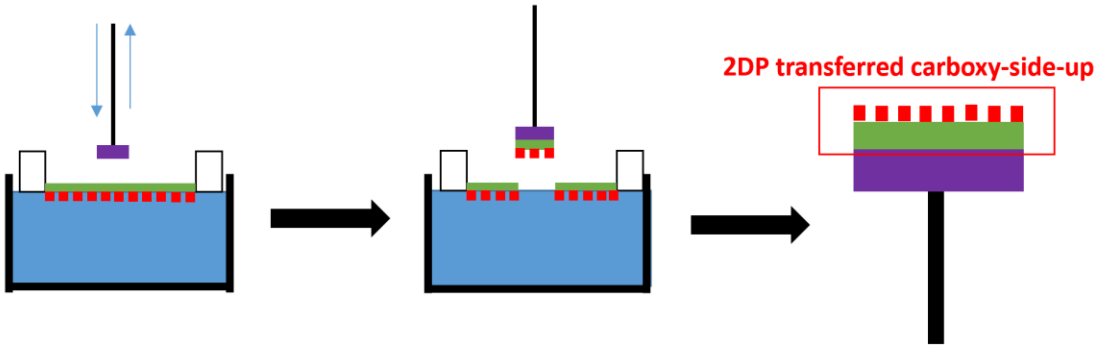

Figure 3. 11 Horizontal transfer of poly(carboxy fantrip): HMDS treated SiO_2/Si chip is lowered down to the films surface (left). Film adheres to the surface of the chip and raised away from the interface (center). Carboxy fantrip film with carboxy acid groups facing away from the substrates surface (right).

Silanization of SiO_2 installs hydrophobicity to the previously hydrophilic surface by treatment with gaseous silanating reagents, hexamethyldisilazane (HMDS) or trimethylsilyl chloride (TMSCl). Through trial and error it was found that transferred poly(carboxy fantrip) on HMDS treated SiO_2 gives a more defect free 2DP than previously reported transfers done on TMSCl treated SiO_2 when using the top-down Langmuir-

Scheafer transfer method. Better adhesion resulting in cleaner transfers most likely is a result of the substrates surface polarity better matching poly(carboxy fantrip).

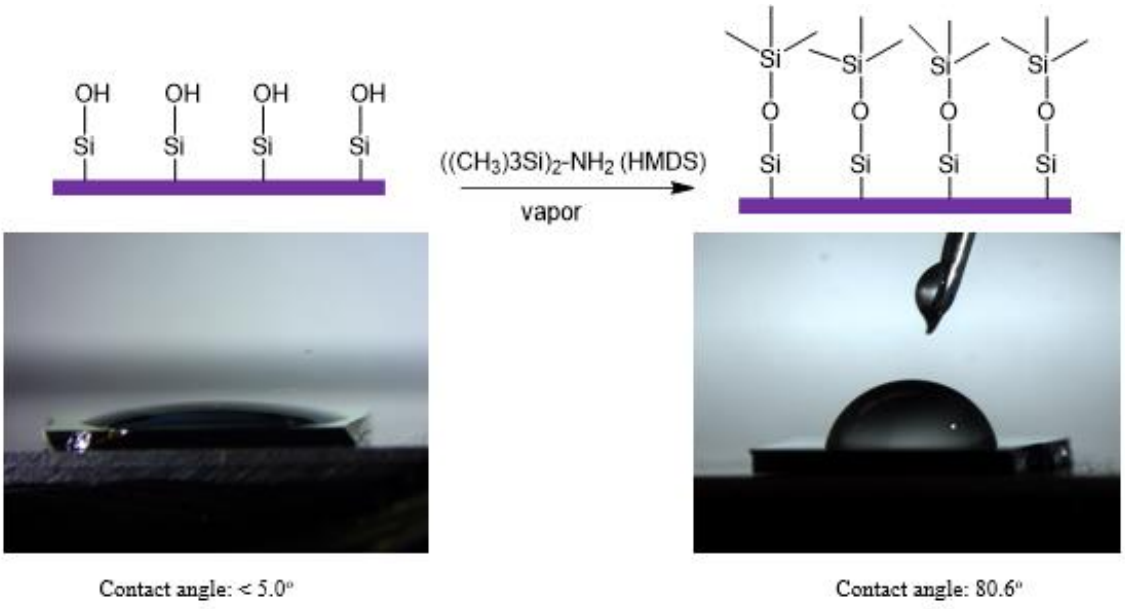

Figure 3.12 Silanization of SiO_2 using HMDS vapor: UVO cleaned wafers are treated with gaseous HMDS for 3 days.

The hydrophobicity of the treated wafer is measured through contact angle assignments of water droplets placed on the substrates surface. Measurements were taken from a homemade optical attachment fitted for a stereomicroscope. Clean, native SiO_2 surface results in a contact angle of almost zero when measured, that is, the surface is fully wetted. Upon treatment with HMDS, surface hydrophobicity increases to ~80.6° for neutral water and 79.3° for basic (1M NH_4OH) (Figure 3.13). The difference in contact angle between basic and neutral droplets is used as a control for the identification of carboxy-side-up poly(carboxy fantrip) transfers since the carboxylic acid is deprotonated at high pH. It is expected for the difference in contact angle between basic and neutral droplets on

HMDS treated wafers to be negligible because the newly formed methyl groups bonded to the oxygen creating a hydrophobic surface (refer to Figure 3.13).

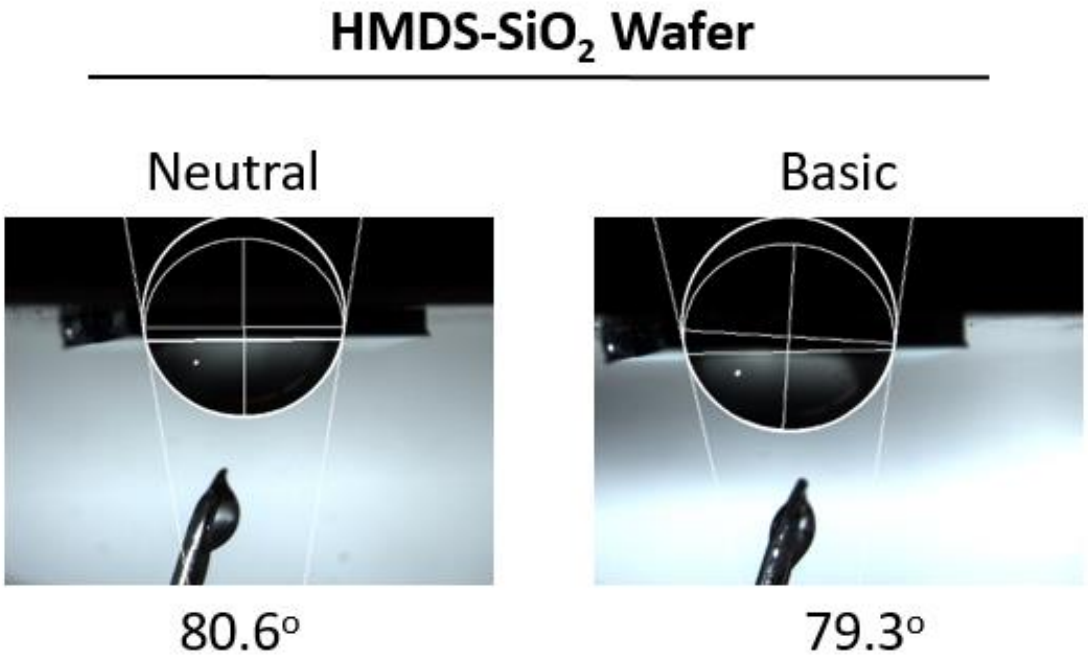

Figure 3.13 Contact angle of HMDS treated SiO_2: Neutral H_2O and basic (NH_4OH) tested as control for post functional modification studies.

3.3.2 Vertical deposition (Langmuir-Blodgett)

Attempts to transfer poly(carboxy fantrip) via vertical downstroke was not successful due to angular stress exhibited on the film causing tears during the transfer. HMDS treated substrates were used having a contact angle of ~80°. This angle does not afford a gradual approach for the film to adhere to the substrates surface. Reducing the effective angle the film during adhesion could be done using a super hydrophobic surface (contact angle ~180°, Figure 3.14). Various materials and fabrication strategies have been

explored to create superhydrophobic surface including chemical vapor deposition (CVD), sputtering, sol-gel, immersion and chemical etching.[85]

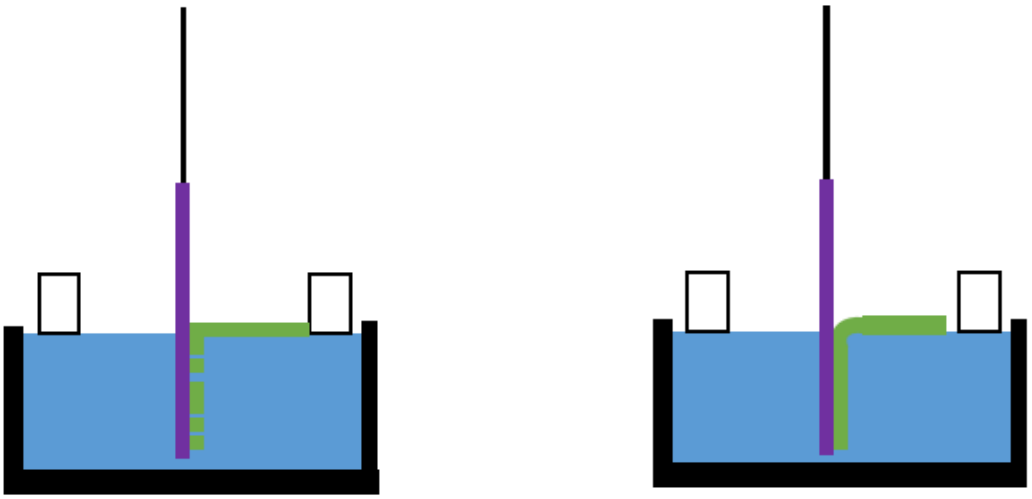

Figure 3.14 Vertical deposition approaches: Contact angle of ~90° forces polymer to deposit onto substrate at a right angle, causing breakage (left). A super hydrophobic surface would offer a gradual slope for the polymer to deposit onto the surface (right).

Most surface tears are a result of vertical deposition and often resemble the shape of a meniscus. As the substrate is lowered into the water, the polymer would adhere to the substrates surface and begin the bend at a right angle as the substrate is submerged into the trough. Eventually the angle caused the film breakage resulting in a horizontal tear (refer to Figure 3.15).

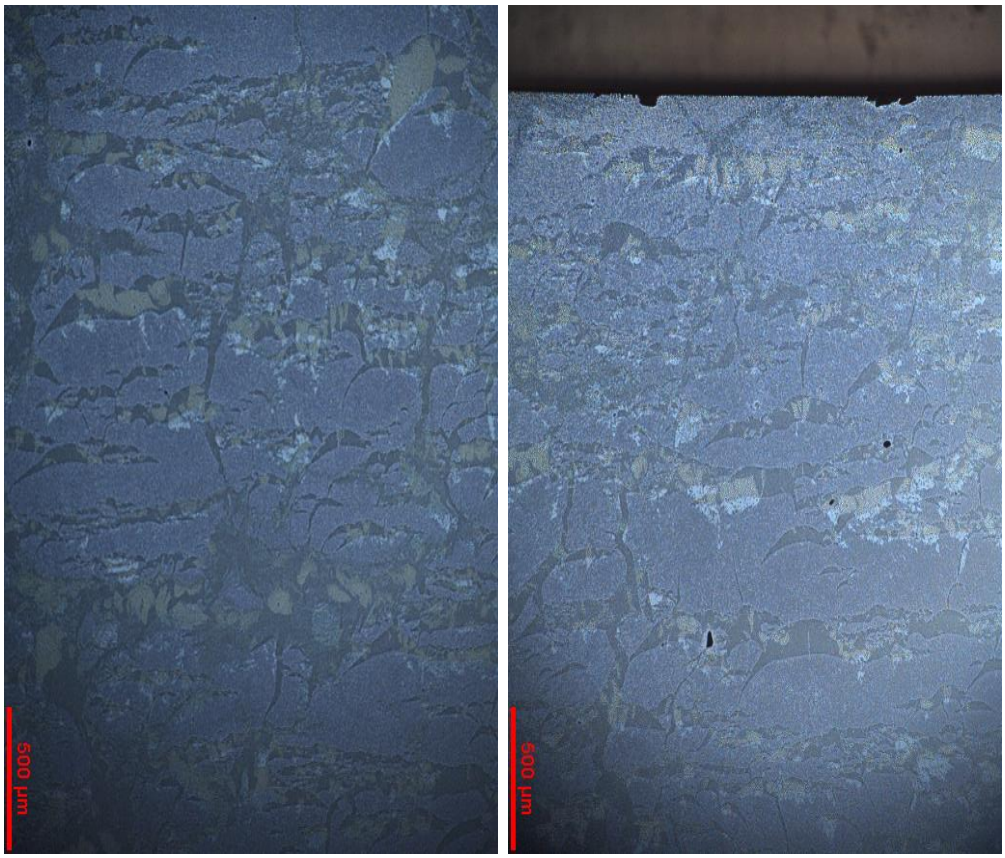

Figure 3.15 Vertical transfer of poly(carboxy fantrip) on HMDS-treated SiO_2: Two different vertical attemps to transfer poly(carboxy fantrip) to HMDS treated SiO_2.

3.3.3 Horizontal Transfer (Langmuir-Schaefer)

Horizontal deposition has successfully achieved transfers of poly(carboxy fantrip) with the carboxy side facing up. This method involves lowering the sample parallel to the water's interface, eliminating the stress generated by vertical transfer methods. HMDS-treated SiO_2 chips are utilized, employing a slow dipping speed (1 mm/min) during the descent to the water interface. Upon establishing contact between the substrate and interface, the substrate is gradually raised (1 mm/min) until it is separated from the interface.

Observation of double layers around the substrate edges is linked to excess film folding onto itself during the upstroke (refer to Figure 3.16). Employing a pasture pipet for aspiration around the chip after contact with water significantly diminishes the occurrence of double layers. Careful aspiration is crucial to prevent disturbing the film around the substrate, which could lead to submersion into the subphase.

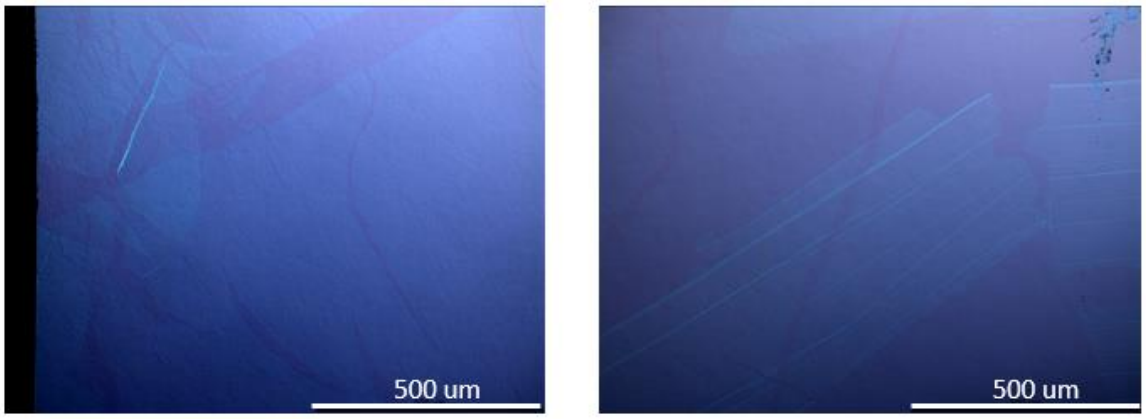

Figure 3.16 Langmuir-Schaefer transfer with double layers: Two optical images taken of poly(carboxy fantrip) transferred onto HMDS treated SiO_2. Both images illistrate double layer formation around the substrates edges.

Imaging defect-free transfers of poly(carboxy fantrip) (>1 mm2) on HMDS-treated SiO_2 chips poses challenges as they visually resemble the native surface. However, closer inspection reveals that much of the surface is not defect-free, often exhibiting linear fractures intersecting at consistent angles of ~70° and ~110°. These angles align with the unit cell of the non-amphiphilic poly(fantrip) crystal structure, implying that poly(carboxy fantrip) likely forms a porous hexagonal structure.[70] The extended length of these well-defined edges (>1 mm) indicates long-range order (see Figure 3.17).

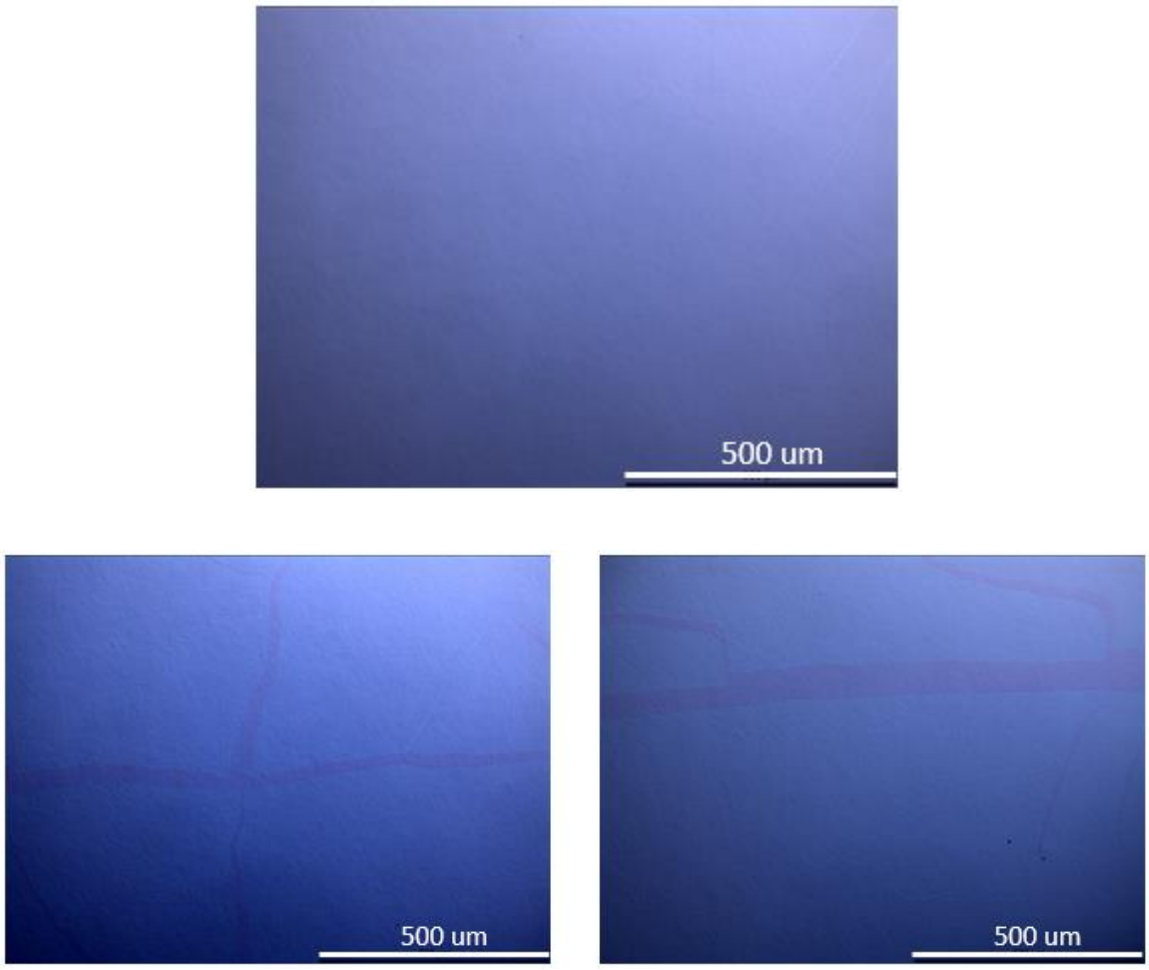

Figure 3.17 Langmuir-Schaefer transfer of poly(carboxy fantrip): Top image is a defect free transfer of poly(carboxy fantrip), no fractures are present but two small wrinkles are observed in the top right of the minage. Bottom images show consistant, clearly defined edges which hint at long range order.

3.3.4 Imaging Techniques of Transferred Poly(carboxy fantrip)

Utilizing differential interference contrast (DIC)[86] makes imaging poly(carboxy fantrip) on reflective surfaces (SiO_2) relatively straightforward. This method capitalizes on the contrast created by differences in thickness and refractive indices between the substrate

and the film, enabling clear visualization of the molecularly thin film on the substrate. Commonly used 300 nm SiO_2 (appearing purple-to-violet) provides optimal contrast for imaging molecularly thin films and is widely employed for observing graphene.[87] It is crucial to source SiO_2 wafers from reliable suppliers, as even a slight variation in thickness can significantly impact contrast.[88] However, imaging poly(carboxy fantrip) on non-reflective surfaces presents challenges. To indirectly visualize films on transparent quartz, gold (Au), and HOPG substrates, vapor condensation is employed by leveraging differences in polarity between the substrate and the transferred film (refer to Figure 3.18).

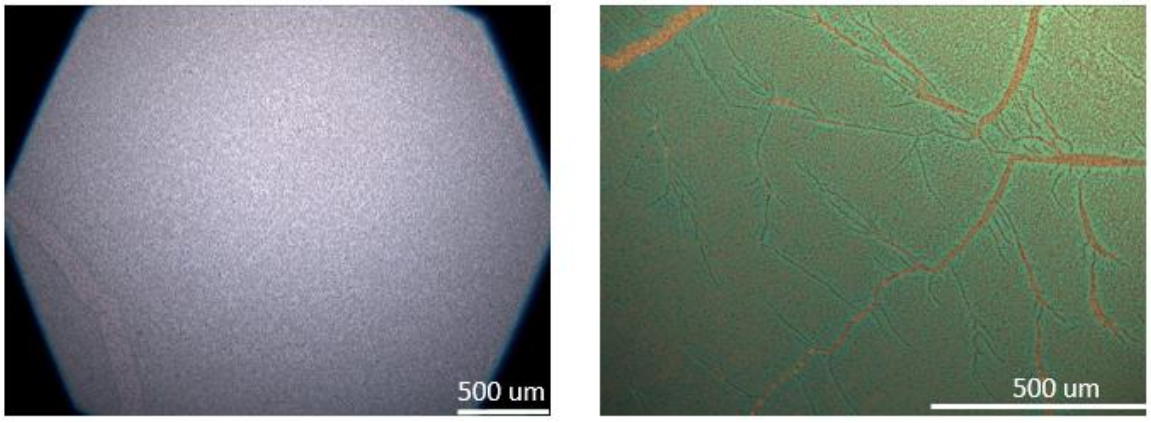

Figure 3.18 Vapor condensation images of poly(carboxy fantrip): Vapor condensation of SiO_2 (left) and gold (right).

Vapor condensation proves effective not only for optical microscopy but also for imaging extensive coverage on substantial areas (>3 cm^2) using a camera. This can be accomplished using a stereo microscope or even a phone camera, offering a convenient way to rapidly capture images of large areas with minimal preparation (refer to Figure 3.19).

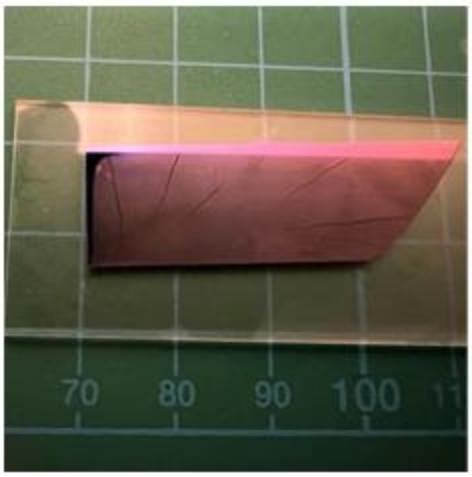

Figure 3.19 Vapor condensation image of poly(carboxy fantrip): Transferred poly(carboxy fantrip) carboxy-side-up. Image taken on Iphone-13.

AFM imaging of the polymer utilized a Nanosurf easyscan II operating in contact mode. The imaging process employed an App Nano silicon cantilever (Applied Nano Structures, Inc.) with a set point of 15nN. The measured height profiles between fractures were approximately 1.8 nm, consistent with the non-amphiphilic poly(fantrip) structure.[70] Lighter mounds visible in the image are likely associated with contaminants trapped beneath the film (refer to Figure 3.20).

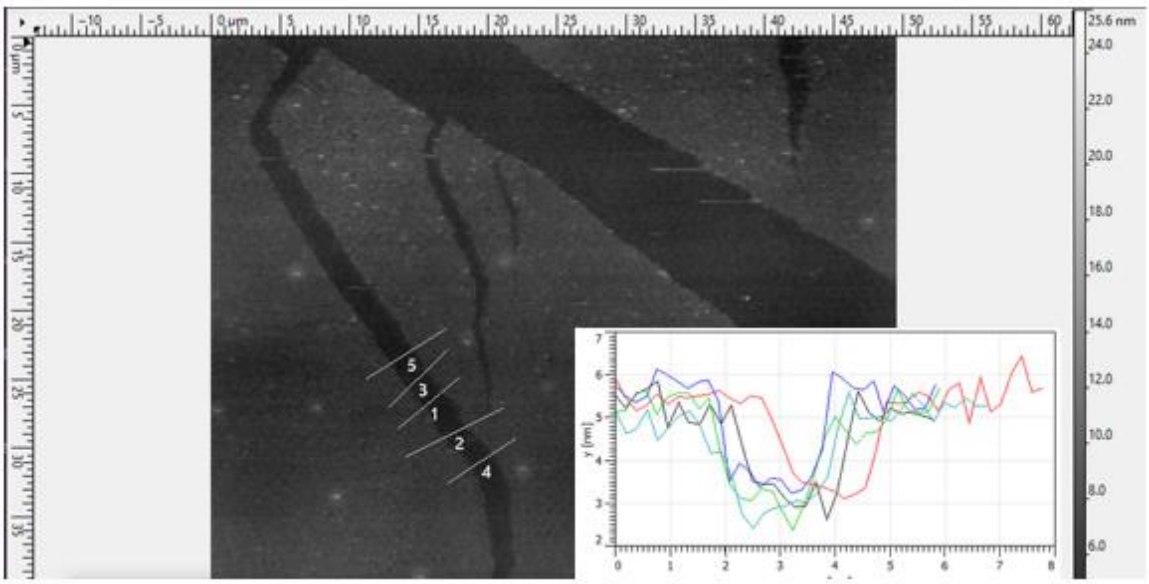

Figure 3.20 AFM image of poly(carboxy fantrip):AFM hight profile between a fracture within the film measured to be ~1.8 nm.

Imaging with AFM posed challenges given the ambient noise from classroom traffic and ventilation airflow during the measurement. To mitigate these issues, a homemade acoustic box was constructed and positioned on a vibration isolation table. Despite these experimental precautions, optimal results were obtained during nighttime when the building was unoccupied.

3.4 Substrate Disruption of the Air/Water Interface

Achieving reproducible monomer transfers of thin films onto solid substrates is often impeded by challenges associated with the three-phase solid-liquid-gas interphase.[89,90] Understanding the thermodynamic factors influencing monolayer transfers from the water's interface to a solid substrate is crucial for obtaining consistent results. The three-phase interphase between the monolayer and substrate is analogous to wetting

properties observed between various liquids and solids.[91–94] Free energy variations during the transfer process can be quantified for each surface through contact angle measurements between the solid substrate and its interaction with the water's interface. Addressing this issue is nontrivial, given the variations in experimental setups and variable assignments across different analyses.

To observe the release of free energy during the adhesion between the film and the substrate, a high-speed camera was set up to record the moment of contact (refer to Figure 3.21). While initial contact may appear gentle from a human perspective, with minimal disturbance to the air/liquid interface, a high frame rate camera reveals that the substrate's contact with water releases enough energy to propagate a wavefront across the entire Langmuir-Blodgett surface. The hydrophobicity of the substrate influences the amount of energy released, and this relationship was explored through a series of experiments designed to record the energy release.

3.4.1 Horizontal Deposition

Recordings of the initial contact between the air/water interface and three different substrates (SiO_2, HMDS-SiO_2, and Teflon) were captured at various angles to observe the displacement of water during adhesion. All three surface chemistries exhibited the propagation of a wavefront upon the initial contact with the water's surface. Figure 3.21 presents a series of snapshots captured during the moment of contact with water on the non-polar HMDS-SiO_2 surface. At time=0, a wave is generated as the lowest part of the substrate touches the water, creating a spherical wave that moves outward. The chip is

lowered at a rate of 1 mm/min, and it takes 84 µs for the water to adhere to the chip's surface.

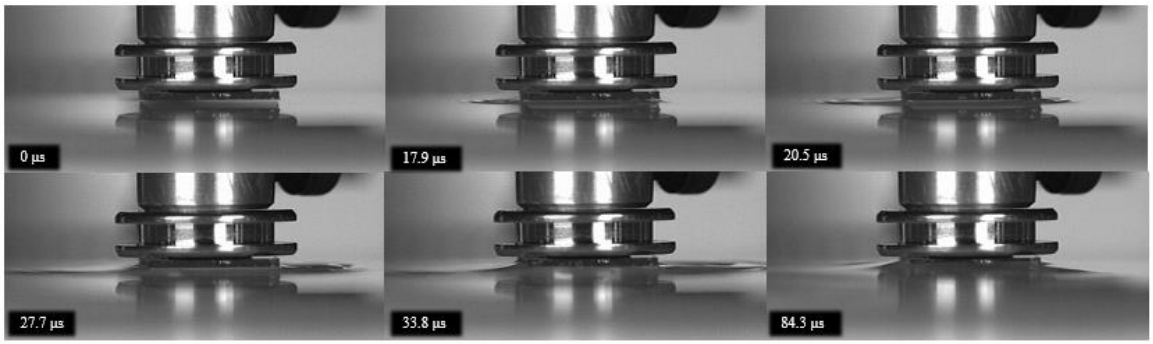

Figure 3.21 High speed imaging of substrate touching interface): HMDS-SiO_2 lowered to water's surface at 1mm/min. A wave is observed propagating out from the substrates initial point of contact.

Fractures caused by adhesive forces during horizontal film transfer mimic defects intentionally induced by forcing the barriers together after polymerization (as observed by BAM microscopy). In both scenarios, long lines and intersecting sharp angles are observed. These closely related fractures result from forces acting on the film and offer insights into defect formation before film transfer. Figure 3.22 illustrates the similarities between film defects generated by different forces, where the left image is a result of barrier compression, and the right is a result of the wave generated by adhesive forces during deposition.

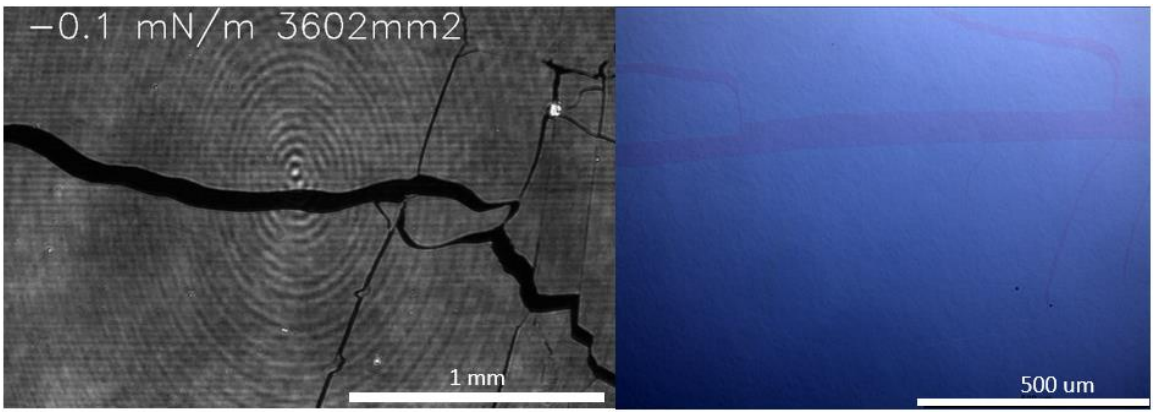

Figure 3.22 Film defect comparison: Fractures generated by barrier compression afer polymerization captured by BAM (left) and fractures generated by film depostion on HMDS-SiO_2.

3.4.2 Vertical and 45° Deposition

Additional deposition angles, including vertical and 45° angles, were recorded, and similarly, wave formations occurred during the initial point of contact with the water's surface. Changing the substrate's angle of approach (45° or 90°) reduced the size of the generated wave but did not lead to a cleaner film transfer. Defects during vertical film deposition result from a meniscus formed after contact with the water interface, as illustrated earlier in Figure 3.23-24.

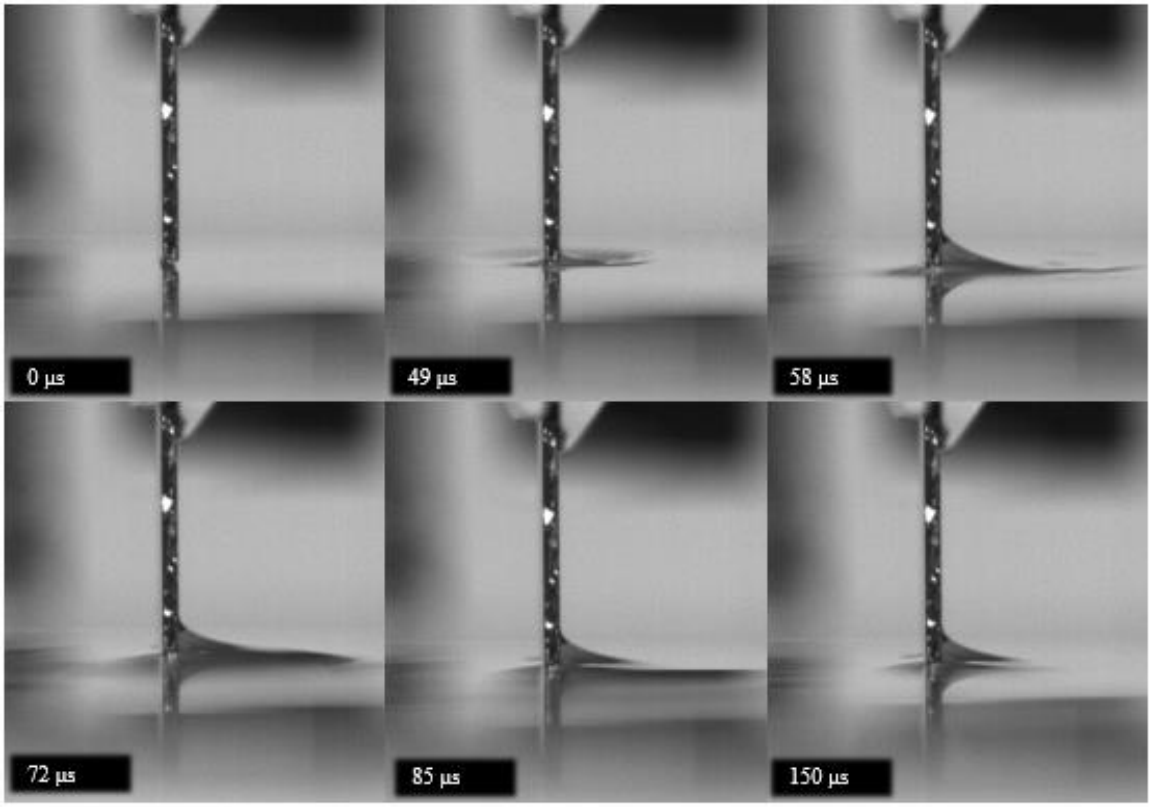

Figure 3.23 High speed imaging of substrate touching interface: HMDS-SiO_2 lowered to water's surface at an angle of 90° and speed of 1mm/min. A small wave is observed propagating out from the substrates initial point of contact. A meniscus forms on the substrate's surface resulting in film defects upon deposition.

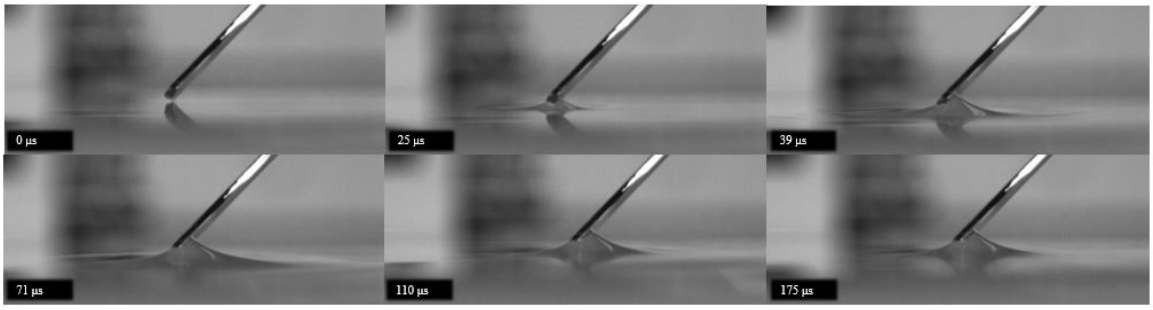

Figure 3.24 High speed imaging of substrate touching interface: HMDS-SiO_2 lowered to water's surface at an angle of 45° and speed of 1mm/min. A small wave is observed

propagating out from the substrate's initial point of contact. A meniscus forms on the substrates surface which results in film defects upon deposition.

In conclusion, adhesion forces between the air/liquid interface and the substrate's surface disrupt the air/liquid interface, forming a wavefront that causes fracture defects within the 2DP. These defects are observed on the substrate's surface after deposition. Changing the angle of approach to a 45° or 90° angle reduces the adhesive force, minimizing the wave but does not improve the deposition process.

3.5 Poly(Carboxy Fantrip) Gas Phase Surface Modification

Over the last three decades, there has been a growing interest in the modification of surfaces containing self-assembled monolayers (SAMs). This focus primarily centers on achieving control over surface modification at the molecular level and the ability to characterize the surface properties of the newly modified interface.[95] This process of assembling molecular building blocks onto a surface is often referred to as molecular nanotechnology. Precise control over the modification of molecular assemblies is crucial for manufacturing nanodevices, providing a means to communicate with the device. This increasing interest in surface control has found applications in various fields, including fuel cells,[96] sensors,[97,98] and molecular electronics,[99–101] as it allows for tailoring surface chemistry and understanding electron transfer processes among conjugated surfaces.

3.5.1 Surface Modification of Self-Assembled Monomers (SAMs)

Researchers commonly achieve surface modifications by employing self-assembled monolayers (SAMs) that are bound to various substrates such as silicon dioxide (SiO_2), silicon (Si), gold (Au), and graphene. SAMs are preferred as a foundation for

modified surfaces due to their well-defined molecular packing and a specific density of repeat units, which can be chemically modified for specific applications. Common reagents used in SAM formation include organosilanes,[102,103] alkanethiols,[104] organosulfur,[105] and aryl diazonium salts.[106]

Each SAM employed for surface modification contains a chemically functional distal moiety that participates in a surface reaction, leading to a chemical change in the surface environment. Distal moieties commonly involve primary amines (-NH2), alcohols (-OH), azides (N3), thiol (-SH), alkynes (-CH), and carboxy groups (-COOH).[107] Surface coupling reactions link relevant molecules to the SAMs distal functional groups in the liquid or gas phase, tailored for specific applications.

3.5.2 Surface Modification of Poly(Carboxy Fantrip)

We achieved surface functionalization on a molecularly thin two-dimensional polymer (2DP), poly(carboxy fantrip). The monomer design incorporates a single bridgehead carboxylic acid to act as an active, periodic tether for surface manipulation. Gaseous thionyl chloride was utilized to activate the carboxylic acid to an acid chloride, which subsequently reacted with alkyl alcohols or amines, forming the corresponding esters and amides.

The transfer protocol dictates the reactivity of the film. Poly(carboxy fantrip) must be transferred carboxy-side-up to provide access to the reactive bridgehead functionality. Figure 3.25 illustrates a carboxy-side-up transfer. The green box represents the polymerized sheet of anthracene blades oriented so that the functional carboxylic acid on each monomer faces away from the surface of the substrate.

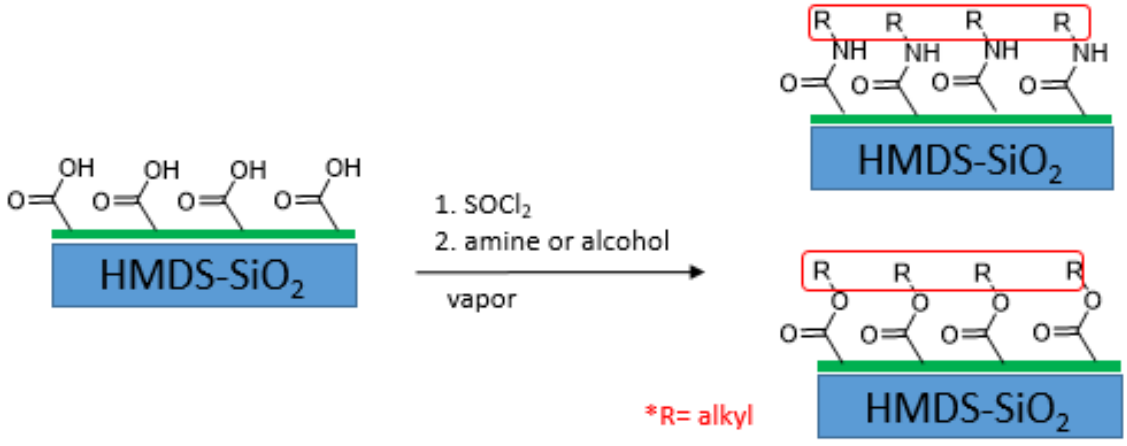

Figure 3.25 Surface modification of poly(carboxy fantrip) deposited on a HMDS-SiO_2 chip: Cartoon dipiction of polymer in grean transferred onto the substrates surface carboxy-side-up followed by functionalization reaction forming respective esters and amides

The carboxy fantrip monomer is photo-polymerized on a Langmuir-Blodgett trough and transferred carboxy-side-up onto HMDS-treated SiO2 chips, as described earlier in the chapter. The resulting molecularly thin films are functionalized using an evacuated vacuum chamber, where gaseous thionyl chloride is introduced using the air-free Schlenk technique. The film is allowed to react with thionyl chloride gas for 30 minutes, followed by a thorough evacuation (minimum 1 hour, 50 mtorr) to remove excess thionyl chloride or HCl. Gaseous alkyl moieties containing a distal primary amine or alcohol are introduced to the chamber to convert the acid chloride to its respective amide or ester (refer to Figure 3.26).

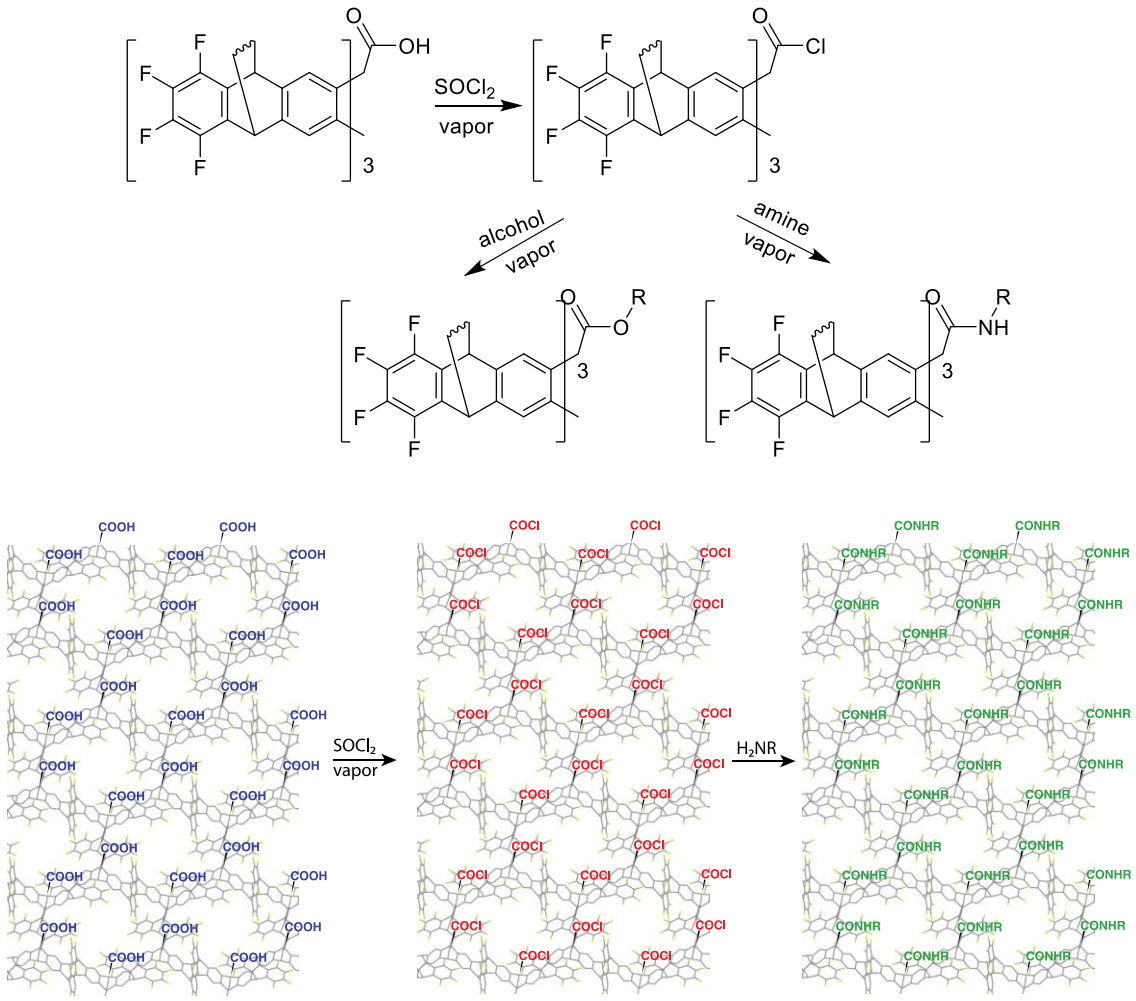

Figure 3.26 Surface modification of poly(carboxy fantrip): Synthetic scheme of involving carboxy activation with thionyl chloride and eseter or amide formation (top). Modification of polymer with carboxilic acids facing up (bottom)

Careful experimental setup is critical for successful functionalization. Thionyl Chloride must be distilled prior to use, and all alcohols and amines must be dried using activated 3A molecular sieves. Removing all water from the reactants reduces the chance of the activated acid chloride being converted back to the carboxylic acid. An air-free environment requiring multiple evacuations and N_2 backfills is necessary to facilitate ester

or amide formation. Below, Figure 3.27 illustrates a basic vacuum apparatus setup wherein the HMDS-SiO_2 chip containing the transferred film sits on the bottom. The septum on the side acts as a port for the introduction of reagents. The top of the apparatus is fitted with a barbed outlet that is connected to a Schlenk manifold.

Figure 3.27 Experimental setup of vacuum chamber used to functionalize poly(carboxy fantrip) surface: Custom made vacuum chamber with HMDS-SiO_2 chip harboring depositied film on bottom.

Surface contamination from airborne oil greatly inhibited reactivity and had to be carefully accounted for before every reaction. Prior to each gas-phase reaction, the substrate surface must be cleaned with electronic-grade isopropanol, followed by HPLC-

grade pentane, then quickly blown dry by a stream of N_2 gas with a 0.3 μm inline filter. This washing technique successfully cleaned oil particles from the surface of the substrate and was gentle enough to not disturb the 2DP film.

3.5.3 Contact Angle Measurement of Functionalized Surfaces

Characterization of the completeness of the reactions proved challenging due to the lack of available characterization techniques. The physical state of the polymer being adhered to a surface and the low concentration of molecules per area on the surface made common laboratory characterization techniques impossible. The modified surface was characterized by measuring a change in hydrophobicity before and after functionalization. The contact angle of water dropped onto the film's surface was measured to gain insight into the surface's polarity before and after surface functionalization.

In surface science, contact angle measurements are commonly used to gauge a surface's wettability. Wettability is defined as the angle between the tangent to the liquid-vapor interface and the solid surface at the three-phase contact line.[108] A surface with high surface energy (polar or hydrophilic) exhibits a low contact angle, while a surface with low surface energy (non-polar or hydrophobic) shows a high contact angle (refer to Figure 3.28).

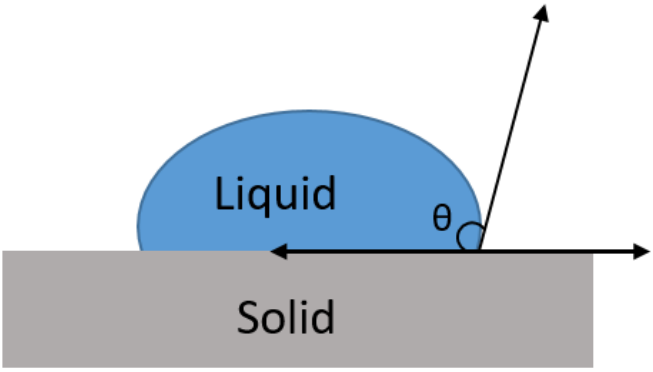

Figure 3.28 Contact angle: A drop of water on a solid surface where contact angle (θ) is an angle tangent to the liquid-vapor interface and the solid surface at the three-phase contact line.

Utilizing the contact angle principle, it becomes possible to track and quantify the chemical modification of the surface. A range of amines and esters with varying alkyl chain lengths were individually reacted on the poly(carboxy fantrip) surface, and their impact was measured by contact angle to assess the surface's wettability. While this method provides insights into the success of surface modification, indicating whether amination or esterification occurred, it does not quantify the percentage of functionalization.

Native SiO_2 is highly hydrophilic, exhibiting a contact angle close to zero, which does not facilitate adhesion of the hydrophobic dimerized anthracene blades of poly(carboxy fantrip) during deposition. However, when SiO_2 is treated with hexamethyldisilane (HMDS), it transforms into a hydrophobic surface with a contact angle of approximately 80°, enabling polymer adhesion. A successful transfer of poly(carboxy fantrip) onto HMDS-treated SiO_2 resulted in a contact angle of about 57°. By measuring

the change in contact angle before and after film transfer, coupled with optical imaging of the film, we could confirm the film's adherence to the surface (refer to Figure 3.29).

Figure 3.29 Contact angle of different substrates: Measuring the differences in contact angle of different surfaces offer insight to a change in surface chemistry.

The contact angle of specific functional surfaces can be pH-dependent, especially if the surface contains hydrogen bond donors, acceptors, acids, or bases. For poly(carboxy fantrip), deprotonation of the carboxylic acid leads to the formation of a carboxylate anion, increasing the surface's hydrophilicity and causing a decrease in the contact angle. This phenomenon is observed when measuring the contact angle of poly(carboxy fantrip) with basic water (pH 11 using NH4OH as the base), where the contact angle decreases to approximately 41° (refer to Figure 3.30).

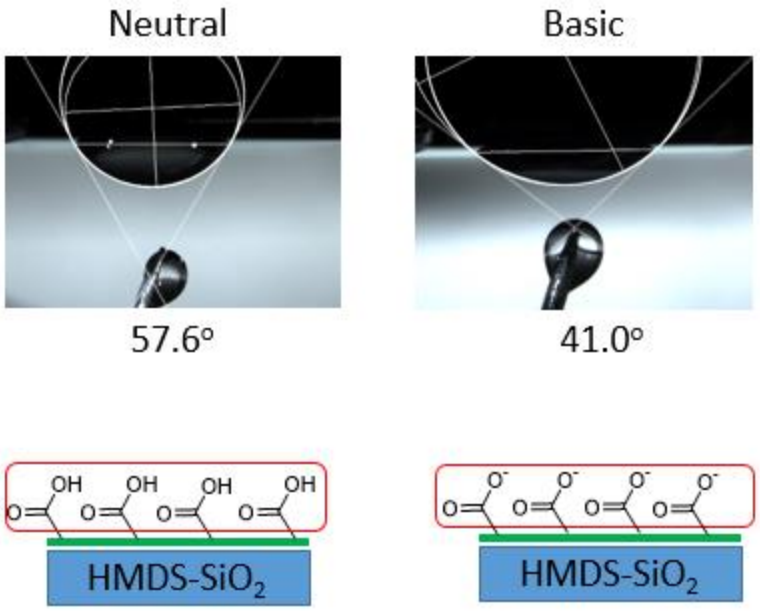

Figure 3.30 Poly(carboxy fantrip) contact angle pH dependence: Contact angle decreases with basic water by deprotination of they carboxy functional groups creating a more polar surface.

The pH dependence of the surface is a result of carboxylate anion formation, causing water to spread over the surface. The HMDS-SiO2 surface does not exhibit a pH-dependent contact angle due to the SiO2 surface being "capped" with alkyl chains. The lack of pH dependence in HMDS-SiO2 provides confidence that the pH dependence of poly(carboxy fantrip) is a measurable result due to the carboxylic acid functionality (refer to Figure 3.31).

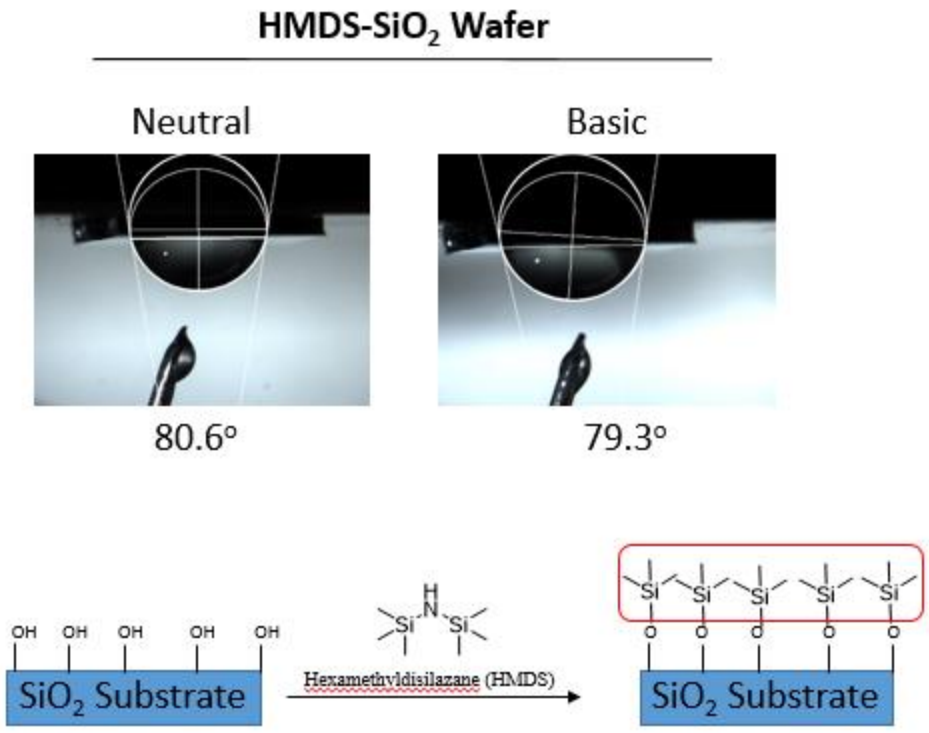

Figure 3.31 Contact angle of HMDS-SiO_2: Surface contact angle is not dependent on pH.

Functionalizing carboxylic acid with alkyl amines and alcohols will "cap" the carboxylic acid in a similar fashion to HMDS-SiO_2, thereby increasing hydrophobicity and effectively eliminating pH dependence. The pH dependence is eliminated by functionalizing the carboxylic acid to alkyl esters and amides, which do not form carboxylate anions in basic water and are less polar than a carboxylic acid. The success of surface modification reactions can be verified by comparing the increase in contact angle and the decrease in pH dependence (refer to Figure 3.32)

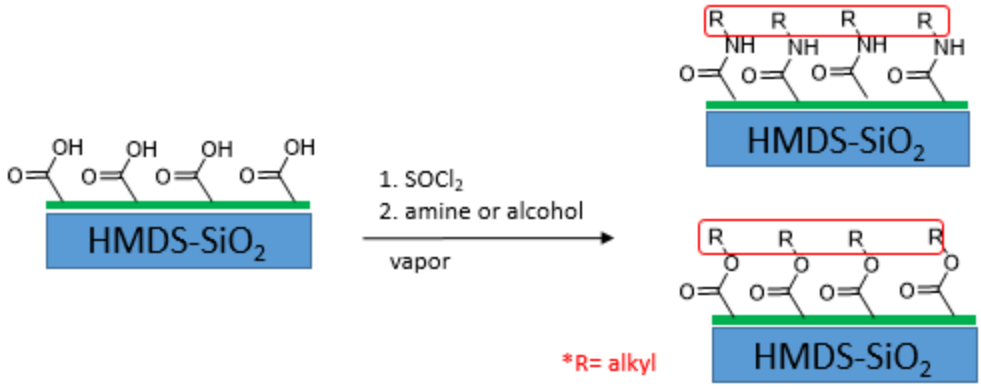

Figure 3.32 Amide and ester functionalization of poly(carboxy fantrip): pH dependence is eliminated by functionalizing the carboxylic acid with alkyl amides and esters.

3.5.4 Ester Functionalization Results

Surface modification of poly(carboxy fantrip) can be analyzed by comparing the neutral and basic contact angles pre and post-modification. A series of alkyl alcohols increasing in chain length (methyl, ethyl, and butyl alcohol) were reacted in the gas phase to form ester functionality on the carboxylic bridgehead. Contact angle measurements were taken of the surface after the modification to confirm the success of the reaction. The chips were washed with water followed by electronic grade isopropanol and pentane before contact angle analysis to ensure the cleanliness of the film's surface.

All three alcohols showed an increase in contact angles compared to unfunctionalized poly(carboxy fantrip) (contact angle of 57.6°). Additionally, the difference between basic and neutral water was much smaller, indicating successful functionalization. Methyl ester functionality had a neutral θ= 69.8° and a basic θ= 66.4°. The difference between basic and neutral θ= 3.4°. Ethyl ester functionality had a neutral

θ= 81.3° and a basic θ= 78.5°. The difference between basic and neutral θ= 2.8°. Butyl ester functionality had a neutral θ= 77.7° and a basic θ= 71.6°. The difference between basic and neutral θ= 6.1°.

The ethyl ester modified surface had the largest difference in contact angle between neutral and basic water, possibly due to the larger alkyl chain exhibiting slower vapor-phase kinetics of esterification, resulting in a lower percent functionalization. Ethyl ester also had contact angles between methyl and butyl ester functionality but is expected to be more hydrophobic, resulting in the largest contact angle. This result may be attributed to a lower percent functionalized surface.

Methyl ester contact angle measurments		
	Neutral	Basic
Trial	Theata C	Theata C
1	68.9	65.3
2	70.6	67.3
3	70	66.7
Average	69.83333	66.43333
std	0.862168	1.02632

Ethyl ester contact angle measurments		
	Neutral	Basic
Trial	Theata C	Theata C
1	80	79.6
2	81.8	76.2
3	82.1	79.7
Average	81.3	78.5
std	1.135782	1.992486

Butyl ester contact angle measurments		
	Neutral	Basic
Trial	Theata C	Theata C
1	76	74
2	78	76
3	79.1	64.7
Average	77.7	71.56667
std	1.571623	4.923639

Figure 3.33 Contact angle of alcohol series: Contact angle measurments of neutral and basic water tested respective esters.

Surface modification using adamantane methanol was also tested as a sterically encumbered ester. Adamantane methanol is a solid at room temperature and had to be sublimed in the vacuum chamber to react with the surface. Adamantane ester functionality had a neutral θ= 71.0° and a basic θ= 66.2°. The difference between basic and neutral θ=

4.8°. This represents an increase in the neutral contact angle of θ= 14° compared to poly(carboxy fantrip).

Adamantane ester contact angle measurments		
	Neutral	Basic
Trial	Theata C	Theata C
1	69.1	65.8
2	72.9	66.6
Average	71	66.2
std	2.687006	0.565685

Figure 3. 34 Contact angle of adamantane ester: Contact angle measurments of neutral and basic water tested on adamantane ester.

3.5.5 Amide Functionalization Results

A series of alkyl amines increasing in chain length (butyl, pentyl, and hexyl amine) were reacted in the gas phase to form amide functionality on the carboxylic bridgehead. Contact angle measurements were taken of the surface after the surface modification was complete to analyze the success of the amide functionalization. The chips were washed with water followed by electronic grade isopropanol and pentane prior to contact angle analysis to ensure the cleanliness of the film's surface.

All three amine contact angles increased from poly(carboxy fantrip). The contact angle difference between basic and neutral water was smaller than poly(carboxy fantrip), indicating the functionalization was successful. Butyl amide functionality had a neutral θ= 71.6° and a basic θ= 65.2°. The difference between basic and neutral θ= 6.4°. Pentyl amide functionality had a neutral θ= 67.4° and a basic θ= 60.5°. The difference between basic and

neutral θ= 6.9°. Hexyl amide functionality had a neutral θ= 70.7° and a basic θ= 66.9°. The difference between basic and neutral θ= 3.8°.

The difference in neutral contact angles between poly(carboxy fantrip) and amide-modified surfaces was smaller than the ester-modified surfaces. The difference between neutral and basic contact angles was larger on average compared to the ester-modified surface. During the gas-phase reactions of amines, it was common to see a slight vapor form within the chamber. The vapor is most likely a result of HCl gas evolved through the reaction of thionyl chloride and water. It is possible that the amines had a slightly higher percentage of water compared to the alcohols, resulting in a lower percent of functionalization.

Butyl amide contact angle		
	Neutral	Basic
Trial	Theata C	Theata C
1	70.3	61.6
2	72.8	68.8
Average	71.55	65.2
std	1.767767	5.091169

Pentyl amide contact angle measurments		
	Neutral	Basic
Trial	Theata C	Theata C
1	63.4	60.9
2	69.6	59.8
3	69.2	60.8
Average	67.4	60.5
std	3.46987	0.608276

Hexyl amide contact angle		
	Neutral	Basic
Trial	Theata C	Theata C
1	69.4	67.4
2	72.2	67.8
3	70.5	65.4
Average	70.7	66.86667
std	1.410674	1.28582

Figure 3. 35 Contact angle of amine series: Contact angle measurments of neutral and basic water tested respective amides.

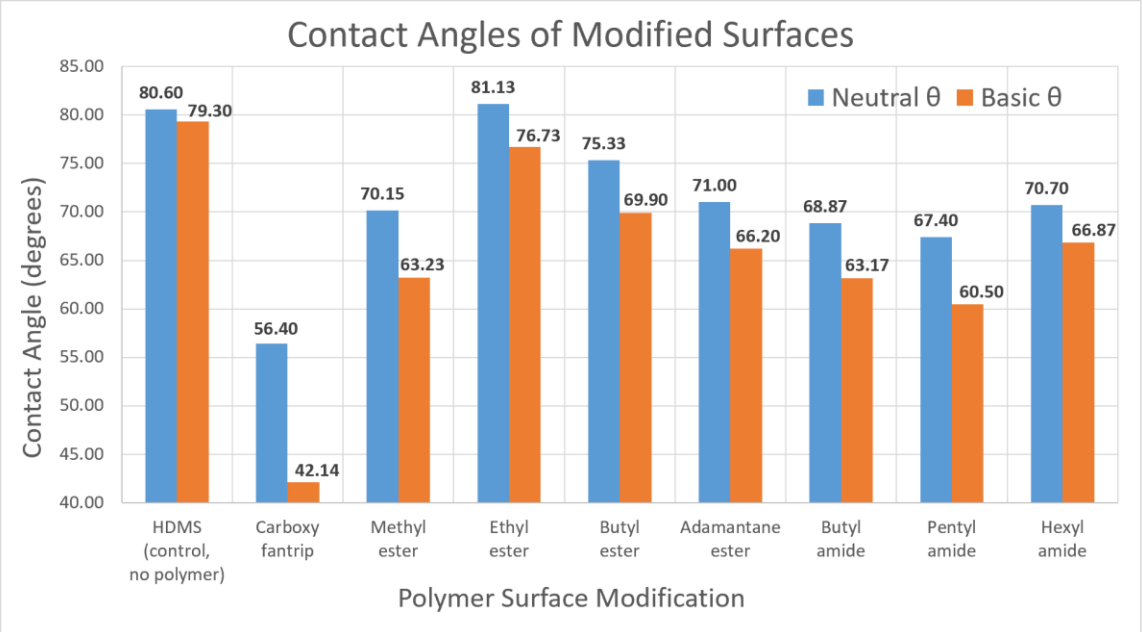

Figure 3. 36 Summary of modified surfaces and their respective contact angles.

3.6 Experimental

General Information:

All experiments were performed using a Kibron G1 microtrough. Surface pressure of the air/water interface was monitored with a Kibron DyneProbe. Freshly dispensed Milli-Q 18.2megohm water was used for the water interface. Fisher chemical HLPC acetone was used for trough cleaning and optima grade chloroform was used for the monomer solutions. Substrates were cleaned with semiconductor grade 2-Propanol (99.5% min). A Hamilton 1710 Gastight Syringe, 100 µL, cemented needle, 22s G, 2" blunt tip was used for loading monomer onto the air/water interface. The substrate used was prime grade 300 µm wet thermal oxide on silicon wafer purchased from University Wafer (ID:

1583). HMDS was freshly distilled before treatment of SiO_2 substrate. A 365 nm 5 W led was used for irradiating the trough.

3.6.1 Preparation of Trough:

The trough basin and barrier arms were cleaned thoroughly with electronic grade isopropanol followed by Milli-Q water then immediately blown dry with N_2 connected to a 3 um inline filter. With the barriers closed to the smallest allowed area, freshly dispensed Milli-Q water was used to fill the trough before each experiment. The trough was cooled to 1^{o}C. Aspiration of the air/water interface inside the barriers was critical to obtain a contaminate free surface. Barriers were then opened to the datum position before adsorption of analyte. An isothermal compression can be ran to ensure the water interface is contaminate free.

3.6.2 Preparation of HMDS-SiO2 Wafer:

Wafers were cut SiO_2 side down to a desired size using a scribe. The cut wafers were then ran under ample DI water. The chips were delicately swabbed with a cotton ball saturated in dilute soapy water then immediately placed under a stream of DI water for 1 minute. N_2 gas was used to blow dry the chip. The chip was then cleaned with a steady stream of electronic grade isopropynol then blown dry ensuring no solvent evaporated to dryness on the surface. The last step was repeated with HPLC grade pentane. The chip was placed under a mercury vapor grid lamp inside UVO-Cleaner to remove any remaining organic contaminants for 20 minutes. The cleaned cut wafers were immediately transferred to a glass desiccator along with a small vial containing HMDS (0.2 mL). The desiccator was sealed at 25 ^{o}C for 3 days. The chips were used as-is following this procedure.

3.6.3 Compression, Polymerization and Transfer onto SiO_2 of Monomer:

A HMDS-SiO_2 chip was centered above the trough parallel to the air/water interface (Schaefer method). Carboxy fantrip monomer was dissolved in a chloroform to a solution of 0.07 mg/ml and carefully adsorbed onto the air water interface by touching a droplet depressed from the tip of a microsyringe to the air/water interface. The adsorbed solution was allowed to spread across the surface for 10 seconds before adsorption of the following droplet. This slow method of adsorption allowed for even spreading and reduced spreading induced turbulent mixing[81]. A 15 minute delay time was allowed for solvent evaporation before compression. The barriers were closed at a rate of 2mm/min until the surface pressure increased from 0mM/m then slowed to 1 mN/m. The pressure was allowed to increase until 12 mN/m then held at constant pressure until an equilibrium was achieved between barrier compression and constant pressure, we call this the annealing process.

The entire area within the barriers were irradiated with a 365nm 5W led light for 1 min. Upon irradiation, surface pressure noticeably drops due to the formation of covalent bonds crosslinking the monomer. The substrate was immersed at 2 mm/min until contact was made with the surface. The dipper was halted for 5 seconds and then immersed at 1 mm/min for 10 seconds or until the substrate began rising above the interface but still touching the water. The surface around the substrate was aspirated to remove excess polymer followed by opening the barriers to the datum. This step was crucial to inhibit formation of double layers when the substrate was lifted from the surface. The substrate was emersed at 1 mm/min until it was freed from the water. The remaining droplet of water on the substrate was carefully aspirated off the chip.

3.6.4 Isothermal Compression Followed by Brewster Angle Microscopy:

A Kibron BAM was set up directly over the center of the LB trough. Carboxy fantrip monomer was dissolved in a chloroform to a solution of 0.07mg/ml and carefully adsorbed onto the air water interface by touching the droplet depressed from the tip of a microsyringe to the air/water interface. The adsorbed solution was allowed to spread across the surface for 10 seconds before adsorption of the following droplet. This slow method of adsorption allowed for even spreading and reduced spreading induced turbulent mixing[81]. A 15 minute delay time was allowed for solvent evaporation before compression. The barriers were closed from the datum position at 1 mm/min while the BAM was video recording. The pressure was allowed to increase until 12mN/m then held at constant pressure until an equilibrium was achieved between barrier compression and constant pressure, we call this the annealing process. The entire area within the barriers were irradiated with a 365nm 5W led light for 1 min. The barriers were opened at 1 mm/min until the video clearly showed the monomer to freely float across the screen. At this point the barriers were stopped. The area was then reduced at 1 mm/min to compress the freely floating film until it fractured. This opening and closing cycle was repeated to further break apart the polymer film.

3.6.5 Vapor Phase Surface Modification

Experimental setup and procedure was kept constant for each vapor phase surface modification. A substrate with transferred polymer was cleaned with electronic grade isopropanol, blown dry with N_2 then washed with HPLC grade pentane then blown dry with N_2. The chip was immediately placed on the bottom of a vacuum chamber and pumped

down to 40 mtorr for 30 minutes. The chamber was backfilled with argon and evacuated to 40 mtorr three times. The chamber was filled with thionyl chloride vapor through air/free Schlenk technique and allowed to react with the substrate for 30 minutes. Excess thionyl chloride was removed by evacuating the chamber to 40 mtorr for one hour. To the evacuated chamber the introduction of gaseous amine or alcohol reagent through Schlenk technique was transferred into the chamber and allowed to react with the substrate for one hour. Evacuation of excess reagent was removed by pumping to 40 mtorr for 30 minutes. The modified chips were removed from the chamber and washed with Milli-Q H_2O followed by a sequence of isoproynol (5 mL), then N_2 blown dry and pentane (5 mL), then N_2 blown dry. The cleaned film was immediately used for contact angle measurements.

3.6.6 Contact Angle Measurements

Contact Angle Measurements were taken on a house-made contact angle instrument mounted on a stereomicroscope. A substrate of interest was centered in the microscopes field of view with a white piece of paper centered behind the chip to offer contrast. A droplet of water was carefully drawn from the tip of the syringe and brought to the surface of the chip using a micro-manipulator. Once contact was made between the droplet and the substrate the needle was raised away from the droplet. An image was immediately taken and analyzed using ImageJ contact angle measurement add on.

3.6.7 High Speed Videography:

A Phantom high speed camera was positioned level with the troughs surface 4 feet away so that the field of view (FOV) was centered on the substrate and air/water interface. The dipper was lowered at 10 mm/min (the speed was chosen in order to capture the

moment of contact in the allowed recording time). For immersion in water: the camera was triggered to start recording just before the moment of contact between the substrate and the surface of water. For emersion from water: the camera was triggered to start recording just before the moment of release between the substrate and the surface of water.

References

(1) Carron, M. P.; Etienne, H.; Lardet, L.; Campagna, S.; Perrin, Y.; Leconte, A.; Chaine, C. Somatic Embryogenesis in Rubber (Hevea Brasiliensis Müll. Arg.). In *Somatic Embryogenesis in Woody Plants: Volume 2 — Angiosperms*; Jain, S. M., Gupta, P. K., Newton, R. J., Eds.; Forestry Sciences; Springer Netherlands: Dordrecht, 1995; pp 117–136. https://doi.org/10.1007/978-94-011-0491-3_8.

(2) Hurley, P. E. History of Natural Rubber. *J. Macromol. Sci. Part - Chem.* 1981, *15* (7), 1279–1287. https://doi.org/10.1080/00222338108056785.

(3) Provost, N. The Development of Synthetic Rubber and Its Significance in World War II. *Hist. Mak.* 2022, *15* (1).

(4) Geyer, R.; Jambeck, J. R.; Law, K. L. Production, Use, and Fate of All Plastics Ever Made. *Sci. Adv.* 2017, *3* (7), e1700782. https://doi.org/10.1126/sciadv.1700782.

(5) Frey, H.; Johann, T. Celebrating 100 Years of "Polymer Science": Hermann Staudinger's 1920 Manifesto. *Polym. Chem.* 2019, *11* (1), 8–14. https://doi.org/10.1039/C9PY90161B.

(6) Abd-El-Aziz, A. S.; Antonietti, M.; Barner-Kowollik, C.; Binder, W. H.; Böker, A.; Boyer, C.; Buchmeiser, M. R.; Cheng, S. Z. D.; D'Agosto, F.; Floudas, G.; Frey, H.; Galli, G.; Genzer, J.; Hartmann, L.; Hoogenboom, R.; Ishizone, T.; Kaplan, D. L.; Leclerc, M.; Lendlein, A.; Liu, B.; Long, T. E.; Ludwigs, S.; Lutz, J.-F.; Matyjaszewski, K.; Meier, M. A. R.; Müllen, K.; Müllner, M.; Rieger, B.; Russell, T. P.; Savin, D. A.; Schlüter, A. D.; Schubert, U. S.; Seiffert, S.; Severing, K.; Soares, J. B. P.; Staffilani, M.; Sumerlin, B. S.; Sun, Y.; Tang, B. Z.; Tang, C.; Théato, P.; Tirelli, N.; Tsui, O. K. C.; Unterlass, M. M.; Vana, P.; Voit, B.; Vyazovkin, S.; Weder, C.; Wiesner, U.; Wong, W.-Y.; Wu, C.; Yagci, Y.; Yuan, J.; Zhang, G. The Next 100 Years of Polymer Science. *Macromol. Chem. Phys.* 2020, *221* (16), 2000216. https://doi.org/10.1002/macp.202000216.

(7) Wei, Q.; Haag, R. Universal Polymer Coatings and Their Representative Biomedical Applications. *Mater. Horiz.* 2015, *2* (6), 567–577. https://doi.org/10.1039/C5MH00089K.

(8) Levkin, P. A.; Svec, F.; Fréchet, J. M. J. Porous Polymer Coatings: A Versatile Approach to Superhydrophobic Surfaces. *Adv. Funct. Mater.* 2009, *19* (12), 1993–1998. https://doi.org/10.1002/adfm.200801916.

(9) Cho, S. H.; White, S. R.; Braun, P. V. Self-Healing Polymer Coatings. *Adv. Mater.* 2009, *21* (6), 645–649. https://doi.org/10.1002/adma.200802008.

(10) Angelopoulos, M. Conducting Polymers in Microelectronics. *IBM J. Res. Dev.* 2001, *45* (1), 57–75. https://doi.org/10.1147/rd.451.0057.

(11) Dimitrakopoulos, C. d.; Malenfant, P. r. l. Organic Thin Film Transistors for Large Area Electronics. *Adv. Mater.* 2002, *14* (2), 99–117. https://doi.org/10.1002/1521-4095(20020116)14:2<99::AID-ADMA99>3.0.CO;2-9.

(12) Lopez, J.; Mackanic, D. G.; Cui, Y.; Bao, Z. Designing Polymers for Advanced Battery Chemistries. *Nat. Rev. Mater.* 2019, *4* (5), 312–330. https://doi.org/10.1038/s41578-019-0103-6.

(13) Novoselov, K. S.; Geim, A. K.; Morozov, S. V.; Jiang, D.; Zhang, Y.; Dubonos, S. V.; Grigorieva, I. V.; Firsov, A. A. Electric Field Effect in Atomically Thin Carbon Films. *Science* 2004, *306* (5696), 666–669. https://doi.org/10.1126/science.1102896.

(14) Novoselov, K. S.; Jiang, D.; Schedin, F.; Booth, T. J.; Khotkevich, V. V.; Morozov, S. V.; Geim, A. K. Two-Dimensional Atomic Crystals. *Proc. Natl. Acad. Sci.* 2005, *102* (30), 10451–10453. https://doi.org/10.1073/pnas.0502848102.

(15) Li, X.; Cai, W.; An, J.; Kim, S.; Nah, J.; Yang, D.; Piner, R.; Velamakanni, A.; Jung, I.; Tutuc, E.; Banerjee, S. K.; Colombo, L.; Ruoff, R. S. Large-Area Synthesis of High-Quality and Uniform Graphene Films on Copper Foils. *Science* 2009, *324* (5932), 1312–1314. https://doi.org/10.1126/science.1171245.

(16) Hoffmann, R. How Should Chemists Think? *Sci. Am.* 1993, *268* (2), 66–73.

(17) Sakamoto, J.; van Heijst, J.; Lukin, O.; Schlüter, A. D. Two-Dimensional Polymers: Just a Dream of Synthetic Chemists? *Angew. Chem. Int. Ed.* 2009, *48* (6), 1030–1069. https://doi.org/10.1002/anie.200801863.

(18) Gee, G.; Rideal, E. K. Reaction in Monolayers of Drying Oils I - The Oxidation of the Maleic Anhydride Compound of β-Elaeostearin. *Proc. R. Soc. Lond. Ser. - Math. Phys. Sci.* 1997, *153* (878), 116–128. https://doi.org/10.1098/rspa.1935.0224.

(19) Evans, A. M.; Strauss, M. J.; Corcos, A. R.; Hirani, Z.; Ji, W.; Hamachi, L. S.; Aguilar-Enriquez, X.; Chavez, A. D.; Smith, B. J.; Dichtel, W. R. Two-Dimensional Polymers and Polymerizations. *Chem. Rev.* 2022, *122* (1), 442–564. https://doi.org/10.1021/acs.chemrev.0c01184.

(20) Payamyar, P.; King, B. T.; Öttinger, H. C.; Schlüter, A. D. Two-Dimensional Polymers: Concepts and Perspectives. *Chem. Commun.* 2015, *52* (1), 18–34. https://doi.org/10.1039/C5CC07381B.

(21) Ritchie, H.; Roser, M. Clean Water and Sanitation. *Our World Data* 2021.

(22) Cohen-Tanugi, D.; Grossman, J. C. Water Desalination across Nanoporous Graphene. *Nano Lett.* 2012, *12* (7), 3602–3608. https://doi.org/10.1021/nl3012853.

(23) Sun, C.; Boutilier, M. S. H.; Au, H.; Poesio, P.; Bai, B.; Karnik, R.; Hadjiconstantinou, N. G. Mechanisms of Molecular Permeation through Nanoporous Graphene Membranes. *Langmuir* 2014, *30* (2), 675–682. https://doi.org/10.1021/la403969g.

(24) Cozzi, F.; Bacchi, S.; Filippini, G.; Pilati, T.; Gavezzotti, A. Synthesis, X-Ray Diffraction and Computational Study of the Crystal Packing of Polycyclic Hydrocarbons Featuring Aromatic and Perfluoroaromatic Rings Condensed in the Same Molecule: 1,2,3,4-Tetrafluoronaphthalene, -Anthracene and -Phenanthrene. *Chem. – Eur. J.* 2007, *13* (25), 7177–7184. https://doi.org/10.1002/chem.200700267.

(25) O'Hern, S. C.; Boutilier, M. S. H.; Idrobo, J.-C.; Song, Y.; Kong, J.; Laoui, T.; Atieh, M.; Karnik, R. Selective Ionic Transport through Tunable Subnanometer Pores in Single-Layer Graphene Membranes. *Nano Lett.* 2014, *14* (3), 1234–1241. https://doi.org/10.1021/nl404118f.

(26) Wang, Z.; Ouyang, L.; Li, H.; Wågberg, L.; Hamedi, M. M. Layer-by-Layer Assembly of Strong Thin Films with High Lithium Ion Conductance for Batteries and Beyond. *Small* 2021, *17* (32), 2100954. https://doi.org/10.1002/smll.202100954.

(27) Wang, L.; Gao, Y.; Wen, B.; Han, Z.; Taniguchi, T.; Watanabe, K.; Koshino, M.; Hone, J.; Dean, C. R. Evidence for a Fractional Fractal Quantum Hall Effect in Graphene Superlattices. *Science* 2015, *350* (6265), 1231–1234. https://doi.org/10.1126/science.aad2102.

(28) Zhao, Y.; Liu, H.; Wu, C.; Zhang, Z.; Pan, Q.; Hu, F.; Wang, R.; Li, P.; Huang, X.; Li, Z. Fully Conjugated Two-Dimensional Sp2-Carbon Covalent Organic Frameworks as Artificial Photosystem I with High Efficiency. *Angew. Chem. Int. Ed.* 2019, *58* (16), 5376–5381. https://doi.org/10.1002/anie.201901194.

(29) Sahabudeen, H.; Qi, H.; Glatz, B. A.; Tranca, D.; Dong, R.; Hou, Y.; Zhang, T.; Kuttner, C.; Lehnert, T.; Seifert, G.; Kaiser, U.; Fery, A.; Zheng, Z.; Feng, X. Wafer-Sized Multifunctional Polyimine-Based Two-Dimensional Conjugated Polymers with High Mechanical Stiffness. *Nat. Commun.* 2016, *7* (1), 13461. https://doi.org/10.1038/ncomms13461.

(30) Griessl, S.; Lackinger, M.; Edelwirth, M.; Hietschold, M.; Heckl, W. M. Self-Assembled Two-Dimensional Molecular Host-Guest Architectures From Trimesic Acid. *Single Mol.* 2002, *3* (1), 25–31. https://doi.org/10.1002/1438-5171(200204)3:1<25::AID-SIMO25>3.0.CO;2-K.

(31) Herbstein, F. H. Structural Parsimony and Structural Variety among Inclusion Complexes (with Particular Reference to the Inclusion Compounds of Trimesic Acid, N-(p-Tolyl)-Tetrachlorophthalimide, and the Heilbron "Complexes"). In *Molecular Inclusion and Molecular Recognition — Clathrates I*; Weber, E., Ed.; Topics in Current Chemistry; Springer: Berlin, Heidelberg, 1987; pp 107–139. https://doi.org/10.1007/BFb0003838.

(32) Rabe, J. P.; Buchholz, S. Commensurability and Mobility in Two-Dimensional Molecular Patterns on Graphite. *Science* 1991, *253* (5018), 424–427. https://doi.org/10.1126/science.253.5018.424.

(33) Yokoyama, T.; Yokoyama, S.; Kamikado, T.; Okuno, Y.; Mashiko, S. Selective Assembly on a Surface of Supramolecular Aggregates with Controlled Size and Shape. *Nature* 2001, *413* (6856), 619–621. https://doi.org/10.1038/35098059.

(34) Lin, N.; Stepanow, S.; Ruben, M.; Barth, J. V. Surface-Confined Supramolecular Coordination Chemistry. In *Templates in Chemistry III*; Broekmann, P., Dötz, K.-H., Schalley, C. A., Eds.; Topics in Current Chemistry; Springer Berlin Heidelberg: Berlin, Heidelberg, 2008; Vol. 287, pp 1–44. https://doi.org/10.1007/128_2008_150.

(35) Lafferentz, L.; Eberhardt, V.; Dri, C.; Africh, C.; Comelli, G.; Esch, F.; Hecht, S.; Grill, L. Controlling On-Surface Polymerization by Hierarchical and Substrate-Directed Growth. *Nat. Chem.* 2012, *4* (3), 215–220. https://doi.org/10.1038/nchem.1242.

(36) Bieri, M.; Nguyen, M.-T.; Gröning, O.; Cai, J.; Treier, M.; Aït-Mansour, K.; Ruffieux, P.; Pignedoli, C. A.; Passerone, D.; Kastler, M.; Müllen, K.; Fasel, R. Two-Dimensional Polymer Formation on Surfaces: Insight into the Roles of Precursor Mobility and Reactivity. *J. Am. Chem. Soc.* 2010, *132* (46), 16669–16676. https://doi.org/10.1021/ja107947z.

(37) Kissel, P.; Erni, R.; Schweizer, W. B.; Rossell, M. D.; King, B. T.; Bauer, T.; Goetzinger, S.; Schlueter, A. D.; Sakamoto, J. A Two-Dimensional Polymer Prepared by Organic Synthesis. *Nat. Chem.* 2012, *4* (4), 287–291. https://doi.org/10.1038/nchem.1265.

(38) Bhola, R.; Payamyar, P.; Murray, D. J.; Kumar, B.; Teator, A. J.; Schmidt, M. U.; Hammer, S. M.; Saha, A.; Sakamoto, J.; Schlu, A. D.; King, B. T. A Two-Dimensional Polymer from the Anthracene Dimer and Triptycene Motifs. 2013, *21*. https://doi.org/10.1021/ja404351p.

(39) Kissel, P.; Murray, D. J.; Wulftange, W. J.; Catalano, V. J.; King, B. T. A Nanoporous Two-Dimensional Polymer by Single-Crystal-to-Single-Crystal Photopolymerization. *Nat. Chem.* 2014, *6* (9), 774–778. https://doi.org/10.1038/nchem.2008.

(40) Kory, M. J.; Bergeler, M.; Reiher, M.; Schlüter, A. D. Facile Synthesis and Theoretical Conformation Analysis of a Triazine-Based Double-Decker Rotor Molecule with Three Anthracene Blades. *Chem. – Eur. J.* 2014, *20* (23), 6934–6938. https://doi.org/10.1002/chem.201400364.

(41) Kory, M. J.; Wörle, M.; Weber, T.; Payamyar, P.; van de Poll, S. W.; Dshemuchadse, J.; Trapp, N.; Schlüter, A. D. Gram-Scale Synthesis of Two-Dimensional Polymer Crystals and

Their Structure Analysis by X-Ray Diffraction. *Nat. Chem.* 2014, *6* (9), 779–784. https://doi.org/10.1038/nchem.2007.

(42) Oliveira, O. N.; Caseli, L.; Ariga, K. The Past and the Future of Langmuir and Langmuir–Blodgett Films. *Chem. Rev.* 2022, *122* (6), 6459–6513. https://doi.org/10.1021/acs.chemrev.1c00754.

(43) Franklin, B.; Brownrigg, W.; Farish, null. XLIV. Of the Stilling of Waves by Means of Oil. Extracted from Sundry Letters between Benjamin Franklin, LL. D. F. R. S. William Brownrigg, M. D. F. R. S. and the Reverend Mr. Farish. *Philos. Trans. R. Soc. Lond.* 1997, *64*, 445–460. https://doi.org/10.1098/rstl.1774.0044.

(44) Strutt, R. J. IV. Measurements of the Amount of Oil Necessary Iu Order to Check the Motions of Camphor upon Water. *Proc. R. Soc. Lond.* 1997, *47* (286–291), 364–367. https://doi.org/10.1098/rspl.1889.0099.

(45) Greene, J. E. Organic Thin Films: From Monolayers on Liquids to Multilayers on Solids. *Phys. Today* 2014, *67* (6), 43–48. https://doi.org/10.1063/PT.3.2419.

(46) Dubault, A.; Veyssié, M.; Liebert, L.; Strzelecki, L. Cross-Linked Polymerization of Monolayers of 1-n-Octadecyloxy-2-3-Diacryloyloxy Propane. *Nat. Phys. Sci.* 1973, *245* (145), 94–95. https://doi.org/10.1038/physci245094a0.

(47) Bodalia, R. R.; Duran, R. S. Polymerization of 2-Pentadecylaniline Monolayers at Fluid Surfaces: Kinetics, Thermodynamics, and Mechanism. *J. Am. Chem. Soc.* 1993, *115* (24), 11467–11474. https://doi.org/10.1021/ja00077a051.

(48) Kloeppner, L. J.; Duran, R. S. Langmuir Film Polymerization of 1,22-Bis(2-Aminophenyl)Docosane: A Two-Dimensional Cross-Linked Polyalkylaniline. *J. Am. Chem. Soc.* 1999, *121* (35), 8108–8109. https://doi.org/10.1021/ja990142x.

(49) Zhou, H.; Stern, R.; Batich, C.; Duran, R. S. Chemical Polymerization and Langmuir-Blodgett Techniques, 1. The Polymerization of a Monolayer of 2-Pentadecylaniline. *Makromol. Chem. Rapid Commun.* 1990, *11* (8), 409–414. https://doi.org/10.1002/marc.1990.030110812.

(50) Michl, J.; Magnera, T. F. Two-Dimensional Supramolecular Chemistry with Molecular Tinkertoys. *Proc. Natl. Acad. Sci.* 2002, *99* (8), 4788–4792. https://doi.org/10.1073/pnas.052016299.

(51) Murray, D. J.; Patterson, D. D.; Payamyar, P.; Bhola, R.; Song, W.; Lackinger, M.; Schlu, A. D.; King, B. T. Large Area Synthesis of a Nanoporous Two-Dimensional Polymer at the Air/Water Interface. 2015, 1–4. https://doi.org/10.1021/ja512018j.

(52) Yoshizawa, M.; Klosterman, J. K. Molecular Architectures of Multi-Anthracene Assemblies. *Chem. Soc. Rev.* 2014, *43* (6), 1885–1898. https://doi.org/10.1039/C3CS60315F.

(53) Roth, H. D. The Beginnings of Organic Photochemistry. *Angew. Chem. Int. Ed. Engl.* 1989, *28* (9), 1193–1207. https://doi.org/10.1002/anie.198911931.

(54) Hauptmann, S. The Aromatic Sextet: Von E. Clar; John Wiley & Sons LTD, London, New York, Sydney, Toronto 1972; 128 Seiten Mit Zahlreichen Formelbildern; Format 13 × 20 Cm; Broschiert £ 1, 50. *Z. Für Chem.* 1973, *13* (5), 200–200. https://doi.org/10.1002/zfch.19730130531.

(55) Hoffmeister, E.; Kropp, J. E.; McDowell, T. L.; Michel, R. H.; Rippie, W. L. Triptycene Polymers. *J. Polym. Sci. [A1]* 1969, *7* (1), 55–72. https://doi.org/10.1002/pol.1969.150070107.

(56) Cheloha, R. W.; Maeda, A.; Dean, T.; Gardella, T. J.; Gellman, S. H. Backbone Modification of a Polypeptide Drug Alters Duration of Action in Vivo. *Nat. Biotechnol.* 2014, *32* (7), 653–655. https://doi.org/10.1038/nbt.2920.

(57) Bouas-Laurent, H.; Castellan, A.; Desvergne, J.-P.; Lapouyade, R. Photodimerization of Anthracenes in Fluid Solution:Structural Aspects. *Chem. Soc. Rev.* 2000, *29* (1), 43–55. https://doi.org/10.1039/A801821I.

(58) Bouas-Laurent, H.; Castellan, A.; Desvergne, J.-P.; Lapouyade, R. Photodimerization of Anthracenes in Fluid Solutions: (Part 2) Mechanistic Aspects of the Photocycloaddition and of the Photochemical and Thermal Cleavage. *Chem. Soc. Rev.* 2001, *30* (4), 248–263. https://doi.org/10.1039/B006013P.

(59) Long, T. M.; Swager, T. M. Minimization of Free Volume: Alignment of Triptycenes in Liquid Crystals and Stretched Polymers. *Adv. Mater.* 2001, *13* (8), 601–604. https://doi.org/10.1002/1521-4095(200104)13:8<601::AID-ADMA601>3.0.CO;2-V.

(60) Gribble, G. W.; LeHoullier, C. S.; Sibi, M. P.; Allen, R. W. Synthesis and Deamination of 7,12-Dihydrobenz[a]Anthracen-7,12-Imines. A New Benz[a]Anthracene Synthesis. *J. Org. Chem.* 1985, *50* (10), 1611–1616. https://doi.org/10.1021/jo00210a011.

(61) Yao, Z.-F.; Wang, J.-Y.; Pei, J. Control of π–π Stacking via Crystal Engineering in Organic Conjugated Small Molecule Crystals. *Cryst. Growth Des.* 2018, *18* (1), 7–15. https://doi.org/10.1021/acs.cgd.7b01385.

(62) Cho, D. M.; Parkin, S. R.; Watson, M. D. Partial Fluorination Overcomes Herringbone Crystal Packing in Small Polycyclic Aromatics. *Org. Lett.* 2005, *7* (6), 1067–1068. https://doi.org/10.1021/ol050019c.

(63) Jadhav, S. Self-Assembled Monolayers (SAMs) of Carboxylic Acids: An Overview. *Open Chem.* 2011, *9* (3), 369–378. https://doi.org/10.2478/s11532-011-0024-8.

(64) Chechik, V.; Crooks, R. M.; Stirling, C. J. M. Reactions and Reactivity in Self-Assembled Monolayers. *Adv. Mater.* 2000, *12* (16), 1161–1171. https://doi.org/10.1002/1521-4095(200008)12:16<1161::AID-ADMA1161>3.0.CO;2-C.

(65) Brancart, J.; Damme, J. V.; Prez, F. D.; Assche, G. V. Substituent Effect on the Thermophysical Properties and Thermal Dissociation Behaviour of 9-Substituted Anthracene Derivatives. *Phys. Chem. Chem. Phys.* 2021, *23* (3), 2252–2263. https://doi.org/10.1039/D0CP05953F.

(66) Yoon, I.; Suh, S.-E.; Barros, S. A.; Chenoweth, D. M. Synthesis of 9-Substituted Triptycene Building Blocks for Solid-Phase Diversification and Nucleic Acid Junction Targeting. *Org. Lett.* 2016, *18* (5), 1096–1099. https://doi.org/10.1021/acs.orglett.6b00169.

(67) Friedman, Lester.; Logullo, F. M. Benzynes via Aprotic Diazotization of Anthranilic Acids: A Convenient Synthesis of Triptycene and Derivatives. *J. Am. Chem. Soc.* 1963, *85* (10), 1549–1549. https://doi.org/10.1021/ja00893a045.

(68) Meek, J. S.; Monroe, P. A.; Bouboulis, C. J. Diels—Alder Reactions of 9-Substituted Anthracenes. VI. 9-Anthryl Acetate, 9-Methoxyanthracene, and 9,10-Dimethoxyanthracene1. *J. Org. Chem.* 1963, *28* (10), 2572–2577. https://doi.org/10.1021/jo01045a021.

(69) Heilbron, I.; Jones, E. R. H.; Sondheimer, F. 129. Researches on Acetylenic Compounds. Part XV. The Oxidation of Primary Acetylenic Carbinols and Glycols. *J. Chem. Soc. Resumed* 1949, No. 0, 604–607. https://doi.org/10.1039/JR9490000604.

(70) Kissel, P.; Murray, D. J.; Wulftange, W. J.; Catalano, V. J.; King, B. T. A Nanoporous Two-Dimensional Polymer by Single-Crystal-to-Single-Crystal Photopolymerization. *Nat. Chem.* 2014, *6* (9), 774–778. https://doi.org/10.1038/nchem.2008.

(71) Cristol, S. J.; Pennelle, D. K. Bridged Polycyclic Compounds. LXI. Synthesis and Some Properties of Tribenzobicyclo[3.2.2]Nonatriene (Homotriptycene) and Derivatives. *J. Org. Chem.* 1970, *35* (7), 2357–2361. https://doi.org/10.1021/jo00832a056.
(72) Yamamoto, G.; Koseki, A.; Sugita, J.; Mochida, H.; Minoura, M. Deamination of 1-Alkyl-9-Aminomethyltriptycenes. Participation of a Neighboring 1-Alkyl Substituent. *Bull. Chem. Soc. Jpn.* 2006, *79* (10), 1585–1600. https://doi.org/10.1246/bcsj.79.1585.
(73) Corey, E. J.; Achiwa, K. Oxidation of Primary Amines to Ketones. *J. Am. Chem. Soc.* 1969, *91* (6), 1429–1432. https://doi.org/10.1021/ja01034a027.
(74) Omura, K.; Sharma, A. K.; Swern, D. Dimethyl Sulfoxide-Trifluoroacetic Anhydride. New Reagent for Oxidation of Alcohols to Carbonyls. *J. Org. Chem.* 1976, *41* (6), 957–962. https://doi.org/10.1021/jo00868a012.
(75) Zhao, M.; Li, J.; Song, Z.; Desmond, R.; Tschaen, D. M.; Grabowski, E. J. J.; Reider, P. J. A Novel Chromium Trioxide Catalyzed Oxidation of Primary Alcohols to the Carboxylic Acids. *Tetrahedron Lett.* 1998, *39* (30), 5323–5326. https://doi.org/10.1016/S0040-4039(98)00987-3.
(76) Kornfeld, E. C.; Barney, P.; Blankley, J.; Faul, W. Triptycene Derivatives as Medicinal Agents. *J. Med. Chem.* 1965, *8* (3), 342–347. https://doi.org/10.1021/jm00327a013.
(77) Roberts, G. G. Transducer and Other Applications of Langmuir—Blodgett Films. *Sens. Actuators* 1983, *4*, 131–145. https://doi.org/10.1016/0250-6874(83)85018-5.
(78) Sheppard, E.; Tcheurekdjian, N. Monolayer Studies: IV. Surface Films of Emulsion Latex Particles. *J. Colloid Interface Sci.* 1968, *28* (3), 481–486. https://doi.org/10.1016/0021-9797(68)90080-5.
(79) Fulda, K.-U.; Tieke, B. Langmuir Films of Monodisperse 0.5 Mm Spherical Polymer Particles with a Hydrophobic Core and a Hydrophilic Shell. *Adv. Mater.* 1994, *6* (4), 288–290. https://doi.org/10.1002/adma.19940060405.
(80) Fulda, K.-U.; Tieke, B. Monolayers of Mono- and Bidisperse Spherical Polymer Particles at the Air/Water Interface and Langmuir-Blodgett Layers on Solid Substrates. *Supramol. Sci.* 1997, *4* (3), 265–273. https://doi.org/10.1016/S0968-5677(97)00012-6.
(81) Nie, H.-L.; Dou, X.; Tang, Z.; Jang, H. D.; Huang, J. High-Yield Spreading of Water-Miscible Solvents on Water for Langmuir–Blodgett Assembly. *J. Am. Chem. Soc.* 2015, *137* (33), 10683–10688. https://doi.org/10.1021/jacs.5b06052.
(82) Joshi, B.; Khatavkar, R.; Iyer, N. Brewster Angle Microscope – An Excellent Tool for Nanoscience Researchers. *Synth. React. Inorg. Met.-Org. Nano-Met. Chem.* 2006, *36* (2), 227–229. https://doi.org/10.1080/15533170500524785.
(83) Desbat, B.; Castano, S. Brewster Angle Microscopy and Imaging Ellipsometry. In *Encyclopedia of Biophysics*; Roberts, G. C. K., Ed.; Springer: Berlin, Heidelberg, 2013; pp 196–200. https://doi.org/10.1007/978-3-642-16712-6_664.
(84) Ramsden, J. J. Chapter 6 - Nanomaterials and Their Production. In *Nanotechnology*; Ramsden, J. J., Ed.; Micro and Nano Technologies; William Andrew Publishing: Oxford, 2011; pp 101–124. https://doi.org/10.1016/B978-0-08-096447-8.00006-5.
(85) Parvate, S.; Dixit, P.; Chattopadhyay, S. Superhydrophobic Surfaces: Insights from Theory and Experiment. *J. Phys. Chem. B* 2020, *124* (8), 1323–1360. https://doi.org/10.1021/acs.jpcb.9b08567.
(86) Differential Interference Contrast Microscopy and Modulation Contrast Microscopy. In *Fundamentals of Light Microscopy and Electronic Imaging*; John Wiley & Sons, Ltd, 2012; pp 173–197. https://doi.org/10.1002/9781118382905.ch10.

(87) Blake, P.; Hill, E. W.; Castro Neto, A. H.; Novoselov, K. S.; Jiang, D.; Yang, R.; Booth, T. J.; Geim, A. K. Making Graphene Visible. *Appl. Phys. Lett.* 2007, *91* (6), 063124. https://doi.org/10.1063/1.2768624.

(88) Geim, A. K.; Novoselov, K. S. The Rise of Graphene. *Nat. Mater.* 2007, *6* (3), 183–191. https://doi.org/10.1038/nmat1849.

(89) Gaines, G. L. From Monolayer to Multilayer: Some Unanswered Questions. *Thin Solid Films* 1980, *68* (1), 1–5. https://doi.org/10.1016/0040-6090(80)90130-3.

(90) Gemma, N.; Egusa, S.; Azuma, M. Thermodynamics of Monolayer Transfer in the Langmuir-Blodgett Method. *Phys. Rev. B* 1992, *46* (3), 1655–1663. https://doi.org/10.1103/PhysRevB.46.1655.

(91) ZISMAN, W. A. Relation of the Equilibrium Contact Angle to Liquid and Solid Constitution. In *Contact Angle, Wettability, and Adhesion*; Advances in Chemistry; AMERICAN CHEMICAL SOCIETY, 1964; Vol. 43, pp 1–51. https://doi.org/10.1021/ba-1964-0043.ch001.

(92) de Gennes, P. G. Wetting: Statics and Dynamics. *Rev. Mod. Phys.* 1985, *57* (3), 827–863. https://doi.org/10.1103/RevModPhys.57.827.

(93) Sullivan, D. E. Van Der Waals Model of Adsorption. *Phys. Rev. B* 1979, *20* (10), 3991–4000. https://doi.org/10.1103/PhysRevB.20.3991.

(94) Hauge, E. H.; Schick, M. Continuous and First-Order Wetting Transition from the van Der Waals Theory of Fluids. *Phys. Rev. B* 1983, *27* (7), 4288–4301. https://doi.org/10.1103/PhysRevB.27.4288.

(95) Gooding, J. J.; Ciampi, S. The Molecular Level Modification of Surfaces: From Self-Assembled Monolayers to Complex Molecular Assemblies. *Chem. Soc. Rev.* 2011, *40* (5), 2704–2718. https://doi.org/10.1039/C0CS00139B.

(96) Zhang, X.; Gong, C.; Akakuru, O. U.; Su, Z.; Wu, A.; Wei, G. The Design and Biomedical Applications of Self-Assembled Two-Dimensional Organic Biomaterials. *Chem. Soc. Rev.* 2019, *48* (23), 5564–5595. https://doi.org/10.1039/C8CS01003J.

(97) Gooding, J. J.; Mearns, F.; Yang, W.; Liu, J. Self-Assembled Monolayers into the 21st Century: Recent Advances and Applications. *Electroanalysis* 2003, *15* (2), 81–96. https://doi.org/10.1002/elan.200390017.

(98) Gooding, J. J. Advances in Interfacial Design for Electrochemical Biosensors and Sensors: Aryl Diazonium Salts for Modifying Carbon and Metal Electrodes. *Electroanalysis* 2008, *20* (6), 573–582. https://doi.org/10.1002/elan.200704124.

(99) Liu, Y.; Flood, A. H.; Stoddart, J. F. Thermally and Electrochemically Controllable Self-Complexing Molecular Switches. *J. Am. Chem. Soc.* 2004, *126* (30), 9150–9151. https://doi.org/10.1021/ja048164t.

(100) McCreery, R. L. Molecular Electronic Junctions. *Chem. Mater.* 2004, *16* (23), 4477–4496. https://doi.org/10.1021/cm049517q.

(101) Vilan, A.; Yaffe, O.; Biller, A.; Salomon, A.; Kahn, A.; Cahen, D. Molecules on Si: Electronics with Chemistry. *Adv. Mater.* 2010, *22* (2), 140–159. https://doi.org/10.1002/adma.200901834.

(102) Kobayashi, S.; Nishikawa, T.; Takenobu, T.; Mori, S.; Shimoda, T.; Mitani, T.; Shimotani, H.; Yoshimoto, N.; Ogawa, S.; Iwasa, Y. Control of Carrier Density by Self-Assembled Monolayers in Organic Field-Effect Transistors. *Nat. Mater.* 2004, *3* (5), 317–322. https://doi.org/10.1038/nmat1105.

(103) Halik, M.; Klauk, H.; Zschieschang, U.; Schmid, G.; Dehm, C.; Schütz, M.; Maisch, S.; Effenberger, F.; Brunnbauer, M.; Stellacci, F. Low-Voltage Organic Transistors with an Amorphous Molecular Gate Dielectric. *Nature* 2004, *431* (7011), 963–966. https://doi.org/10.1038/nature02987.

(104) Love, J. C.; Estroff, L. A.; Kriebel, J. K.; Nuzzo, R. G.; Whitesides, G. M. Self-Assembled Monolayers of Thiolates on Metals as a Form of Nanotechnology. *Chem. Rev.* 2005, *105* (4), 1103–1170. https://doi.org/10.1021/cr0300789.

(105) Ulman, A. Formation and Structure of Self-Assembled Monolayers. *Chem. Rev.* 1996, *96* (4), 1533–1554. https://doi.org/10.1021/cr9502357.

(106) Delamar, M.; Hitmi, R.; Pinson, J.; Saveant, J. M. Covalent Modification of Carbon Surfaces by Grafting of Functionalized Aryl Radicals Produced from Electrochemical Reduction of Diazonium Salts. *J. Am. Chem. Soc.* 1992, *114* (14), 5883–5884. https://doi.org/10.1021/ja00040a074.

(107) Geißler, D.; Nirmalananthan-Budau, N.; Scholtz, L.; Tavernaro, I.; Resch-Genger, U. Analyzing the Surface of Functional Nanomaterials—How to Quantify the Total and Derivatizable Number of Functional Groups and Ligands. *Microchim. Acta* 2021, *188* (10), 321. https://doi.org/10.1007/s00604-021-04960-5.

(108) Huhtamäki, T.; Tian, X.; Korhonen, J. T.; Ras, R. H. A. Surface-Wetting Characterization Using Contact-Angle Measurements. *Nat. Protoc.* 2018, *13* (7), 1521–1538. https://doi.org/10.1038/s41596-018-0003-z.